EXPERIMENTAL INVESTIGATION OF THE EFFECT OF COOLING ON NEAR WAKE OF CIRCULAR CYLINDER AT MACH NUMBER SIX

Thesis by

Mathagondapally A. Ramaswamy

In Partial Fulfillment of the Requirements

For the Degree of

Doctor of Philosophy

California Institute of Technology

Pasadena, California

1971

(Submitted March 22, 1971)

ACKNOWLEDGEMENTS

I would like to express my sincere appreciation and thanks to Professor Toshi Kubota for his invaluable guidance and encouragement, and to Professor Lester Lees for his interest and advice throughout the course of this research program.

I would also like to thank Professor Wilhelm Behrens for initiating me into the Hot-Wire Techniques and for his continued help during the course of the experimental investigation. The many useful suggestions given by Dr. Donald J. Collins both during the course of this work and in writing the thesis are gratefully acknowledged.

My grateful appreciation is extended to Mrs. T. Van Harreveld for her conscientious efforts in the reduction of the data and preparation of many figures; to Mrs. Judy Alder for her assistance in calculations and card punching; to the staff of the GALCIT Hypersonic Wind Tunnel, Messrs. P. Baloga, G. Van Halewyn, S. Roman, J. Van Dijk and H. Mazurowski for their assistance during the Wind Tunnel tests; to the staff of the Aeronautics Shop under Mr. G. Carlson for their skillful construction of models and equipment; to Mrs. B. Wood, Mrs. Jewel Colbert and the staff of Graphic Arts for their assistance in the preparation of the illustrations; and to Mrs. V. Conner for her excellent typing of this thesis.

I wish to acknowledge with much appreciation the financial support provided me by the California Institute of Technology throughout my graduate education in this institution. The work discussed in this thesis was carried out under the sponsorship and with the financial

support of the U. S. Army Research Office and the Advanced Research Projects Agency under Contract No. DA-31-124-ARO(D)-33. The study leave granted to me by the National Aeronautical Laboratory, Bangalore, India, is sincerely acknowledged.

I wish to express my deepest appreciation and thanks to my wife, Uma, for her cooperation and encouragement, which were so essential for the completion of this work.

ABSTRACT

An experimental investigation has been conducted to study the near wake of a two-dimensional circular cylinder of 0.2 in. diameter at $M_\infty = 6$. Mean flow properties were determined from Pitot pressure, static pressure, and hot-wire recovery temperature measurements at free stream Reynolds number of 0.905×10^4 and 2.95×10^4 for both adiabatic and cooled models, the latter at $0.19\ T_o$.

The near-wake was laminar for the adiabatic model at both the Reynolds numbers tested. For the cold model, the near-wake was laminar for the lower Reynolds number and transition occurred in the near wake at the higher Reynolds number. The wake shocks, the shear layer edge and the thermal layer edge moved closer to the wake centerline with cooling and with increase in Reynolds number. The base pressure decreased with cooling and the sonic point moved closer to the model on cooling. In the recirculating region, the total temperature distributions exhibited a minimum close to the dividing stream line for all the cases, and the total temperature on the centerline was nearly constant and equal to the value at the rear stagnation point ($0.5\ T_o$ for the cold models) indicating that the heat transfer in this region was mainly by convection. The existence of a thin thermal layer on the base was evident for the cold models.

Preliminary experiments on the two-dimensionality of the flow and an emperical formulation for the viscous corrections to the measured Pitot pressure have been included in the Appendices.

TABLE OF CONTENTS

Table of Contents (Cont'd)

LIST OF FIGURES

List of Figures (Cont'd)

List of Figures (Cont'd)

LIST OF SYMBOLS

a_0, a_1, a_2	coefficients in the curve fit for $\rho u/\rho_\infty u_\infty$
C	Chapman-Rubesin factor
c_p	specific heat at constant pressure
c_v	specific heat at constant volume
D	diameter of the cylinder model
d	diameter of the hot wire or probe
F	$Re_{2r}\left(\frac{\rho_2}{\rho_1}\right)^{\frac{1}{2}} \frac{M^2}{M^2-1}$
G	gap between the protruding cylinder model and the tunnel side wall (Figure A-1)
f_1	function of $M\sqrt{\frac{\gamma}{2}}$
g_1	function of $M\sqrt{\frac{\gamma}{2}}$
H	thickness of the flattened probe
h	heat transfer coefficient
h_m	measured heat transfer coefficient of the hot wire
I	hot wire current
Kn	Knudsen Number
K_t	thermal conductivity of air at T_t
K_w	thermal conductivity of hot wire at T_{awm}
L	extent of the wedge fairing projection into the flow (Figure A-6)
ℓ	hot wire length
M	local Mach number
M_∞	free stream Mach number

List of Symbols (Cont.)

Nu	Nusselt number
Nu_*	infinite wire Nusselt number
Nu_m	measured Nusselt number
P	local static pressure
P_∞	free stream static pressure
P_b	base pressure
$P_{o,\infty}$	free stream stagnation pressure
PP_i	ideal Pitot pressure
PP_m	measured Pitot pressure
PP_∞	Pitot pressure in free stream (i.e. stagnation pressure behind a normal shock in free stream)
R	radius of curvature of the shock
R_{hw}	hot wire resistance
R_{awm}	measured adiabatic wire resistance
R_r	reference wire resistance (at 0^oC)
R_{aw*}	adiabatic wire resistance for infinite wire
Re_d	Reynolds number based on probe diameter $\left(\frac{\rho u d}{\mu}\right)$
Re_H	Reynolds number based on probe thickness $\left(\frac{\rho u H}{\mu}\right)$
Re_r	Reynolds number based on probe radius $\left(\frac{\rho u r}{\mu}\right)$
$Re_{\infty, D}$	Reynolds number based on model diameter and free stream conditions $\left(\frac{\rho_\infty u_\infty D}{\mu_\infty}\right)$
Re_{2d}	Reynolds number based on conditions downstream of a normal shock and diameter of the probe $\left(\frac{\rho_2 u_2 d}{\mu_2}\right)$

List of Symbols (Cont.)

Re_{2r}	Reynolds number based on conditions downstream of a normal shock and radius of the probe $\left(\frac{\rho_2 u_2 r}{\mu_2}\right)$
Re_{2H}	Reynolds number based on conditions downstream of a normal shock and thickness of the probe $\left(\frac{\rho_2 u_2 H}{\mu_2}\right)$
Re_{2R}	Reynolds number based on conditions downstream of a normal shock and radius of curvature of the shock $\left(\frac{\rho_2 u_2 R}{\mu_2} = \frac{\rho_1 u_1 R}{\mu_2}\right)$
$Re_{o, D}$	Reynolds number based on free stream conditions, diameter of the model and viscosity taken corresponding to free stream stagnation temperature $(\rho_\infty u_\infty D/\mu_o)$
$Re_{t, d}$	Reynolds number based on local conditions, diameter of the probe and viscosity corresponding to local total temperature $\left(\frac{\rho u d}{\mu_t}\right)$
r	radius of the probe
T	static temperature
T_o	free stream stagnation temperature
T_r	reference temperature (273^oK)
T_s	support temperature
T_t	local stagnation temperature
T_W	wall temperature of the model
T_w	hot wire temperature
T_∞	free stream static temperature

List of Symbols (Cont.)

T_{awm}	measured adiabatic wire temperature
T_{aw*}	infinite wire recovery temperature
u	local velocity
u_∞	free stream velocity
V_b	bucking voltage
V_{hw}	hot wire voltage
X	distance downstream of the center of the cylinder model
X_r	location of rear stagnation point from the center of the cylinder model
Y	transverse distance from the center of the model
Z	distance along the spanwise direction of the model from the center
α_r	slope of the wire calibration curve for zero current
γ	ratio of specific heats (c_p/c_v)
η	temperature recovery factor
η_c	recovery factor for continuum flow
η_f	recovery factor for free molecular flow
η_*	recovery factor for infinite wire (T_{aw*}/T_t)
η_m	measured recovery factor (T_{awm}/T_t)
$\bar{\eta}_*$	$(\eta_*-\eta_c)/(\eta_f-\eta_c)$
ρ	local density
ρ_1	density ahead of the shock
ρ_2	density after the shock
ρ_∞	free stream density

List of Symbols (Cont.)

ψ_n	Nusselt number end loss correction factor (Nu_*/Nu_m)
ψ	stream function
ω_o	$\frac{\tanh \nu_o}{\nu_o}$
ν_o	$\frac{\ell}{d}\sqrt{\frac{Nu_* K_t}{K_w}}$

Subscripts

0	free stream stagnation conditions
1	conditions upstream of the shock or initial value during an iteration
2	conditions downstream of the shock or revised value after an iteration
*	conditions corresponding to infinite wire
∞	conditions based on upstream infinity
aw	adiabatic wall conditions (equilibrium recovery conditions)
c	corresponding to continuum flow
d	based on the diameter of the probe or diameter of the hot wire
f	based on free molecular flow
H	based on the height or thickness of the probe
hw	referred to the hot wire
m	measured quantities
r	reference conditions or based on radius of the probe
R	based on the radius of curvature of the shock in front of the probe

List of Symbols (Cont.)

t	based on local stagnation temperature
W	referred to the wall condition
w	referred to the hot wire condition at any current I

I. INTRODUCTION

Wakes behind bodies moving at high speeds in air have been the subject of study by many investigators over the past several years. Initially the interest in these studies originated from a need for base drag estimates and hence was primarily a "base pressure problem." However, with the advent of hypersonic reentry vehicles, and the need to understand and evaluate the wake observable phenomena from a point of view of base heat transfer and wake discrimination, investigations have been directed towards a more detailed study of the various aspects of both the near and far-wake flow field. Apart from their application, the understanding of the physical processes associated with these complex flows has always posed a great challenge. Hence, attempts to meet this challenge have been made by many investigators for more than a decade.

A brief account of the theoretical and experimental studies, made to date, is given below in order to show the inadequacy of the theories and as well a lack of any experimental data to describe the near-wake flow field of a cold blunt body at hypersonic speeds and thus establishing the need for the present experimental investigation.

Crocco-Lees Mixing Theory[1] and Chapman's base pressure model[2] are two of the earliest theoretical attempts at understanding the near wake of bodies moving at supersonic speeds.

In Crocco-Lees' theory, the flow is determined from the criteria that the solution must pass smoothly through the critical point of the equations obtained from the conservation of overall mass

and momentum of the viscous layer. However, an empirical constant to take account of the mass entrainment rate was used in this theory. This basic idea later developed into the Integral Moment Method put forward by Reeves and Lees[3] and later extended by Grange et al.[4] and by Klineberg,[5] where no empirical data are introduced.

Chapman[2] postulated that the base pressure was determined by the criteria that the isentropic compression of the flow along the dividing streamline should be equal to the static pressure after isentropic turning of the outer flow through the wake shock, implying that compression of the flow along the dividing streamline takes place over an infinitesimally short distance close to the rear stagnation point. Chapman[6] proposed a heat transfer model also, where he assumes the temperature in the recirculating region (considered to be a dead air region) to be equal to the temperature of the wall. Baum, Denison and King[7] have extended the basic idea of Chapman to include the effects of initial boundary layer at separation and further determine the temperature in the recirculating region by considering a base boundary layer and energy balance in the recirculating region. The outer conditions for calculating the base boundary layer are obtained from a mass balance in the recirculating region.

Theories for the growth of both laminar and turbulent far wake, including the effects of transition and pressure gradient, once the initial profiles are provided, have been developed by many investigators (references 8 to 13).

Experimentally a fairly detailed picture of both the near wake and far wake of an adiabatic cylinder is known from the investigations

of McCarthy,[14] Dewey,[15] and Behrens.[16] The experimental investigations of Mohlenhoff,[17] Kingsland,[18] Herzog,[19] and Collins[20] deal with the problem of mass diffusion in the wake of an adiabatic cylinder. Except for the recirculating region, the flow field in the near wake and far wake of both the adiabatic and cold wedges have been mapped in detail by Batt.[21]

From these theoretical and experimental studies the following observations could be made:

a. The far wake results of Behrens[16] for cylinders and of Batt[21] for wedges were in reasonable agreement with the theories for far wakes thus indicating that further studies should emphasize the near wake region.

b. Chapman's assumption that the compression region is small was found to be incorrect from these experimental studies, where the region of compression extended considerably both upstream and downstream of the rear stagnation point for the range of Reynolds number of these investigations.

c. Though Batt[21] was unable to make measurements in the recirculating region of cold wedges, it was evident from the total temperature distribution on centerline beyond the rear stagnation point, that the temperature in the recirculating region was considerably higher than the temperature of wall as assumed by Chapman,[6] but considerably less than that obtained by Baum, Denison and King.[7]

d. Since no measurements in the recirculating region could be made by Batt[21] due to various experimental difficulties, the existence or otherwise of the base boundary layer was not clarified.

e. The integral moment method applied to the case of an adiabatic circular cylinder gave results in reasonable agreement with the experimental results of Dewey for the near wake. However, an attempt to apply the same method to the cold cylinder gave some physically unrealistic results for the centerline enthalpy distribution. This was possibly due to lack of any guide from experimental results as to a proper choice of enthalpy profiles, which are essential for the success of the integral method.

From the above observations it is evident that theories based on Chapman's model are very inadequate and that for the success of the integral moment method, experimental data are necessary to provide a guide for the choice of the profiles. The investigations of Mohlenhoff[17] and Kingsland[18] do not deal with the near wake. Since the investigations of Herzog and Collins deal with mass injection over only part of the cylinder, the analogous thermal problem would be partial cooling of the cylinder. Thus the effect of cooling in a cold blunt body cannot be inferred from these mass diffusion experiments. It is hard to infer the effects of cooling on the near wake of a blunt body from the results of Batt[21] on a cold wedge, since, (a) the separation on a wedge is essentially fixed unlike that on a blunt body; (b) the boundary layer on a blunt body is subjected to a much greater favorable pressure gradient than on a wedge; and (c) the local Mach number at the outer edge of the shear layer is much higher for a wedge as compared to that for a cylinder, and correspondingly the local

Reynolds number for a wedge is much lower than that for a cylinder. Thus a need to experimentally investigate the near wake of a cold blunt body existed.

Therefore the present experimental investigation was undertaken in order to:

a) find out the effect of cooling on the near wake of a blunt body;

b) compare these effects with that found for the wedge by Batt;[21]

c) find out the existence or otherwise of the thermal boundary layer on the base;

d) provide a guide for choosing the enthalpy profiles for the integral moment method.

The near-wake flow fields of both an adiabatic and cold ($77^{o}K$) circular cylinder of 0.2" diameter at a nominal Mach number of six and, $Re_{\infty, D} = 0.905 \times 10^{4}$ and $Re_{\infty, D} = 2.95 \times 10^{4}$ were mapped using Pitot pressure, static pressure and hot wire measurements.

II. EXPERIMENTAL TECHNIQUE

II. 1. Wind Tunnel

The experiments were conducted at a nominal Mach number of 6 in Leg 1 of the GALCIT Hypersonic Wind Tunnel.[22] This is a continuous flow, closed return tunnel with a 5" x 5" test section. The stagnation pressure is variable from 25 psia to 115 psia with an accuracy of ± 0. 02 psia and the stagnation temperature is maintained at 408°K with an accuracy of± 1°K to avoid nitrogen condensation in the test section. The model was located 23 inches downstream of the throat on the horizontal center plane of the tunnel, in the forward portion of the 10 inch long test rhombus. Tests were made with stagnation pressures of 25 and 80 psia corresponding to free stream Reynolds numbers, $Re_{\infty, D} = 0.905 \times 10^4$ and 2.95×10^4.

All data were taken 2 hours after the tunnel was started to allow sufficient time for the tunnel wall to reach equilibrium temperature. The existing probe actuator system which is repeatable within ± 0. 001 in. was used for all pressure and hot wire measurements except for the preliminary tests described in Appendix A. Helipot potentiometers driven by the actuator mechanism provided linear electrical signals corresponding to the probe position for use in a Moseley XY recorder.

II. 2. Model

The details of the model geometry and installation are given in Fig. 1. The model consisted of a hollow steel cylinder of 0. 2" outside diameter spanning the test section horizontally. In order to minimize the interaction of the cylinder with the tunnel wall boundary

layer and thus provide as nearly a two-dimensional flow as possible, some preliminary tests were made to determine the most favorable end configuration for the cylinder (see Appendix A). From these tests it was found that the 20°, 5/8" long wedges mounted on the cylinder in the vicinity of the wall, as used by Behrens,[16] were the most effective among all the configurations tested. These wedges, which are almost completely inside the wall boundary layer, were aligned visually to within $\pm 2^{\circ}$ of the free stream.

Two copper-constantan thermocouples were imbedded 2 inches apart in the center of the base region of the cylinder as shown in Fig. 1.

The model was mounted in the tunnel in a manner similar to that used by Batt[21] (see Fig. 1). A schematic diagram of the liquid nitrogen cooling system is shown in Fig. 2 (cf also Batt[21]). The cooling baths were provided at the inlet and outlet of the model in order to obtain spanwise uniformity in temperature. An inlet pressure of about 3 psig was required to cool the model to a temperature of 77°K.

II. 3. Pitot Pressure Probes

Pitot pressure surveys were made with a 0. 042 in. diameter probe flattened at the forward end to a 0. 004 in. by 0. 035 in. opening. The outside dimensions of the probe at the tip were 0. 008 in. by 0. 051 in. (see Fig. 3). A 5-psi Statham pressure transducer, model No. PA 208 Te-5-350, was used for most measurements. The transducer was calibrated against a silicon manometer and was found to be linear in the region of interest (Fig. 4). The Pitot pressures on

the centerline, close to the base, were more accurately measured by means of a silicon oil micromanometer, using a vacuum reference pressure of less than 0. 5 microns.

In order to measure the reverse flow in the base region of the model a special Pitot pressure probe shown in Fig. 5 was used. Using this probe, the Pitot pressure of the reverse flow was measured only on the centerline, since it was felt that the measurements at any significant distance away from the center line would not be reliable because of the narrow region of the reverse flow and the two-dimensional nature of the probe. For the same reason, measurements close to the rear stagnation point could be erroneous. Hence, reliance was placed only on the data obtained on the center line away from the rear stagnation point, where measurements were expected to be reasonably accurate. The silicon oil micromanometer was used for these measurements.

II. 4. Static Pressure Probes

For static pressure measurements beyond the rear stagnation point, the cone tipped static pressure probe illustrated in Fig. 3 was used. This is the same probe as used by Behrens[16] except for the distance of the reference edge from the orifice holes. The silicon oil micromanometer was used for the static pressure measurements along the wake centerline, and the 5-psia Statham pressure transducer was used for the transverse surveys at a few stations. The static pressure on the centerline at axial locations closer than $x/D = 2.0$ could not be measured with this probe because of the probe geometry.

The static pressures on the centerline for axial locations, $0.5 \leq x/d \leq 2.0$, were measured one at a time by using the special probes shown in Fig. 6. The silicon oil micromanometer was used for these measurements. The tips of these probes were flat, and during measurement the tip was positioned against the base of the cylinder model so that the influence of the tip on the pressure measurement was minimized. Hence, for each axial location, a probe with pressure taps at the corresponding distance from the tip had to be used. The special probe holder shown in Fig. 6 allowed quick interchange of probes and also insured leak-proof assembly because of the O-ring seal.

II. 5. Hot Wire Anemometer

Fig. 7 shows the hot-wire probes used in the current set of measurements. Each probe consisted of a platinum-10% rhodium wire approximately 0.20 inch in length and 0.000497 inch in diameter (manufacturer's specification), soft soldered to two needle supports. Chromel-Alumel thermocouple wires (.001 inch) were spot welded to within 0.01 inch of one support tip for each of the probes. All wires were calibrated in a manner outlined by Dewey.[15] Since the calibration of the wires before and after the run agreed within 2% which was within the measurable accuracy, no attempt was made to anneal the wires. From these calibration measurements, wire resistivity coefficients (α_r) and reference resistance (R_r) for zero current at $0^{\circ}C$ were determined.

For runs with a cooled model, at 80 psia tunnel stagnation pressure, the wires 0.2 inch long broke frequently, because of the

frost particles flying off of the model. Hence, for these runs the length of the wire was reduced to 0.125 inch.

It was necessary to provide some slight sag in the hot wire to avoid frequent breakage. A typical magnified view of the hot wire is shown in Fig. 8, where the relevant dimensions were obtained by the use of a comparator. The assumed mean location of the hot wire from the slightly protruding tip of the needle was determined as illustrated in Fig. 8. The hot-wire shape was assumed to be a circular arc, and the effective location was taken to be such that the portions of the wire ahead and behind this location were equal. To obtain the reference for positioning the hot wire at any desired axial location, the protruding tip was touched to the center of the cylinder base under running conditions, the contact being detected by an electrical circuit. This setting was repeatable to within 0.002 in.

The flow measurements were made using the instrumentation system developed by Herzog[19] (Fig. 9), modified to be compatible with the larger diameter wire. A detailed description of the system is given by Herzog[19] and a brief description is given here.

The current through the hot wire was measured by measuring the voltage across a 100 ohm resistance. Since variations in the hot wire voltage caused by changes in the flow variables were expected to be small compared to the mean value, the measurement was made more sensistive by amplifying the difference between the hot wire voltage and an accurately determined bucking voltage. The amplified signal was digitized by means of a shaft encoder attached to a Speedomax self-balancing potentiometer, and the digitized output was

punched on IBM cards, along with a digital signal proportional to the probe transverse position.

The bucking voltage and the amplification of the signal, for each of the five currents, were adjusted so that the speedomax recorder reading varied approximately between 25% to 75% of its full range as the hot wire traversed across the wake at any axial location. The difference between the hot wire voltage and the bucking voltage was amplified by a Beckman amplifier and was recorded on an XY recorder.

The output of the thermocouple on the tip of the hot wire support was amplified in order to read the temperature directly in ^{o}C on a digital voltmeter, and the reading was also punched on the cards. The linear, output versus temperature, relation assumed in such a setting did not result in an error for the support temperature of more than a fraction of a degree. The last 10 columns of the IBM card were used for identification, such as run number, date, and sequence of cards.

The automatic sequencing and recording was controlled by the Datex control unit. The sequence of events in a typical run, after noting the five hot wire currents, the five bucking voltages, and the corresponding settings of the signal amplification, was as follows:

a) Probe was moved to a position and the position reading punched on the IBM card.

b) The highest current was passed through the hot wire and, after some time delay to allow for equilibrium to be attained, the digitized output of the Speedomax recorder was punched on the IBM

card and also point plotted on the XY recorder.

c) The remaining four currents were used in sequence, as in (b) above, with the exception that no analog recording was made.

d) Following the hot-wire output for the lowest current, the support temperature was punched on the IBM card, followed by the identification number in the last 10 columns.

The sequence was repeated for each point in the profile.

The five currents, the five bucking voltages and the amplification factors were measured again at the end of the run, and the mean of the values before and after the run were used for data reduction. In each case, these values were found to agree within $\pm$ 0.5%.

III. DATA REDUCTION

III. 1. Corrections for Flow Gradients in Empty Tunnel

Since Behrens[16] and Batt[21] have shown that the maximum variation of the free stream static pressure in the region of interest was less than 2%, no corrections were applied to the measured data to take account of these gradients. However, the variation of free stream Mach number with tunnel stagnation pressure was taken into account.

III. 2. Pitot Pressure Correction

On the basis of the results of Dewey[15] which indicate no measurable influence on the Pitot pressure measurements for angles of attack less than 12°, no corrections for this effect was applied for any of the Pitot pressure data, since the maximum flow inclination in the near wake, except in the recirculating region, is $\simeq 14^{\circ}$.

Viscous corrections to measured Pitot pressure data at low Reynolds numbers have been studied by Homann,[23] Sherman,[24] Potter and Bailey,[25] Sedov, Michailova and Chernyi,[26] Schaaf[27] and others. But none of these consider the corrections in the Mach number range 0.7 to 1.7. Since viscous correction to measured Pitot pressure was found to be necessary in a considerable portion of the near wake flow, it was felt desirable to include the viscous correction in the mean-flow data reduction program. In order to do this it was first necessary to make plausible estimates to the corrections in the Mach number range 0.7 to 1.7 consistent with the corrections known experimentally in the rest of the Mach number range. It was also considered necessary that the corrections should vary smoothly as the Mach

number changes from subsonic to supersonic values. With this in mind an empirical formulation for the Pitot pressure corrections at low Pitot tube Reynolds numbers, agreeing closely with the experimental results, was developed. The details of this formulation are discussed in Appendix B. The formulation is based on the idea that the corrections to the measured Pitot pressure data at supersonic Mach numbers may be considered to be made up of two parts, the first being the loss in Pitot pressure caused by the curvature of the shock in front of the Pitot tube as indicated by Sedov et al.[26] and the second being the viscous correction associated with the subsonic flow behind the shock. For lack of any experimental data close to Mach number 1, an analytical expression fitted to match Sherman's subsonic results[24] was assumed to be valid up to Mach number 1. For supersonic flow, the same result was used for the correction due to the viscous subsonic flow after the shock, by taking the Reynolds number based on flow quantities after the shock. This was then subtracted from the overall corrections to the measured Pitot pressure given by the experimental results of Potter and Bailey[25] to obtain the corrections due to shock curvature and other effects. An analytical expression to match these corrections associated with the shock, as functions of Mach number and Reynolds number, was then obtained.

The Pitot probe (Fig. 3) used in most of the regions was 0.008 in. by 0.051 in. outside dimensions, an aspect ratio of more than 6. The probe used for measuring the centerline reverse flow Pitot pressure, shown in Fig. 5 is in fact two-dimensional. Hence it was thought that the corrections based on a two-dimensional probe

would be more appropriate than that based on the three-dimensional probe. Unfortunately no experimental data are available on the Pitot pressure corrections for two-dimensional probes. However, the theoretical analysis of Homann[23] for subsonic flow shows that, for the same tangential velocity gradient at the stagnation point at the edge of the boundary layer, the corrections for a two-dimensional probe are half the corrections for a three-dimensional probe. From the theoretical analysis of Sedov et al.[26] for the corrections due to shock curvature, it is again seen that for the same shock curvature the corrections for a two-dimensional shock is half that for a three-dimensional shock. It is expected that for a two-dimensional probe the shock radius of curvature would be at least as much as that for a three-dimensional probe of the same lateral dimension. Since the corrections, if anything, reduce as the radius of curvature increases, it is reasonable to assume that the corrections for a two-dimensional probe is half that of a three-dimensional probe. Therefore, the Pitot pressure corrections for the probes used in the present set of measurements were taken to be half that of the corrections for the three-dimensional probes whose experimental data have been used in the empirical formulation. The expressions for the correction factors are given in Appendix B.

The viscous corrections to the measured Pitot pressures at $x/D = 1.75$ and 2.0, for the adiabatic model at $Re_{\infty, D} = 0.905 \times 10^4$, shown in Fig. 10, were chosen for illustration, since the local Reynolds number was minimum for the adiabatic case at $Re_{\infty, D} = 0.905 \times 10^4$ and since the Mach number varied from low subsonic to supersonic

values. The variation of $(PP_m - PP_i)/PP_i$ across the wake, shown in Fig. 10 illustrates that this correction does not necessarily decrease with increase of Reynolds number, though $(PP_m - PP_i)/\rho u^2$, for subsonic flow, varies roughly as the inverse of the Reynolds number, since $\rho u^2/PP_i$ increases with Mach number up to $M = \sqrt{2}$. The maximum correction was of the order of 10%.

III. 3. Viscous Correction to Measured Static Pressure

On the basis of the results obtained by Behrens[16] for viscous corrections to the measured static pressure, the maximum correction to the measured static pressure in the present investigation was found to be less than 2%, and since the accuracy of measurement was of the same order, no correction was applied.

III. 4. Hot-Wire Raw Data Reduction

Hot-wire raw data reduction has been described by Dewey,[15] Behrens,[16] and Batt.[21] However, a brief description is given here.

Hot-wire raw data reduction consisted of calculating, for the finite hot wire used, the mean recovery temperature (T_{awm}), and the product of the Nusselt number and thermal conductivity of air corresponding to the local stagnation temperature of the flow ($Nu_m K_t$) using the following data:

a) the calibration of the hot-wire ;

b) the values of the five currents used and the corresponding settings of the bucking voltage and the amplification factors;

c) the amplified, punched output of the difference between the hot-wire voltage and the bucking voltage.

The hot-wire voltage for a particular current was obtained by dividing the output by the appropriate amplification factor and adding the bucking voltage, and the hot wire resistance was obtained by dividing the hot-wire voltage by the current. In this manner the hot-wire resistance R_{hw} and the heat loss to the flow I^2R_{hw} was found for each of the five currents. A straight line fit, with least square error, for R_{hw} versus I^2R_{hw} was used to obtain the adiabatic wire resistance (R_{awm}) at I = 0 and the slope ($d R_{hw}/d I^2R_{hw}$). The adiabatic recovery temperature of the hot wire (T_{awm}) corresponding to R_{awm} was obtained using the resistance calibration of the hot-wire, $R_{hw} = R_r\{1 + \alpha_r(T_w - T_r)\}$.

Nu_m, the measured Nusselt number is defined as

$$Nu_m = \frac{h_m d}{K_t}$$

where d = diameter of the hot wire

K_t = thermal conductivity of air at the local stagnation temperature of the flow

h_m = average measured heat transfer coefficient

$$= \frac{I^2 R_{hw}}{\pi d \ell (T_w - T_{awm})}$$

$$= \frac{R_r \alpha_r}{\pi d \ell} \quad \frac{I^2 R_{hw}}{(R_{hw} - R_{awm})} = \frac{R_r \alpha_r}{\pi d \ell (\text{slope})}$$

ℓ = length of the hot wire

T_w = mean temperature of the wire at the current I

T_{awm} = mean recovery temperature of the wire (i.e. T_w at I = 0)

R_{hw} = resistance of the hot wire at the current I

$$\text{slope} = \frac{d R_{hw}}{d I^2 R_{hw}}$$

R_r = reference resistance of hot wire at I = 0 and 0^oC

α_r = coefficient of thermal resistance of hot wire

Therefore $Nu_m K_t = h_m d$ could be calculated.

III. 5. Hot Wire End Loss Correction

The calculation of mean flow quantities by means of hot wire anemometry is based on the correlation of dimensionless quantities such as the recovery factor and Nusselt number for an infinite hot wire in terms of the Mach number and Reynolds number. Therefore, the measurements made with a hot wire of finite length must be corrected for the heat loss to the supports in order to obtain equivalent infinite wire values.

Dewey[15] formulated these end loss corrections, by analyzing the conduction of heat from a finite wire, kept in a uniform flow with uniform temperature, to its end supports maintained at temperature T_s. He assumed that the thermal conductivity of the wire remained constant and that the electrical resistance varied linearly with temperature. His results have been used in applying the end-loss correction to the present set of data. His results are

$$T_{aw*} = \frac{(T_{awm} - T_s)\,\omega_0}{1 - \omega_0}$$

$$Nu_* = \psi_n\, Nu_m$$

where

$$\omega_0 = \frac{\tanh \nu_0}{\nu_0}$$

$$\nu_0 = \frac{\ell}{d}\sqrt{\frac{Nu_* K_t}{K_w}}$$

$$\psi_n = (1-\omega_0)\left[1 + \frac{\alpha_n(T_s - T_{awm})\left\{(2\omega_0-1)\omega_0 - \frac{1}{\cosh^2 \nu_0}\right\}}{2\{1 + \alpha_n(T_{awm}-T_r)\}(1-\omega_0)^2}\right]$$

The expression for the Nusselt number end loss correction factor ψ_n given here is that derived by Behrens[16] as a corrected version to the one formulated by Dewey.[15] It is seen that T_{aw*} and ψ_n are functions of $Nu_* K_t$ and hence an iteration procedure is necessary to find T_{aw*} and $Nu_* K_t$.

The procedure is briefly as follows:

1) Assume ψ_n
2) Then $Nu_* K_t = \psi_n Nu_m K_t$
3) Find $\nu_0 \rightarrow \omega_0 \rightarrow \psi_n$.
4) Go to step (2) if ψ_n is not converged.
5) When ψ_n converges, find $Nu_* K_t$, and T_{aw*}

Batt[21] included these end-loss corrections, directly in the mean flow calculations. However, it was felt that it was better to carry out the end-loss corrections independently and then use the corrected infinite wire values in the mean flow calculations for the following reasons. First, the programs become simpler. Second, information on the infinite wire temperature in the reverse flow region is obtained, though the mean flow properties in that region are difficult to find for a number of reasons. As stated in the next section, the T_{aw*} for

low Mach numbers is nearly equal to T_t, the total temperature, and hence we would get information on the total temperature distribution, which would otherwise be lost if the end-loss program and mean flow program are combined.

III. 6. Mean Flow Calculations

III. 6. 1. Procedure Used in the Present Study

The mean flow quantities were obtained using the following data:

a) the Pitot pressure;

b) the static pressure, assumed constant across the wake and equal to the measured value on the centerline;

c) the infinite wire recovery temperature obtained after end-loss correction to the hot-wire data;

d) correlation of the infinite wire recovery factor ($\eta_* = T_{aw*}/T_t$), with Mach number and Reynolds number.

Correlation of infinite-wire recovery temperature with Mach number and Reynolds number.

Dewey,[15] by combining the data of several investigators with his own measurements, found that a single curve could satisfactorily describe the variation of the normalized recovery factor, $\bar{\eta}_* = (\eta_* - \eta_e)/\eta_f - \eta_c)$ with Knudsen number from continuous flow to free molecular flow. This correlation of $\bar{\eta}_*$ with Kn has been used in the present calculations. η_c, the recovery factor for continuum flow, varies from 1.0 for M = 0 to 0.95 for M = 2.0 and remains the same for higher Mach numbers. η_f, the recovery factor for the free molecular flow, is given by $\eta_f = (f_1/g_1)/(1 + \frac{\gamma-1}{2} M^2)$, where f_1 and g_1

are functions of the molecular speed ratio $M\sqrt{\gamma/2}$. η_f tends to 1.0 at M = 0 and increases asymptotically to 1.166 as M increases to infinity. Thus, near M = 0 both η_f and η_c tend to 1.0 and hence η_* would also be close to 1.0. Therefore T_{aw*} would be close to T_f in the low Mach number regions such as the recirculating region, as indicated earlier. The variation of η_c vs. M, g_1 and f_1 vs. $M\sqrt{\gamma/2}$, and $\bar{\eta}_*$ vs. Kn were given in the form of tables in the mean flow program.

Details of the calculation.

The Pitot pressure vs. Y/D, the static pressure on the centerline, and the infinite-wire recovery temperature T_{aw*} vs. Y/D, at any desired X/D location were read into the computer (IBM 360/75). Correlation data on η_f vs. M, η_c vs. M, and $\bar{\eta}_*$ vs. Kn, were also read into the computer in the form of tables. Since Pitot pressure and hot-wire measurements were made separately, the Y/D locations of the two measurements were not the same, and hence the Pitot pressure data were interpolated to correspond to the same Y/D locations as the hot-wire data.

The iteration scheme needed for calculating the mean flow quantities is given below:

a) Assume $\eta_* = \eta_{*1}$ say.

b) Assume $PP = PP_m$, the measured Pitot pressure.

c) Find $T_t = \eta_{*1}\ T_{aw*}$.

d) Find M from P/PP

e) Knowing M, PP, and T_t any flow quantity can be calculated and thus viscous correction PP_m/PP_i and Kn are calculated.

(See Appendix B for viscous corrections).

f) Find $\overline{\eta_*}$, η_c and η_f corresponding to the mean flow quantities calculated.

g) Find $\eta_* = \eta_{*2}$ from $\eta_* = (\eta_* - \eta_c)/(\eta_f - \eta_c)$

h) Find PP_i knowing PP_m and PP_m/PP_i

i) Check η_{*2} and PP_i with the initially assumed η_{*1} and PP. If they satisfy the convergence criterion, then the calculated flow quantities are written out and punched.

j) If convergence is not satisfied, take $PP = PP_i$ and $\eta_{*1} = \eta_{*2}$ and go to step c) andcontinue the iteration until convergence is obtained. (Convergence was generally obtained within about 4 to 5 iterations.)

It may be pointed out that the $Nu_* K_t$ data, available from the hot wire measurements after end-loss correction, have not been used in the mean flow calculations by the above procedure. Therefore a correlation of Nu_* with Mach number and Reynolds number could also be obtained from these calculations.

III. 6. 2. Other Procedures for Mean Flow Calculations

In Section III. 6. 1 the mean flow calculations are based on Pitot pressure, static pressure and T_{aw*} data. Since $Nu_* K_t$ data would always be available from hot-wire measurements, it is also possible, at least in principle, to obtain the mean flow quantities using either T_{aw*}, $Nu_* K_t$ and Pitot pressure data or T_{aw*}, $Nu_* K_t$ and static pressure data. For ease of reference, let us call the mean flow calculations based on Pitot pressure, static pressure, and T_{aw*} data as

in Section III. 6. 1 as procedure (a), that based on T_{aw*}, $Nu_* K_t$, and Pitot pressure as procedure (b) and that based on T_{aw*}, $Nu_* K_t$ and static pressure as procedure (c). For procedures (b) and (c) correlation of both Nu_* and T_{aw*} with Mach number and Reynolds number are needed. The correlation of T_{aw*} with Mach number and Reynolds number has already been described in Section III. 6. 1. The correlation of Nu_* with Reynolds number for various Mach numbers from zero to high supersonic values were obtained by Dewey[15] after a comprehensive review of data from various sources. Since the assumption of constant static pressure across the wake, used in Section III. 6. 1, is definitely valid at least over a narrow region close to the centerline, the mean flow data obtained over that region from procedure (a) could be taken as correct, and since $Nu_* K_t$ data were also available, Nu_* could be calculated and a correlation of Nu_* with Reynolds number and Mach number could be obtained. Results of such a correlation are shown in Fig. 11 along with Dewey's results. It is seen that the two correlations agree reasonably well for subsonic Mach numbers, but the correlations for supersonic Mach numbers are somewhat different. The discrepancy in the two correlations may perhaps be caused by inaccuracies in the determination of wire conductivity and wire aspect ratio because of measurement difficulties. Using the correlation of Nu_* with Reynolds number and Mach number obtained from the present investigations, an attempt was made with procedure (b) to extend the mean flow data to the regions where static pressure could not be assumed equal to that on the centerline. The iteration scheme for procedure (b) is as follows:

a) Assume η_{*1}.

b) Assume PP = PP_m, the measured Pitot pressure.

c) Find $T_t = \eta_{*1} T_{aw*}$.

d) Find K_t corresponding to T_t and hence Nu_*.

e) Assume M the Mach number.

f) Find $Re_{t,d}$ from M, PP and T_t - say = $(Re)_1$

g) Find $Re_{t,d}$ from the infinite wire Nu_*-Re correlation corresponding to that M - say = $(Re)_2$

h) If $(Re)_1$ and $(Re)_2$ do not agree within the convergence criteria, change Mach number and go to step (f) and repeat until convergence is obtained.

i) Then from converged M, PP and T_t viscous correction to Pitot pressure PP_m/PP_i, $\bar{\eta}_*$, η_f and η_c can be calculated and hence η_{*2} can be found.

j) Check for convergence of PP and PP_i, and η_{*1} and η_{*2}. If converged find all the mean flow quantities required. Otherwise take $\eta_{*1} = \eta_{*2}$ and PP = PP_i and go to step (c) and repeat the iteration.

Typical Mach number distribution obtained by procedure (b) is shown in Fig. 12, along with the results obtained from procedure (a) described in Section III. 6. 1. In view of the fact that the Nu_* - M - Reynolds number correlation obtained from the results of procedure (a) have been used in procedure (b), the agreement over the center region is reassuring. However, the Mach number distribution over the other regions obtained from procedure (b) shows considerable scatter.

Fig. 13 shows a comparison of the static pressure distribution obtained from procedure (b) with the measured static pressure distribution. Though the measured static pressure distribution might be somewhat in error in the shear layer region and the wake-shock region because of probe interference and flow inclinations, the trend for the static pressure to decrease away from the centerline is at least qualitatively correct from the general stream line curvatures in that region. The static pressure obtained from procedure (b) shows considerable scatter and there is absolutely no agreement with the measured data.

The scatter in the mean flow data obtained from procedure (b) may possibly be caused by some mismatch in the Pitot pressure and hot-wire data which were taken separately, and also possibly due to the extreme sensitivity of the results to small errors in the input data, when the correlation of Nu_* with Reynolds number and Mach number is used for mean flow calculations. Therefore, procedure (b) was considered unsatisfactory for mean flow calculations for the present investigation. It was further felt that the mean flow calculations of procedure (c) using hot-wire data and the centerline static pressure data would also be unsatisfactory, since Nu_* correlation with Reynolds and Mach number, which make the results very sensitive to slight errors in input data, has to be used even in this case.

III. 7. Accuracy Estimates

The accuracy estimates given below refer mostly to the measurement accuracy and no quantitative estimates could be made for errors caused by extraneous factors, such as say non-two-dimensionality effects in spite of the optimum end devices used, the frost buildup

on the model, etc. It is, however, believed that the errors due to these extraneous factors are small.

a) Positioning

In order to eliminate the mechanical backlash effects, all vertical and axial positionings of a probe were carried out by moving the probe upward and forward respectively. The traverse mechanism had an accuracy of 0.001" in both axial and vertical settings. The use of electrical contact of the probe with the model, for reference, permitted repeatability of the axial settings to within 0.002". For measuring the centerline static pressure, the probe was traversed in the vertical direction around the centerline and the centerline determined from the hump in the pressure distribution. After thus locating the probe on the centerline of the wake, the final reading was taken on the silicon micromanometer. This was particularly needed in the neck region and it is estimated that the probe was located to within ± 0.002" of the center of the wake.

b) Pitot Pressure Measurements

The measured Pitot pressure outside the recirculating region is estimated to be accurate to within ± 1%. Since the probe interference of the looped Pitot pressure probe is unknown, it is hard to estimate the accuracy of the Pitot pressure measurement on the centerline in the recirculating region. It is expected, however, that away from the rear stagnation point and close to the base the measured values are reasonably accurate. The final Pitot pressure data, after taking into account the viscous corrections, are expected to be accurate to ± 2% in most of the regions.

c) Static Pressure Measurements

The repeatability of the static pressure measurement was within ± 2%. As mentioned earlier, no viscous correction to the measured static pressure was applied, as the correction was found to be at most 2%.

d) Base Pressure Measurement

Base pressure data were taken using the silicon micromanometer with the Pitot pressure probe positioned within 0.002" of the base on the centerline. The results of Collins[20] for the interference of the probe on the base pressure measurement is made use of in correcting the measured base pressure in the present investigation. The base pressure being very small in magnitude, the measurement accuracy is expected to be of the order of 5% only.

e) Hot Wire Measurements

The variation in R_r and α_r before and after the run was less than 2%. The resistance measurement at zero current, taking a linear extrapolation of R vs. I^2R is expected to be accurate to ± 0.02 ohms. The overall accuracy in the measurement of T_{awm} is estimated at ± 3°K. It is hard to estimate accurately the error associated with the end-loss correction and the correlation of the infinite wire data, on the final total temperature. A rough estimate is that the total temperature may be in error by as much as ± 5°K.

f) Errors as a Result of the Matching of Pitot Pressure and Hot-Wire Data:

Since Pitot pressure data and hot-wire data were not taken simultaneously, it was necessary to match the two profiles at any x/D

station in order to obtain mean flow properties. It was noticed that when the shocks were matched the center bucket region was not very well matched. This was caused by the fact that the profiles were not quite repeatable in the central region, although beyond the shocks the profiles were quite repeatable. The deficit region was found to shift between tests by about ± 0.004" (±0.02 D) for the cold model at $Re_{\infty, D} = 2.95 \times 10^4$ and by about ± 0.002" (± 0.01 D) for the other cases. Naturally, the midpoint of the shocks did not agree with the center of the deficit region. Since the profiles beyond the shocks were steady, it was decided that the profiles of the Pitot pressure data and the hot wire data should be matched so that the shock locations agreed, and the bucket region was shifted to be symmetrical with respect to the shocks. Such shifting was necessary, as otherwise the mean flow properties obtained from the mismatched Pitot and hot-wire data would be spurious and erroneous. The error committed by shifting and matching is considerably less than it would be otherwise.

g) Mean Flow Calculations

From a few static pressure traverses made, it was clear that the error made in the static pressure by assuming static pressure constant across the wake was less than 10%. Since the Pitot pressure data are estimated to be accurate to ± 2% in most of the regions, the resulting Mach number can be expected to be accurate to about 5%. Since the total temperature is accurate to within ± 5°K which is about 1% for the adiabatic models and about 2% for the cold models, taking uncertainty in M of 5%, the uncertainty in the static temperature would be about 6% and uncertainty in the velocity would be about 8%, and

uncertainty in mass flux would be about 5%. In view of the fact that interference of the looped Pitot pressure probe on the measurement of the Pitot pressure of the reverse flow is not known, no definite estimate of the accuracy of mean flow calculations of the reverse flow can be made.

IV. RESULTS AND DISCUSSION

IV. 1. Pitot Pressure

The measured Pitot pressure profiles are shown in Figure 14. The general picture for all the cases is similar. However, the separation shock is not as well defined for the adiabatic model for the low Reynolds number case. The narrowing of the width of the wake with cooling and with increasing Reynolds number can be easily noticed. For the adiabatic model, at $Re_{\infty, D} = 0.905 \times 10^4$, the separation shock and the wake shock merge with one another, whereas they are distinct for the other cases, and further, this distinction between the two seems to be enhanced with increasing Reynolds number and with cooling.

These profiles have been used to determine the separation shock, wake shock and the shear layer edge in the near wake. Because of the interaction of the oblique shock wave with the subsonic region behind the bow shock on the probe, the Pitot pressure profiles exhibit considerable width even for a thin shock wave. Therefore, the location of the shock wave was assumed to be the mean of the intersections of the vertical lines at the maximum and the minimum of the measured Pitot pressure profiles with the maximum gradient of the profiles between them. In some cases, such as determining the separation shock for the adiabatic model at $Re_{\infty, D} = 0.905 \times 10^4$, where there were no maximum and minimum in the Pitot pressure distributions, the mean of the locations of the kinks was assumed to be the location of the shock. The shear layer edge was assumed to be given by the intersection of the maximum slope of the Pitot pressure profile in the

center bucket with the maximum measured value. The location of the shock and the shear layer edge as determined from the opposite sides of the profiles agreed within 0.02 Y/D, and these will be discussed later.

The centerline Pitot pressure distribution is shown in Figure 15. This is essentially a crossplot of Figure 14, except that close to the base the measurements made on the centerline using silicon micromanometer have been used. The pressure measured by the standard probe (Figure 3), when its tip was located close to the base with a gap of the order of 0.002" was taken to be the base pressure. The silicon micromanometer was used for this measurement also.

From the investigations of Behrens,[16] it is known that the near wake is laminar for the adiabatic model at both $Re_{\infty, D} = 0.905 \times 10^4$ and 2.95×10^4. Since the behavior of the Pitot pressure distribution for the cooled model at $Re_{\infty, D} = 0.905 \times 10^4$ is very similar to that for the adiabatic model, the wake is taken to be laminar for this case also. However, the distribution for the cooled model at the higher Reynolds number departs from the other cases in a manner typical of transition. It was found during measurements that, for this case, there was considerable variation from run to run and the measurements were not very repeatable. This unsteadiness was perhaps a result of the movement of separation point on the cylinder due to frost buildup and breaking-off of the model, coupled with transition effects. Therefore, scatter in the measured data for this case was considerably more. Because of this transition at the higher Reynolds number, for the cold model, comparison of the results of the adiabatic and

cooled models are relevant only for the lower Reynolds number case.

IV. 2. Static Pressure

The centerline static pressure distribution is shown in Figure 16. The base pressure was obtained by the standard Pitot probe kept close to the base with a gap of the order of 0. 002 in., as already mentioned. It can be noticed from Figure 16 that the peak in the static pressure is higher and closer to the model for the cold cases, compared to the adiabatic cases. The location of the static pressure peak is a good indication of the wake-neck location, and it is seen that the wake-neck moves closer to the model on cooling. The effect of Reynolds number on the neck location is negligible. Effect of Reynolds number on the measured base pressure for the adiabatic model is seen to be negligible from Figures 15 and 16. However, after applying the corrections for probe interference based on Collins'[20] results, it was found that the base pressure increased slightly with Reynolds number agreeing with the trend obtained by other investigators. Figures 15 and 16 also show that the base pressure decreased with cooling. The base pressure for the cold model at $Re_{\infty, D} = 2.95 \times 10^4$, being much less than that for the cold model at $Re_{\infty, D} = 0.905 \times 10^4$ is caused by the transition in the wake at the higher Reynolds number for the cold model. For comparison, it may be mentioned that for a wedge, Batt[21] found that the base pressure decreased with increase of Reynolds number, and with cooling. The base pressure for a wedge is lower than the free stream static pressure, whereas

the base pressure for the cylinder is about the free stream static pressure or even slightly more. Also, the static pressure after re-compression in the neck region of the cylinder wake is nearly three times the free stream static pressure. The overall pressure level in the near wake of a cylinder is considerably higher than that for the wedge because of the blast-wave-like behavior of blunt bodies at hypersonic Mach numbers.

IV. 3. Rear Stagnation Point Location

The rear stagnation point location is defined by the equality of the Pitot pressure and the static pressure on the center line. For this purpose, the Pitot pressure as measured by the standard probe shown in Figure 3 was used. Figure 17 clearly shows the manner in which the rear stagnation point was determined.

The variation of the rear-stagnation point with Reynolds number and cooling will be discussed later when these results will be compared with the results of other investigators.

IV. 4. Centerline Pitot Pressure of Reverse Flow

In order to obtain the mean flow quantities of the reverse flow in the recirculating region, the Pitot pressure of the reverse flow was measured using a looped Pitot probe shown in Figure 5. As discussed earlier in Section II. 3, the measurements were restricted to the centerline only. The results of the measurement are shown in Figure 18. The static pressure distribution of Figure 16, and the location of the rear stagnation point obtained from Figure 17 are also shown in Figure 18, in order to show the magnitude of the interference effects

of the looped Pitot probe near the rear stagnation point. It is seen that the Pitot pressure measured by the looped Pitot probe becomes less than the static pressure, even before the rear stagnation point is reached. In spite of this interference near the rear stagnation point, since the Pitot pressure measurements of the looped Pitot probe do approach the base pressure as the base is approached, it is believed that these measurements could be taken to be reasonably correct at least at x/D = 0.7 and 0.8 for the low Reynolds number cases, and at x/D = 0.7, 0.8, and 1.0 for the higher Reynolds number cases. Therefore in obtaining the centerline distribution of the mean flow quantities, reliance is placed mainly on the data obtained at these points and on the location of the rear stagnation point obtained from Figure 17.

IV. 5. Hot Wire Measurements

The infinite wire recovery temperature variation is shown in Figure 19. These infinite wire values were obtained from the raw hot-wire data after applying end-loss correction as described in Sections III. 4 and III. 5.

Except for the adiabatic model at the higher Reynolds number, the locations of separation and wake shocks cannot be determined accurately from the infinite wire temperature profiles. The positions of the shock as determined by these temperature profiles were generally 0.01 Y/D farther from the centerline as compared to those obtained from Pitot pressure distributions. This may just be caused by the error in the assumption of the shock location within the width exhibited by the pressure and temperature profiles.

The characteristic overshoot of the temperature profiles in the shear layer of the adiabatic models is clearly observed. The cold model profiles do not exhibit such overshoots. In the case of adiabatic models, the edge of the thermal layer was assumed to be given by the intersection of maximum slope beyond the overshoot and the minimum temperature beyond the overshoot. Whereas in the case of the cold models, the edge of the thermal layer was assumed to be given by the intersection of maximum slope of the temperature distribution in the bucket and the maximum temperature. Hence it is probable that the edge of the thermal layer so determined, in the case of adiabatic model, may be closer to the actual edge than that for the cold model. The mean edge of the thermal layer so determined from the top and bottom profiles is discussed later.

IV. 6. Mean Flow Calculations

Using the Pitot pressure data and the infinite wire temperature data, and assuming the static pressure to be constant across the wake and equal to the centerline value, mean flow properties were calculated as described in Section III. 6. 1. The static pressure was assumed to be constant up to the edge of the shear layer. From the Pitot pressure measurements with the normal probe, flow properties in the reverse flow region could not be calculated, since the measured pressure was naturally less than the static pressure. The Pitot pressure measured using the looped probe was used to obtain the centerline reverse flow properties.

i) Centerline Mach Number Distribution

Figure 20 shows the centerline Mach number distribution for the four cases. For the cooled model at $Re_{\infty, D} = 2.95 \times 10^4$, the Mach number beyond the rear stagnation point increases much more rapidly than for the other cases as a result of the transition in the wake for this particular case. The maximum Mach number of the reverse flow on the centerline increases with increasing Reynolds number and with cooling. This maximum Mach number reaches a value as high as 0.6 in the case of the cooled model for the higher Reynolds number. The sonic point on the centerline moves closer to the model with cooling. The effect of Reynolds number on the location of sonic point for the adiabatic model is negligible. For the cold model, the sonic point location at the higher Reynolds number being closer to the model compared to its location at the lower Reynolds number is again a result of transition in the wake at this Reynolds number.

ii) Centerline Velocity Distribution

This is shown in Figure 21, non-dimensionalized with respect to the free stream velocity. The scatter in the data for the cooled model at $Re_{\infty, D} = 2.95 \times 10^4$ is caused by various factors discussed already in Section IV. 1. Just comparing the lower Reynolds number cases, cooling has only a small effect on the variation of the centerline velocity distribution which indicates that the differences in Mach number distribution noted earlier are due to temperature effects. From comparing the results for the two Reynolds number for the adiabatic case, the centerline velocity increases at a slightly faster

rate for the higher Reynolds number case as compared with the lower Reynolds number case.

The maximum velocity in the reverse flow region again increases with increasing Reynolds number and with cooling. It may be observed that the effect of cooling on this maximum reverse velocity is not as much as on the maximum Mach number in the reverse flow region.

iii) Centerline Stagnation Temperature Distribution

The centerline stagnation temperature distribution for both the adiabatic and cooled models is shown in Figure 22. It is seen that the rate of increase of the stagnation temperature along the centerline for the adiabatic model at $Re_{\infty, D} = 0.905 \times 10^4$ is very small and it can almost be considered constant. The slight initial dip in the distribution could not be accounted for. For the higher Reynolds number, the increase along the centerline beyond the rear stagnation point is noticeable though still quite small.

For the cold model, at $Re_{\infty, D} = 0.905 \times 10^4$, the stagnation temperature from X/D = 0.7 up to the rear stagnation point is almost constant and then begins to increase, and considerable temperature defect exists even at X/D = 10 for this case. The stagnation temperature measured upstream of the rear stagnation point is of the order of 0.48 times the free stream stagnation temperature, whereas the model was cooled to 0.19 times the free stream stagnation temperature. It is evident that there is a thin boundary layer on the model base.

The rapid increase of the stagnation temperature beyond the rear stagnation point for the cold model at $Re_{\infty, D} = 2.95 \times 10^4$ is again a result of the transition occurring in the wake for this case. There is considerable scatter in the data for this case, perhaps as a result of the movement of the separation point on the cylinder due to frost buildup and breaking-off of the model, coupled with transition effects. The stagnation temperature is reasonably constant, within the experimental scatter, from X/D = 0.7 up to the rear stagnation point for this case also and it is about 0.5 times the free stream stagnation temperature. A thin boundary layer on the base is evident in this case also.

The results of Zakkay and Cresci[28] on the near wake of a slender cone also show that the stagnation temperature on the centerline is nearly constant up to the rear stagnation point except for a thin layer on the base. Since Batt[21] could not make any temperature measurements in the recirculating region of the wedge, for reasons already stated, the presence of a thin thermal layer on the base was not evident from his experiments.

The temperature at the rear stagnation point of sharp cones and wedges, for the same wall temperature, have been found to be about the same by many investigators (for example Batt,[21] Muntz and Softley[29]). The temperature at the rear stagnation point for wedges and cones for a wall temperature of 0.2 times the free stream stagnation temperature (T_o), is about 0.3 T_o. However, Muntz and Softley[29] found that the temperature at the rear stagnation point increased with increasing nose bluntness and for a 0.3 nose bluntness,

9^{o} sphere cone at M = 12.8, the temperature at the rear stagnation point was about 0.6 T_o for a wall temperature of about 0.27 T_o. Since, in the present investigation, we have found the temperature at the rear stagnation point of a cylinder cooled to 0.2 T_o is about 0.5 T_o, it appears that the bluntness of the body affects the temperature at the rear stagnation point (which generally corresponds to the maximum static temperature in the wake) more than the two-dimensional or three-dimensional nature of the body.

The fact that, in the reverse-flow region behind the cooled models, the stagnation temperature on the centerline is constant and equal to that at the rear stagnation point, except very close to the base, indicates that there is very little conduction in the fluid in the recirculating flow and that the heat is mostly convected in this region.

iv) Centerline Static Temperature Distribution

The centerline static temperature distribution is a direct consequence of the stagnation temperature distribution and Mach number distribution and is shown in Figure 23.

For the adiabatic model, since the variation of the stagnation temperature is small, whereas the Mach number increases as one proceeds downstream, the static temperature decreases as one proceeds downstream of the rear stagnation point.

For the cold model, the variation of the stagnation temperature and the Mach number happens to be such that the static temperature is nearly constant at four times the free stream static temperature except close to the base, where the base boundary layer is evident. Again scatter in data for the cold model at $Re_{\infty,D} = 2.95 \times 10^4$ is noticed because of

the various factors already mentioned.

v) Mach Number Profiles

The transverse variation of Mach number is shown in Figure 24. It should be noted that the origin for different X/D stations have been shifted by a constant amount. In the reverse flow region, the Mach number on the centerline was taken from the faired curves of the centerline Mach number distribution. Dashed curve shows fairing of the Mach number profiles through the point on the centerline. The edge Mach number in all cases is nearly 2.5.

For the adiabatic model at $Re_{\infty, D} = 0.905 \times 10^4$, the Mach number profiles for X/D = 0.7 and 0.8 look reasonable even beyond the separation shock even though the static pressure is assumed constant and equal to that on the centerline indicating that the separation shock is very weak for this case.

This is not the case for the cold models, where the Mach number instead of continuously increasing tends to decrease as one passes through the separation shock. This indicates that the separation shock is of sufficient strength and assuming static pressure across the shear layer to be constant and equal to the centerline value, even beyond the separation shock, is erroneous.

For the adiabatic model at $Re_{\infty, D} = 2.95 \times 10^4$, the profiles do not go beyond the separation shock, but it is likely that the behavior would be similar to that of the cold model.

vi) Velocity Profiles

The velocity profiles are shown in Figure 25. Again, the

values obtained from the faired curves of the centerline velocity distribution have been used for fairing these velocity profiles in the reverse flow region. The u = 0 location was determined from these profiles. It is believed that the location of the u = 0 is determined more accurately by this method than by taking it to be the location where the Pitot pressure is equal to the centerline static pressure, as was done by some previous investigators. Since the Pitot pressure profile cuts the constant static pressure line at a very acute angle, this raises some ambiguity in the exact location of the intersection point. Further, since at u = 0, the velocity is perpendicular to the probe, the basic criteria of the two pressures being equal at u = 0 is incorrect.

The edge velocity is around 0.8 times the free stream velocity in all the cases.

vii) Stagnation Temperature Profiles

The stagnation temperature profiles are shown in Figure 26. Note that the scales for the adiabatic model and the cold model are different. Since for low subsonic Mach numbers the infinite wire recovery temperature is very close to unity for both continuum and free molecular flow, it was felt that the infinite wire recovery temperature shown in Figure 19 would be close to the stagnation temperature in the reverse flow. Therefore, it was felt that the infinite wire recovery temperature distribution shown in Figure 19 could be used in the reverse flow region to represent the stagnation temperature distribution in that region. In Figure 26 the infinite wire recovery temperature distribution in the reverse flow region is shown by dotted

lines. It may be observed that this infinite-wire recovery temperature distribution fairs smoothly into the stagnation temperature distribution outside of the reverse flow region. The stagnation temperature on the centerline obtained from Pitot pressure of the reverse flow, the static pressure and hot wire data on the centerline are also shown by dark dots. It can be seen that these data agree closely with the infinite recovery temperature data on the centerline, confirming our expectation that the infinite wire recovery temperature and the total temperature are nearly equal for low subsonic Mach numbers.

For some cases, the stagnation temperature profiles were extended somewhat into a region where static pressure could not be assumed constant by using the infinite wire temperature data given in Figure 19 and assuming the recovery factor to be the same as that obtained for the end point in the mean flow calculations.

For the adiabatic model, the characteristic overshoot of the total temperature in the shear layer can be observed at both the Reynolds numbers tested. No such overshoot is observed for the cold model. Except for the cold model at $Re_{\infty, D} = 2.95 \times 10^4$, where the behavior is somewhat irregular because of the various causes already mentioned, for all the other three cases the temperature profiles at the axial stations ahead of the rear stagnation point show an off-axis minimum. It was found that the location of the off-axis minimum was close to the location of the dividing streamline, the determination of which would be discussed in the next section. For the cold models, the cold boundary layer separating from the cylinder and the cold base boundary layer flow merges along the dividing stream

line and hence, the minimum stagnation temperature can be expected to be close to the dividing streamline. Since the recovery temperature of the cylinder model for the adiabatic case is about 0.92 times the free stream stagnation temperature, the effect is similar to a cold cylinder and an off-axis minimum for the stagnation temperature occurs for this case also. The recirculating flow gets heated as it flows along the dividing streamline towards the rear stagnation point and returns back to the base along the center. Therefore, the off-axis minimum and a hump around the center region in the total temperature distribution is fully understandable.

IV. 7. Flow Field Structure

The dividing streamline was found in the following manner. Centerline mass flow values obtained from the faired curves of the centerline mass flow distribution shown in Figure 27 were used in completing the transverse mass flow profiles shown in Figure 28. The mass flow profiles in the reverse flow region were assumed to be of the form

$$\rho u/\rho_\infty u_\infty = a_0 + a_1(Y/D)^2 + a_2(Y/D)^4 \qquad \text{and}$$

the coefficients a_1 and a_2 were chosen so that these profiles faired smoothly with the rest of the measured profiles; a_0 was given by the faired centerline value. Though even powers were chosen from the theoretical point of view that the profiles should be symmetrical, the coefficients a_1 and a_2 had to be different for the top and bottom profiles in order to match with the measured profile. The mass flow profiles being thus determined (Figure 28), the $\psi = 0$ location was determined by

integration. The assumed analytical profiles, in most cases, matched so well with the measured profiles that the analytical expression itself was used for determining $\psi = 0$. The locations of $\psi=0$ are also indicated on Figure 28.

It was checked that the Y/D positions of $\rho u = 0$ as given by these profiles agreed well with the Y/D positions of $u = 0$ given by the velocity profiles shown in Figure 25. The mean of the $\psi = 0$ and $u = 0$ locations from the top and bottom profiles have been used in Figure 29.

The separation shock, the wake shock and the shear layer edge as determined from Pitot pressure profiles (Section IV. 1) and the edge of the thermal layer as determined from the infinite wire temperature profiles (Section IV. 5) are also shown in Figure 29.

It is clear from Figure 29 that there is considerable difference between the thermal layer edge and the shear layer edge in all the cases. The difference between the two edges is more for the cold model compared to the adiabatic model. It may be pointed out, for the sake of comparison, that Batt[21] did not make any difference between the shear layer edge and the thermal layer edge in his investigation of the wake behind wedges. In fact he could not find the shear layer edge near the base from Pitot pressure profiles, because of the enormous expansion around the wedge corner, and he took the shear layer edge to be the same as the thermal layer edge found from the temperature measurements. The difference between the thermal layer edge and the shear layer edge is attributed to the fact that the boundary layer on the cylinder is subjected to a much higher favorable pressure gradient compared to that on a wedge and, consequently, the velocity boundary layer becomes thinner compared to the thermal

layer and this is felt in the shear layer as well. The fact that the difference between the thermal layer and the shear layer for the cold model reduces as the wake-neck is approached can again be attributed to the fact that the flow is subjected to an unfavorable pressure gradient as it approaches the neck. For the case of adiabatic model, it should be borne in mind that, because of the temperature overshoot and the manner in which the thermal layer is determined (see Section IV. 5), the difference between the thermal layer and the shear layer might be somewhat exaggerated. The edge of the thermal layer for the adiabatic model at $Re_{\infty, D} = 0.905 \times 10^4$ for X/D less than 1.5 could not be determined since the temperature overshoot was not well defined for these profiles.

It can be seen from Figure 29 that the separation shock and the wake shock merge with one another for the adiabatic model at $Re_{\infty, D} = 0.905 \times 10^4$, whereas they are distinct for the other three cases. For comparison it may be stated that the separation shock and the wake shock merged with one another for the wedge for all cases investigated by Batt.[21]

The shock positions, the thermal layer edges, and the shear layer edges for the four cases have been superposed in Figure 30a for easy comparison. By comparing the thermal layer edges and the shear layer edges for the adiabatic and cold models at $Re_{\infty, D} = 0.905 \times 10^4$, it is clear that cooling reduces the wake width to somewhere between 2/3 to 3/4 of its adiabatic value. Comparing the thermal layer edges and the shear layer edges for the adiabatic model for the two Reynolds numbers, it is seen that the wake width at $Re_{\infty, D} = 2.95 \times 10^4$ is nearly

2/3 to 3/4 of the wake width at $Re_{\infty, D} = 0.905 \times 10^4$. Since transition occurred in the wake for the cold model at $Re_{\infty, D} = 2.95 \times 10^4$, similar statements regarding the effect of cooling at higher Reynolds number, or the effect of Reynolds number for a laminar wake of a cold model, cannot be made apart from just stating that the wake width for this case was the minimum of all the four cases tested.

The variation in the wake shock locations qualitatively correlates with the variation of the shear layer edge for all the cases.

It may be mentioned that the effect of Reynolds number and cooling on the wake width discussed above, for the cylinder, is qualitatively the same as that found by Batt[21] for wedges.

The wake neck for all the cases lies somewhere between X/D = 2.0 to 3.0, the exact location being hard to determine because of the slow variation of the shear layer edge position with distance. However, one can observe the tendency for the neck to move closer to the model with increase of Reynolds number and with cooling. By comparing the X/D locations of the peaks of the centerline static pressure distribution shown in Figure 16 and the shear layer edges shown in this Figure 30a, it seems reasonable to assume that the neck positions are given by the X/D location of the peaks in the static pressure distribution. The trend in the variation of the neck location on this basis with Reynolds number and with cooling is more easily noticeable, and has already been discussed in Section IV. 2.

Figure 30b shows a comparision of the separation shock, $\psi = 0$, and $u = 0$ lines to a larger scale. Except for the adiabatic model at the higher Reynolds number of 2.95×10^4, for which the separation

shock is higher up; for the others, the shock location is nearly the same. The recirculating region lengthens and the rear stagnation point is moved downstream with increase of Reynolds number for the adiabatic model. At the lower Reynolds number for which the near wakes are laminar for both adiabatic and cold models, cooling shifts the rear stagnation point away from the model. However, because of transition in the wake, for the cold model at the higher Reynolds number, the rear stagnation point shifts closer to the model with increase of Reynolds number for the cold model, and with cooling at the higher Reynolds number.

IV. 8. Comparison with the Results of Other Investigators

Figure 31 shows a comparison of the centerline static pressure distribution. There is general agreement, but the base pressure and the peak pressure are lower for the present set of results.

Figure 32 shows the variation of base pressure in terms of free stream Pitot pressure (i. e. the pressure at the forward stagnation point on the cylinder, with Reynolds number based on cylinder diameter and viscosity corresponding to free stream stagnation temperature. The results of Dewey,[15] Herzog,[19] and Collins[20] are also included. Dewey and Herzog measured the base pressure directly using a base tap. Collins[20] measured the base pressure using a Pitot probe, the tip being kept close to the base within a few thousandths of an inch. He corrected for the probe interference, and the corrected base pressure is shown in Figure 32. In the present study also, the base pressure was measured using a Pitot probe, the tip being kept close to the base. No calibration of the Pitot pressure against the pressure measured by a base tap could be made in the

present study because of the hollow model needed for cooling. The uncorrected base pressures obtained in the present study are shown in this figure. Since the experimental conditions of the present study are close to that of Collins, the corrections to probe interference can be taken from his results and applied for the present results. If that is done, the base pressure for the lower Reynolds number is reduced by about 0.5% and increased by about 4% for higher Reynolds number. These corrected values are also indicated. Taking into account the fact that the end devices used by the various investigators are different and that the accuracy of measurement of such low pressures is only about ± 5%, the agreement among the results of the various investigators can be considered to be reasonable.

Figure 33 shows the variation of the location of the rear stagnation point with Reynolds number. The results of the other investigators are also included. The rear stagnation point being somewhat closer to the model for the present investigation compared to the experimental results of the other investigators is consistent with the fact that the base pressures were lower in the present investigations compared to the result of the others.

The difference in the results of Reeves and Lees[3] and that of Klineberg,[5] as pointed out by Collins[20] is due to slightly different approaches adopted by them in their theoretical analysis. Klineberg treats a supercritical separation on the cylinder coupled to the near wake flow, whereas Reeves and Lees consider a fixed separation point.

The results of the cold model are also included in this figure.

The near wake structure obtained from the present set of measurements for the adiabatic model is compared with that obtained by Collins[20] in Figure 34. They agree reasonably well except for the location of the rear stagnation point, which has been discussed already. The u = 0 line of the present results, at $Re_{\infty, D} = 0.905 \times 10^4$, lie somewhat lower than that of Collins'[20] results.

V. SUMMARY OF RESULTS

An experimental investigation has been carried out to determine the mean flow properties for the near wake behind a two-dimensional circular cylinder of 0.2 in. diameter at $M_\infty = 6.0$. Tests were conducted for both the adiabatic and cold model at $Re_{\infty, D} = 0.905 \times 10^4$ and 2.95×10^4. For the cold model tests, the model was cooled to 77°K by an internal flow of liquid nitrogen through the hollow cylinder model.

The main results which have been obtained from this investigation are as follows:

1) Except for the case of the cold model at $Re_{\infty, D} = 2.95 \times 10^4$ for which transition occurred in the near wake, for all the other three cases, the near wake was laminar.

2) The base pressure decreased with cooling. The base pressure for the adiabatic model (after correcting for the probe interference) increased slightly with increase of Reynolds number. For the cold model, because of transition at the higher Reynolds number, the base pressure decreased with increase of Reynolds number.

3) For the adiabatic model, the rear stagnation point moved from $X/D = 1.45$ at $Re_{\infty, D} = 0.905 \times 10^4$ to $X/D = 1.70$ at $Re_{\infty, D} = 2.95 \times 10^4$. At $Re_{\infty, D} = 0.905 \times 10^4$, on cooling, the rear stagnation point moved to $X/D = 1.65$. The rear stagnation point was at $X/D = 1.61$ for the cold model at $Re_{\infty, D} = 2.95 \times 10^4$, and this slight movement of the rear stagnation point towards the model with increase of Reynolds number for the cold case was caused by the transition in the near wake of the cold model at $Re_{\infty, D} = 2.95 \times 10^4$.

4) The location of the wake neck moved towards the model on cooling.

5) The location of the sonic line on the wake center line also moved upstream with cooling. The location of the sonic point for the adiabatic model was hardly affected by Reynolds number and was around $X/D \simeq 3.2$. For the cold model, the location was at $X/D \simeq 2.75$ at $Re_{\infty, D} = 0.905 \times 10^4$ and moved to $X/D \simeq 2.25$ at $Re_{\infty, D} = 2.95 \times 10^4$ because of transition at this Reynolds number for the cold model. For comparison with the wedge data, it may be noted that Batt found that wake centerline became supersonic for all his cases within an axial distance of two base heights.

6) The wake shocks, the shear layer edge and the thermal layer edge moved closer to the wake centerline with increasing Reynolds number and decreasing wall temperature.

7) The separation shocks became stronger with increase of Reynolds number and with cooling. The location of the separation shock was nearly the same for all the cases, except for the adiabatic model at $Re_{\infty, D} = 2.95 \times 10^4$, for which the location was slightly higher than for the others.

8) Batt found that the separation shock coalesced with the wake shock for the wedges for all cases, whereas for the cylinder, this happened for the adiabatic model at $Re_{\infty, D} = 0.905 \times 10^4$ only and for the other cases the wake shock was quite distinct from the separation shock.

9) The shear layer edge was closer to the centerline than the thermal layer edge for all the cases, because of the favorable pressure

gradient acting along the boundary layer on the cylinder prior to separation. This is particularly evident for the cold cases. Further, for the cold cases, the effect of the unfavorable pressure gradient along the shear layer, as the wake neck is approached, tending to bring the shear-layer and thermal-layer edges closer, is also evident.

10) From the centerline total temperature distribution, for the cold model, it was apparent that there was a thin boundary layer on the base of the model. The total temperature was nearly constant between the rear stagnation point and close to the base and approximately equal to 0.5 times the free stream stagnation temperature for the cold models and dropped to the model temperature of 0.19 times the free stream stagnation temperature within the thin boundary layer. For the adiabatic model, at the lower Reynolds number of 0.905×10^4, there was initially a slight decrease in the total temperature below that of the model recovery temperature and then it very gradually started to increase beyond the rear stagnation point. The distribution could almost be considered constant. For the adiabatic model at $Re_{\infty, D} = 2.95 \times 10^4$, the total temperature was constant up to the rear stagnation point and further downstream increased gradually to reach 0.98 times the free stream stagnation temperature at X/D = 10. The fact that the total temperature on the centerline in the recirculating region, except close to the base, is nearly constant indicates that there is very little heat transferred to the recirculating flow by conduction, and most of the heat transfer is by convection.

11) It was found that in the recirculating region, the transverse temperature distribution exhibited a minimum close to the dividing streamline indicating again that the heat transfer process in the recirculating region is mainly by convection, except for the base heat transfer to the base boundary layer.

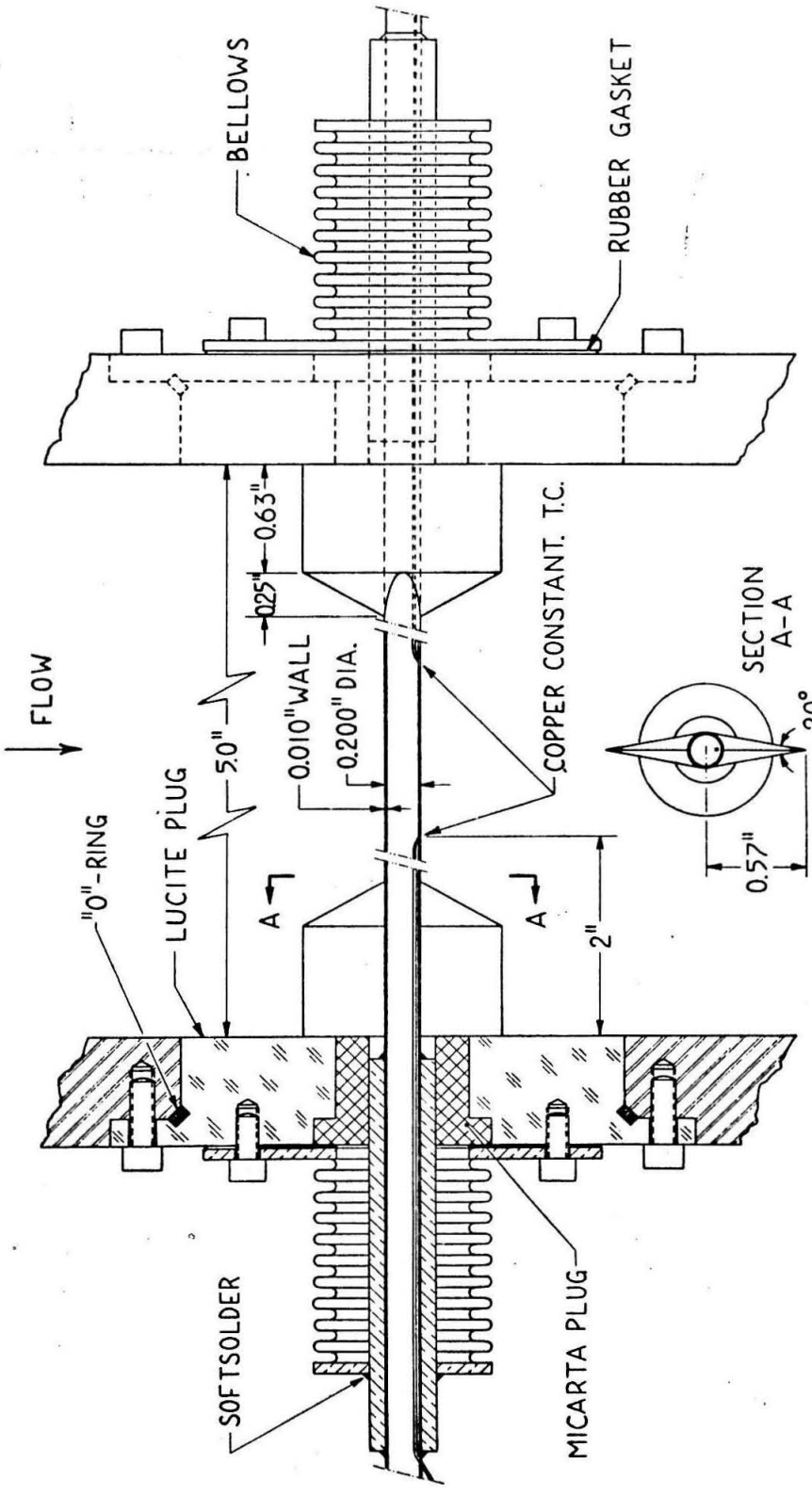
BELLOWS
RUBBER GASKET
0.63"
.025"
FLOW
5.0"
0.010" WALL
0.200" DIA.
COPPER CONSTANT. T.C.
SECTION
A-A
20°
"O"-RING
LUCITE PLUG
A
A
2"
0.57"
SOFTSOLDER
MICARTA PLUG

FIG. I MODEL

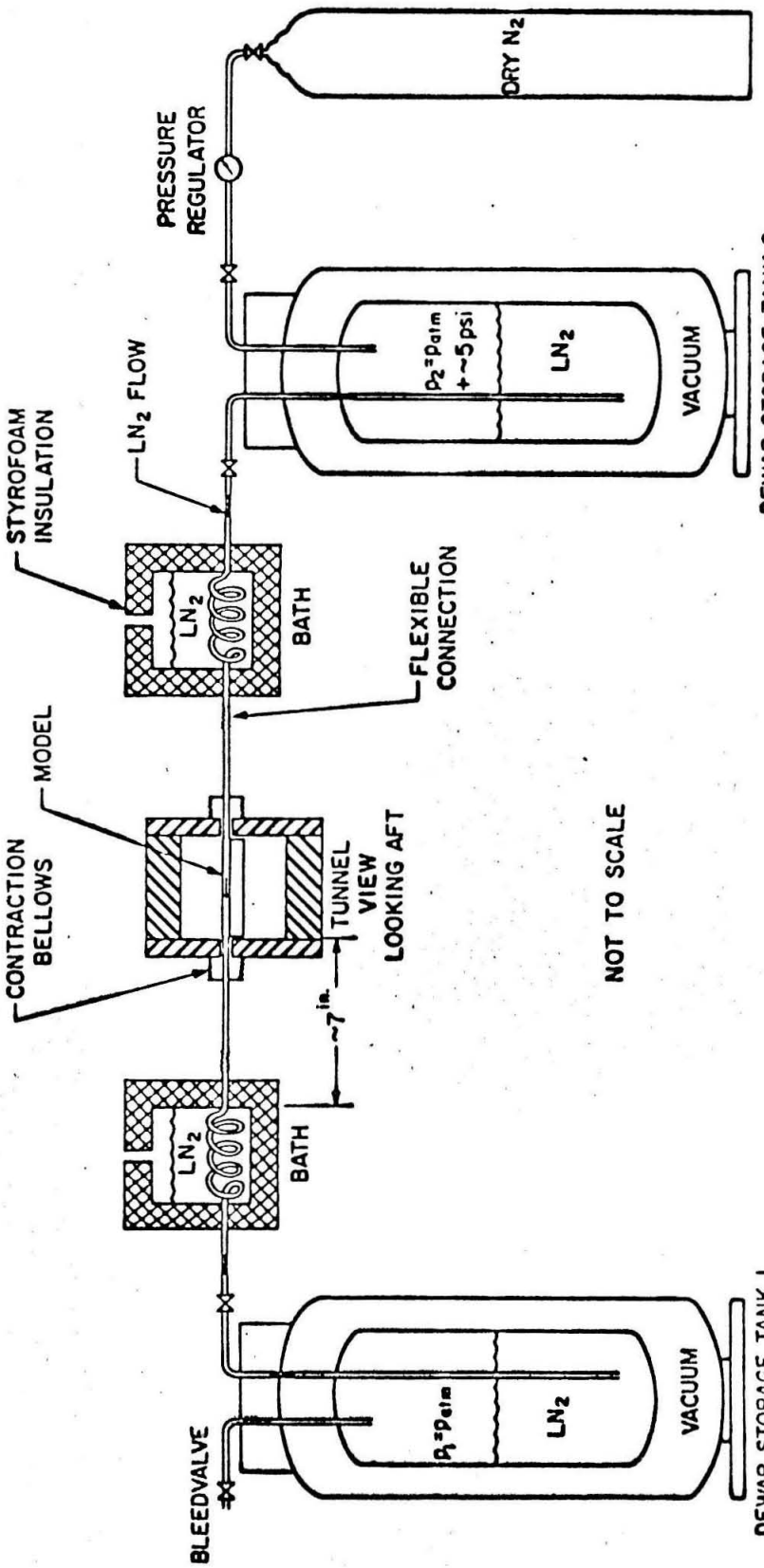

FIG. 2. LIQUID NITROGEN COOLING SYSTEM

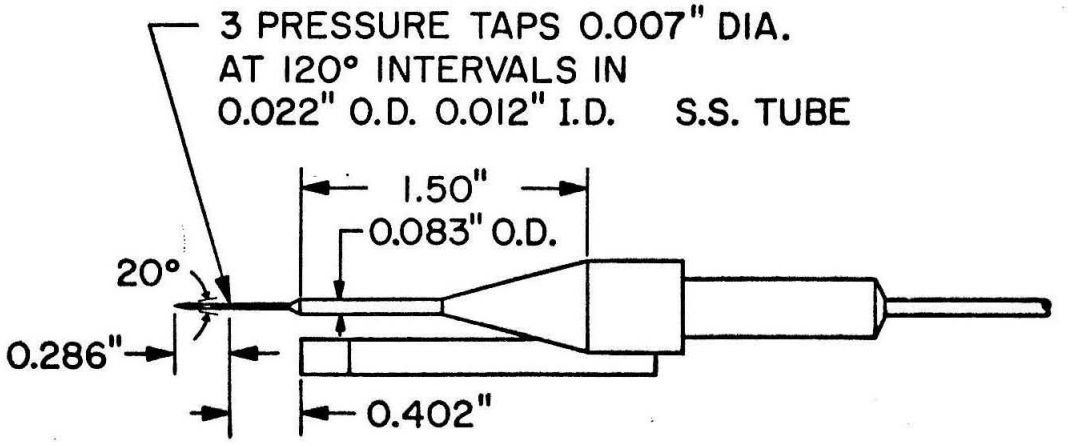

CONE TIPPED STATIC PRESSURE PROBE

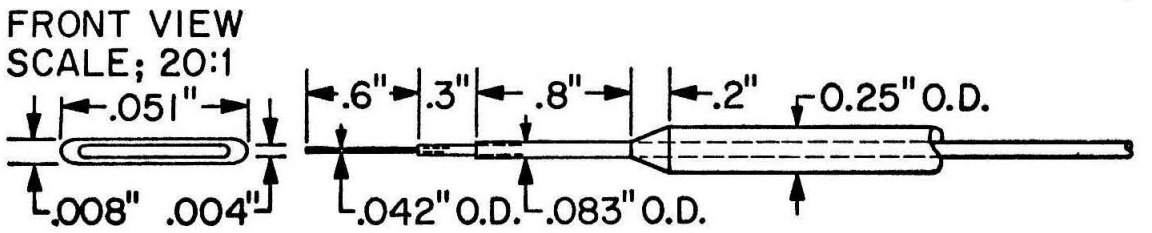

PITOT PRESSURE PROBE

Fig. 3 PITOT AND STATIC PRESSURE PROBES

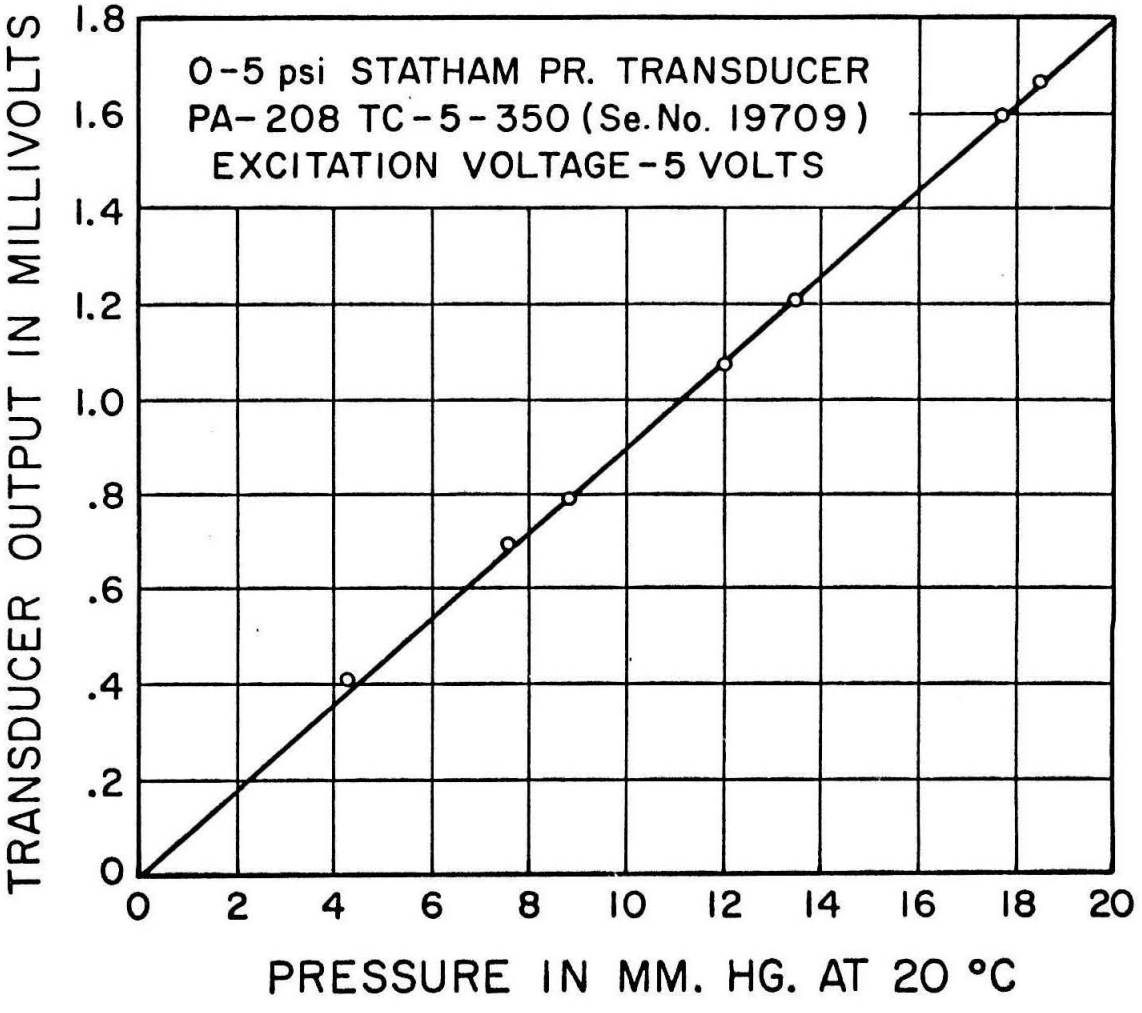

Fig. 4 CALIBRATION OF PRESSURE TRANSDUCER

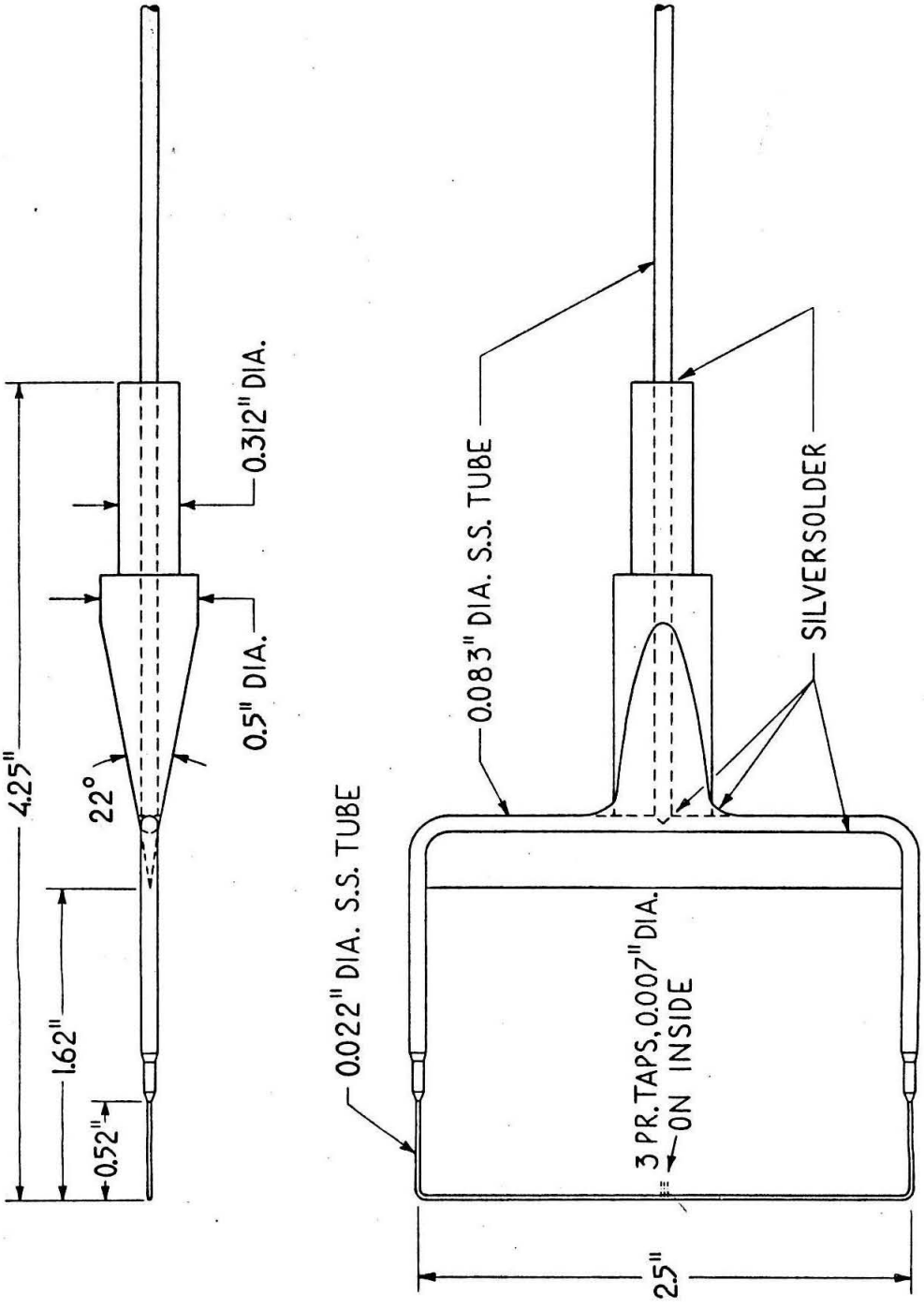

FIG. 5 LOOPED PITOT PRESSURE PROBE

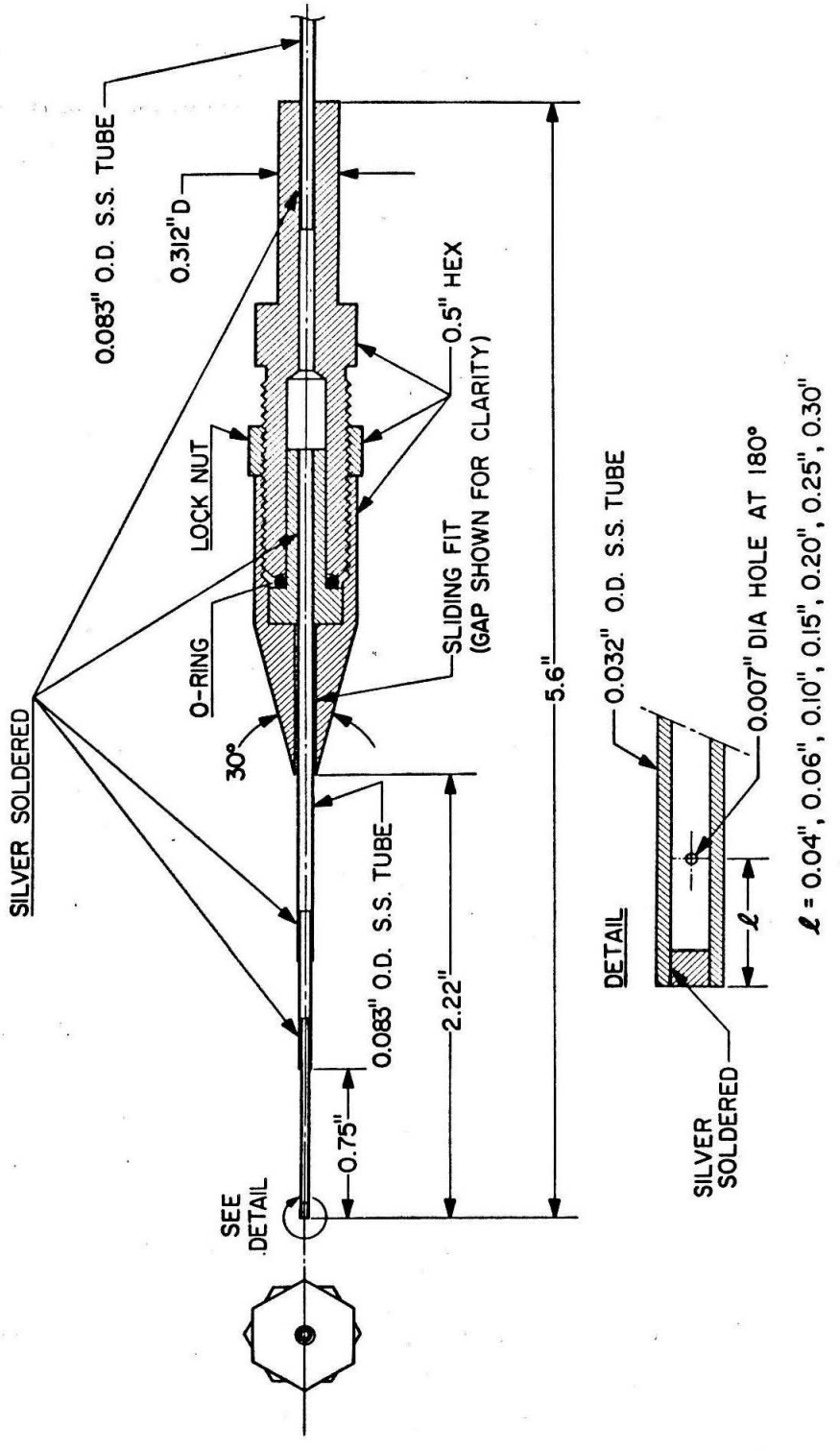

Fig. 6 STATIC PRESSURE PROBE

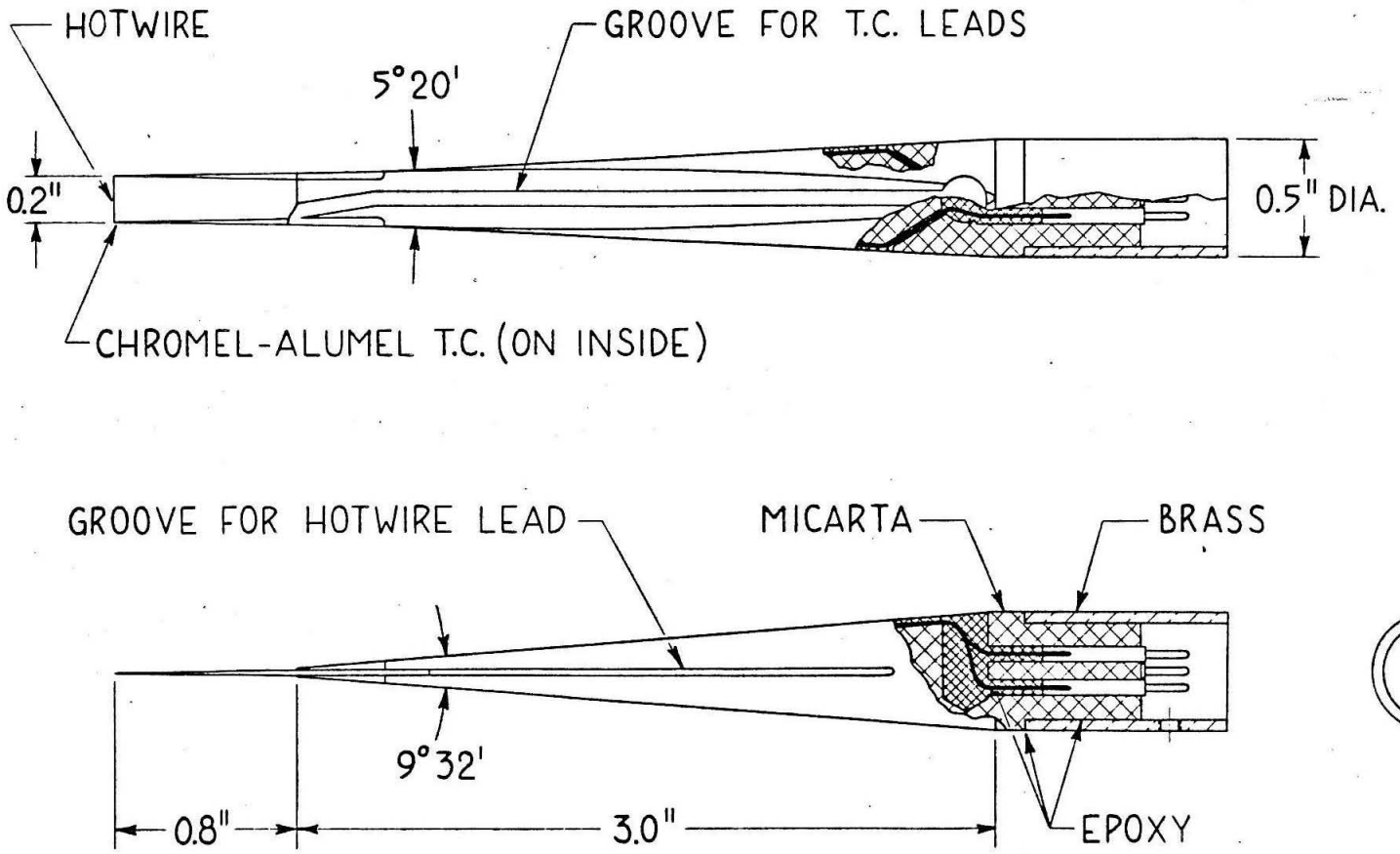

FIG. 7 HOT WIRE PROBE

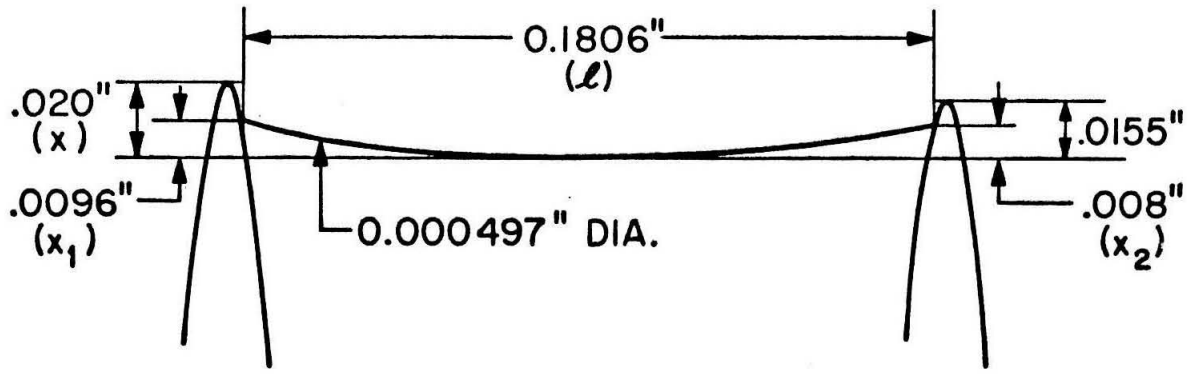

TYPICAL HOT WIRE CONFIGURATION

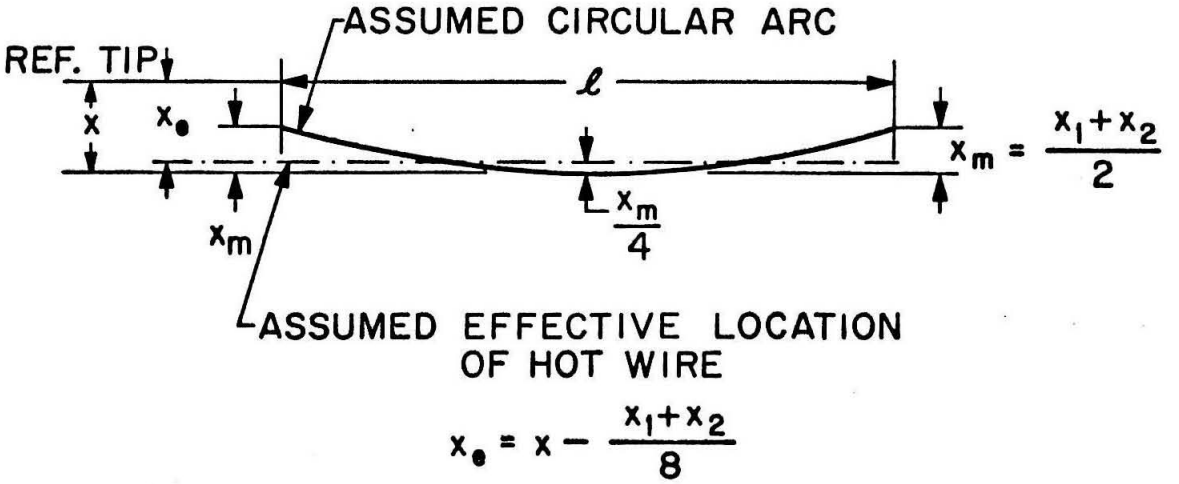

Fig. 8 HOT WIRE SAG AND EFFECTIVE LOCATION

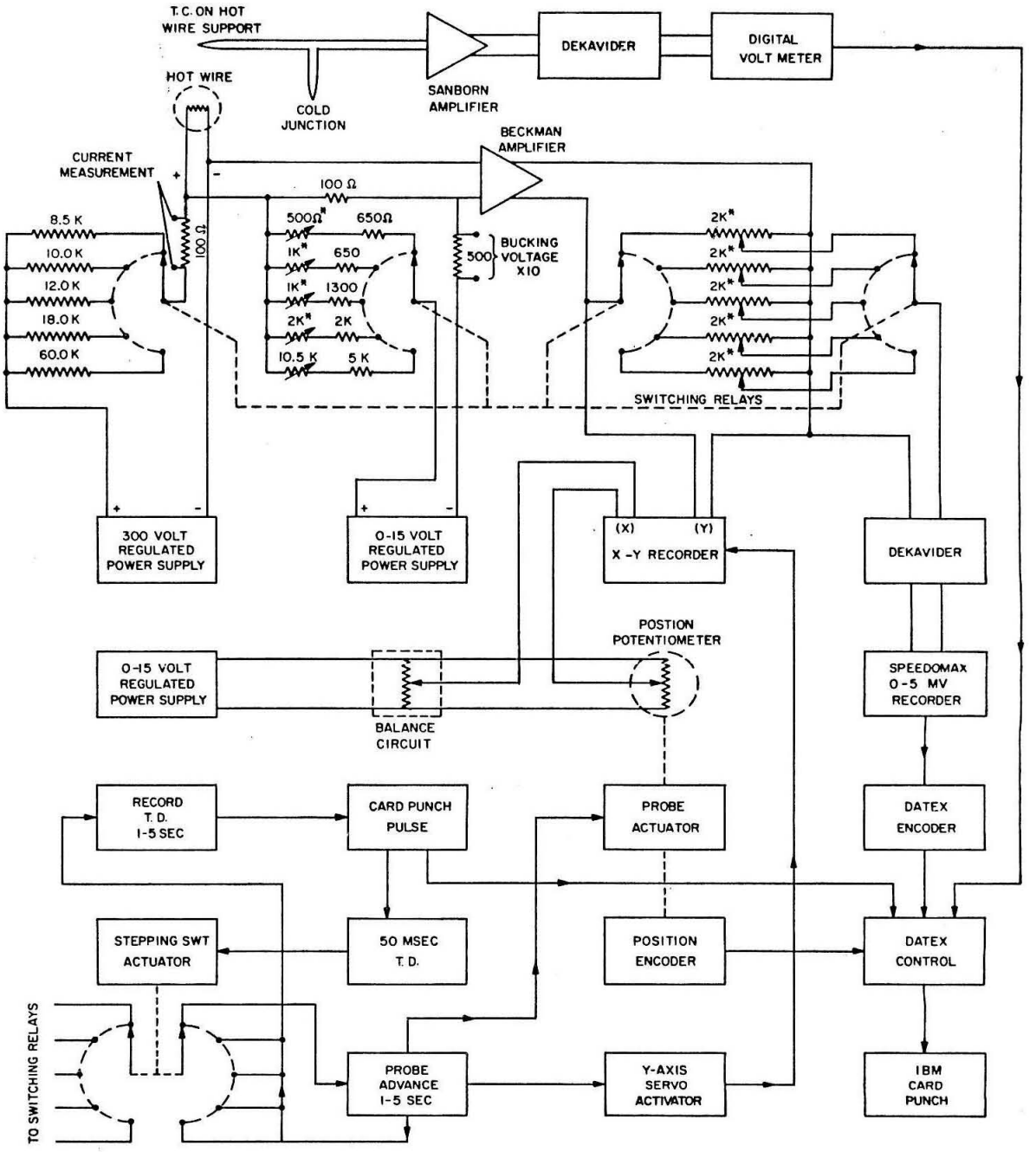

*10-TURN PRECISION POTENTIOMETERS

SWITCHING RELAYS SHOWN IN HIGH CURRENT POSITION

FIG. 9 SCHEMATIC DIAGRAM OF HOT-WIRE SYSTEM

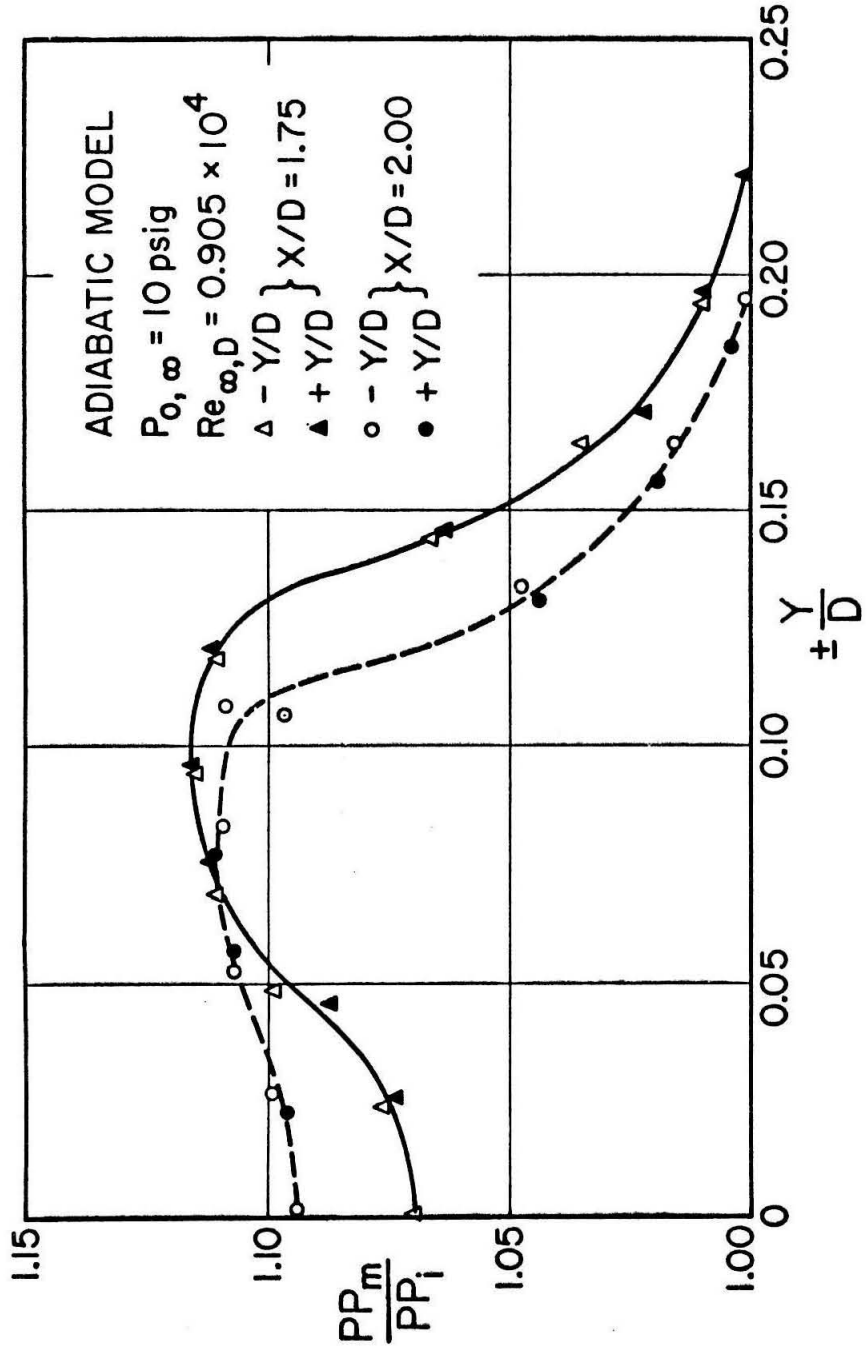

Fig. 10 TYPICAL RESULTS OF VISCOUS CORRECTIONS TO MEASURED PITOT PRESSURE

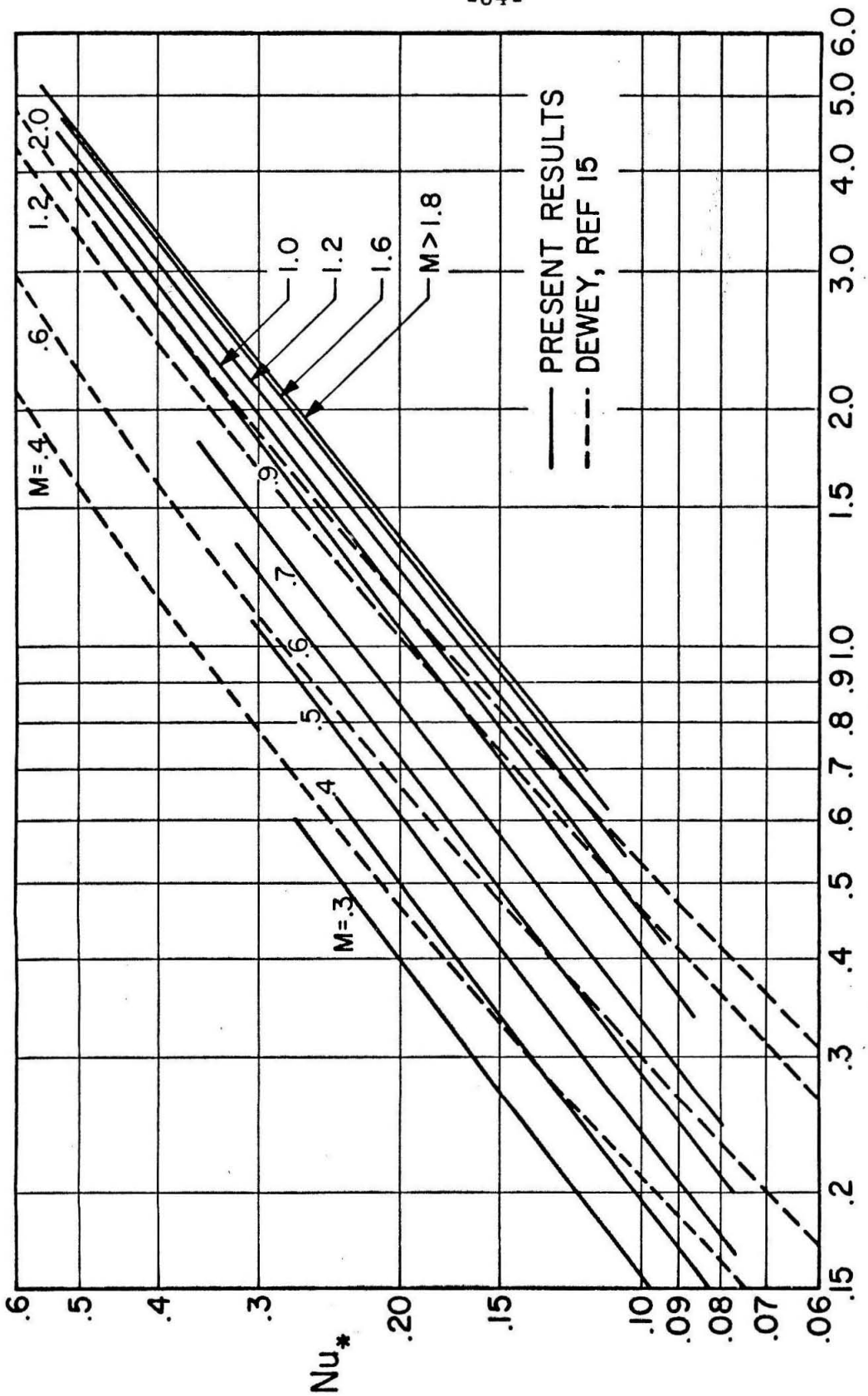

Fig. 11 NUSSELT NUMBER - REYNOLDS NUMBER CORRELATION

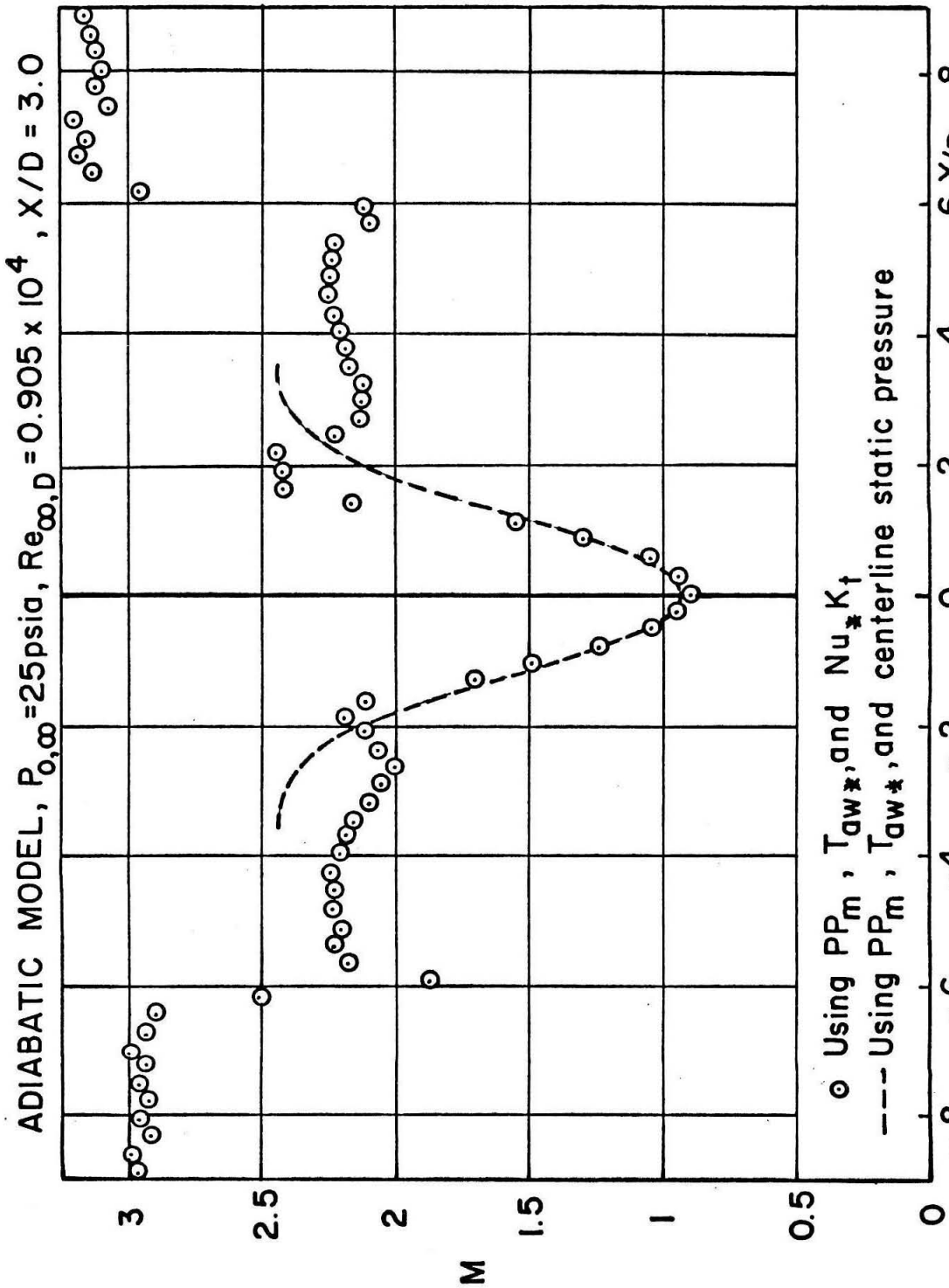

FIG. 12 COMPARISON OF MACH NUMBER DISTRIBUTIONS

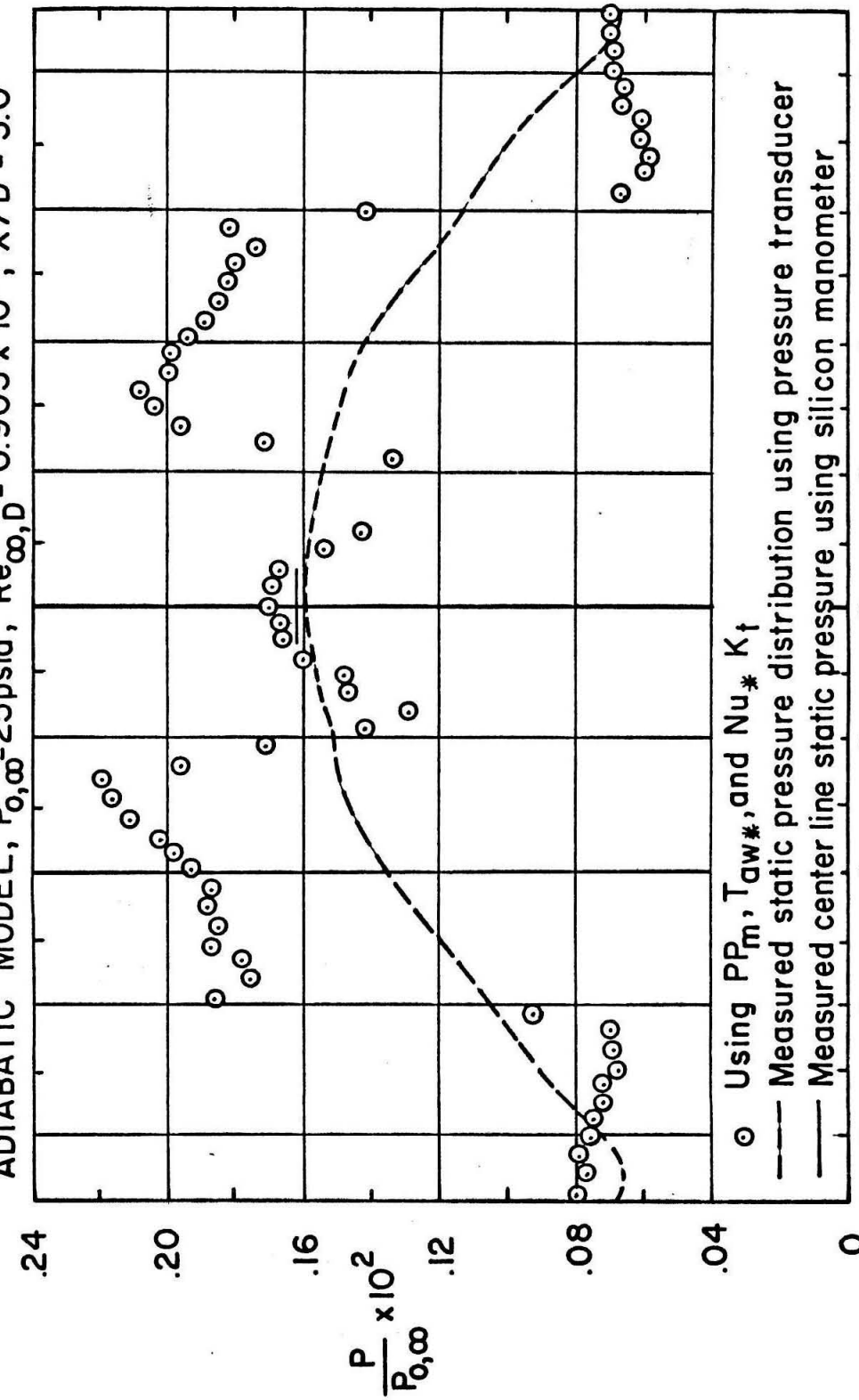

FIG. 13 TRANSVERSE STATIC PRESSURE DISTRIBUTION

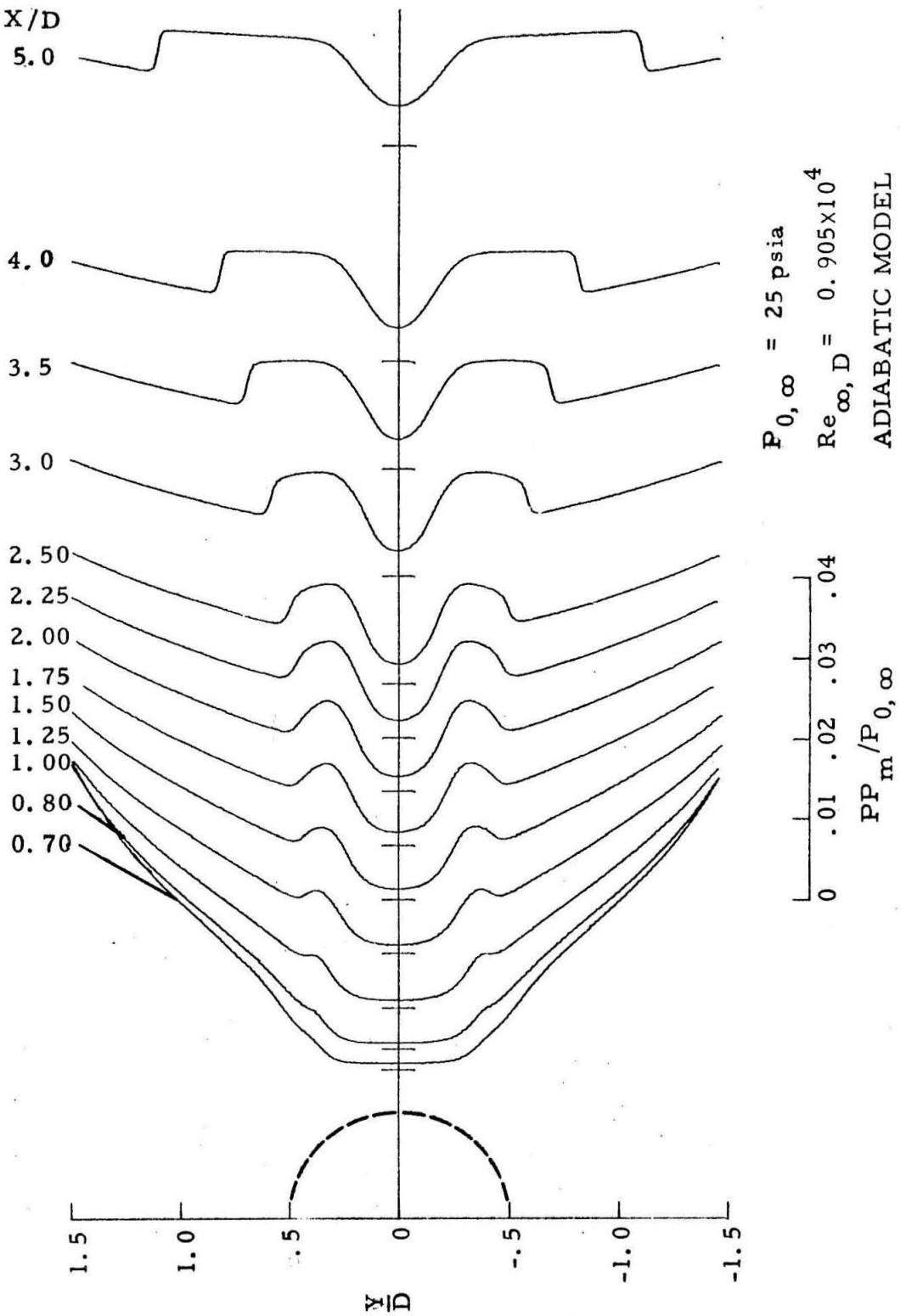

FIG. 14a MEASURED PITOT PRESSURE PROFILES

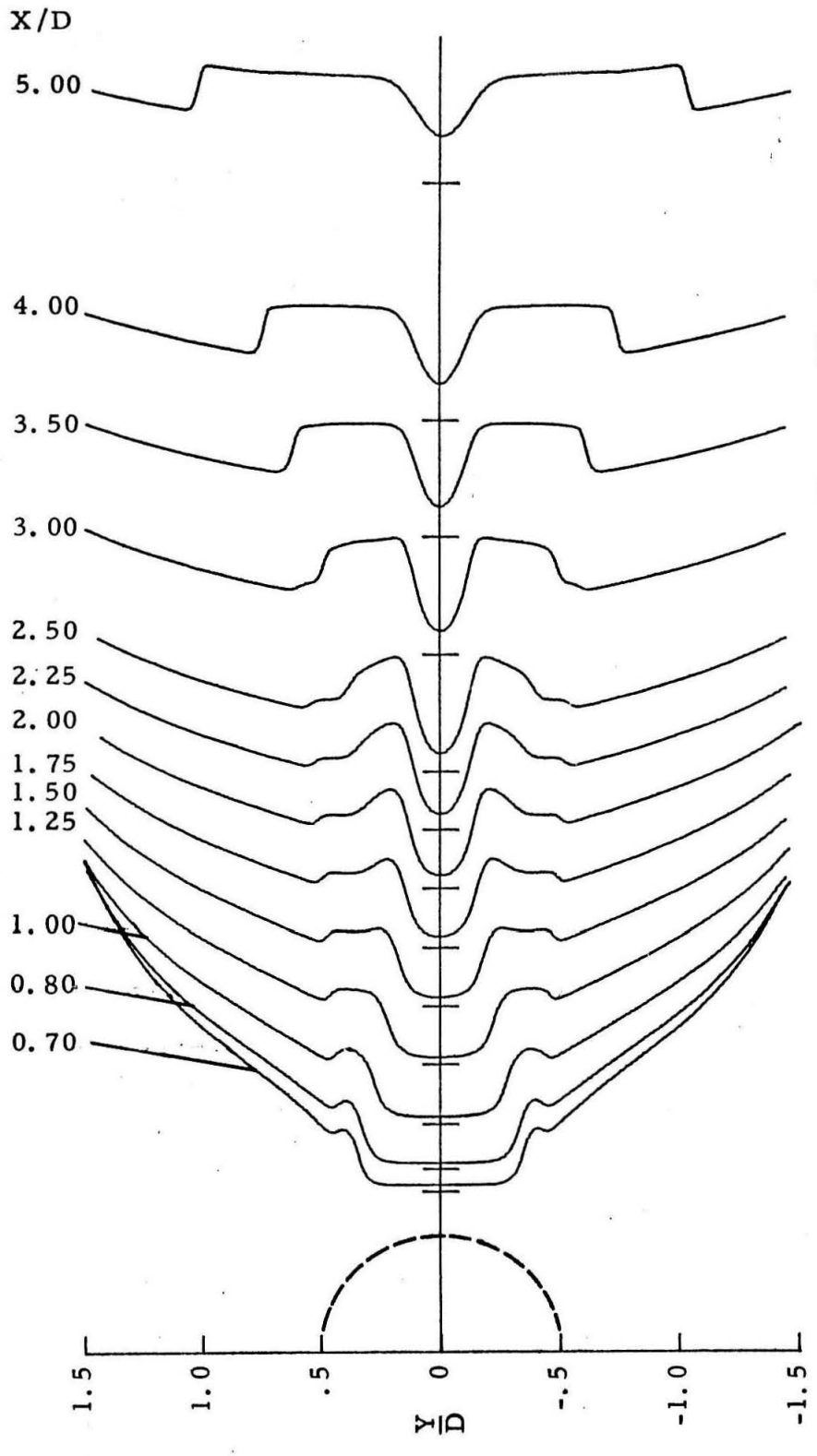

FIG. 14b MEASURED PITOT PRESSURE PROFILES

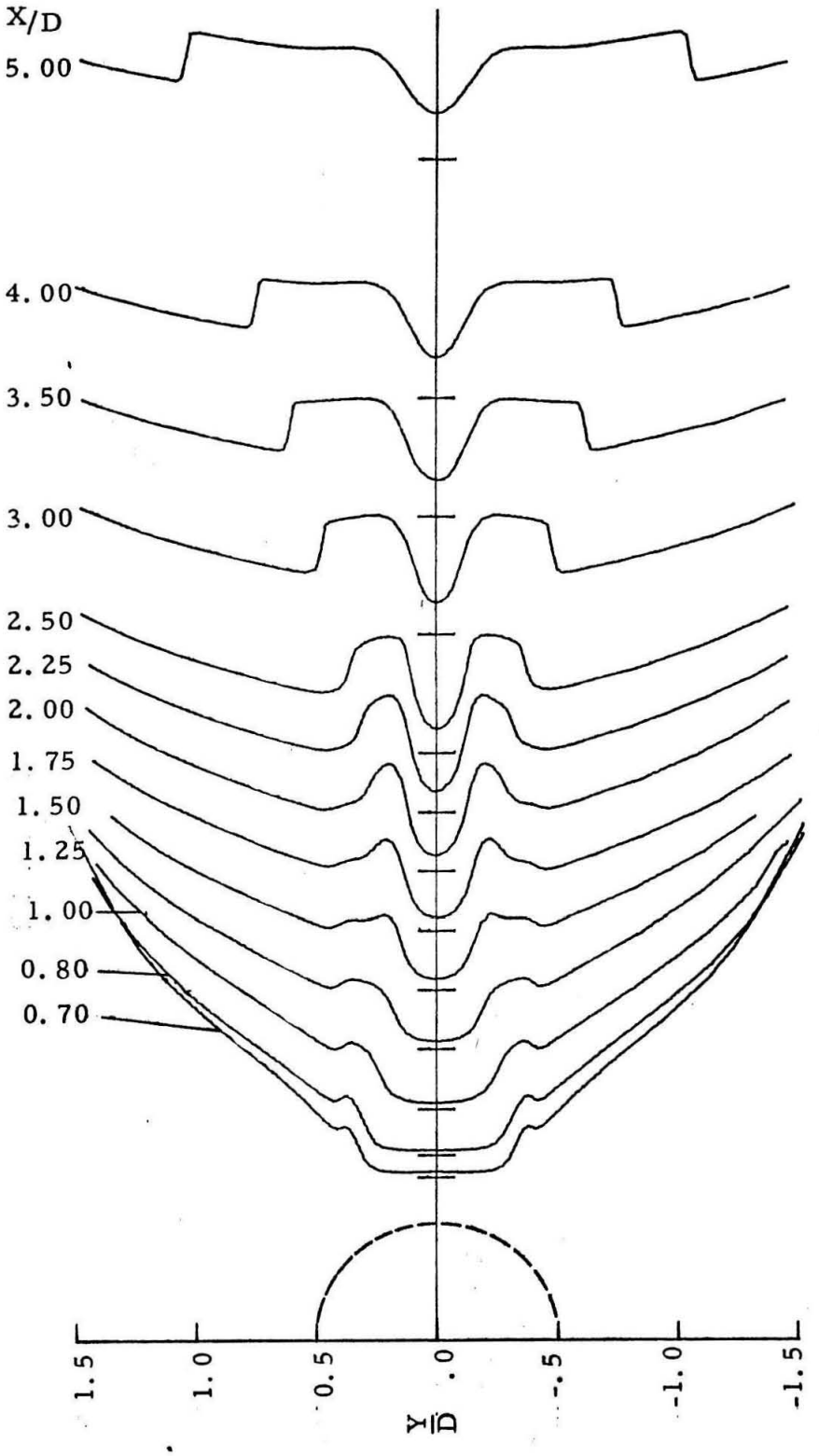

FIG. 14c MEASURED PITOT PRESSURE PROFILES

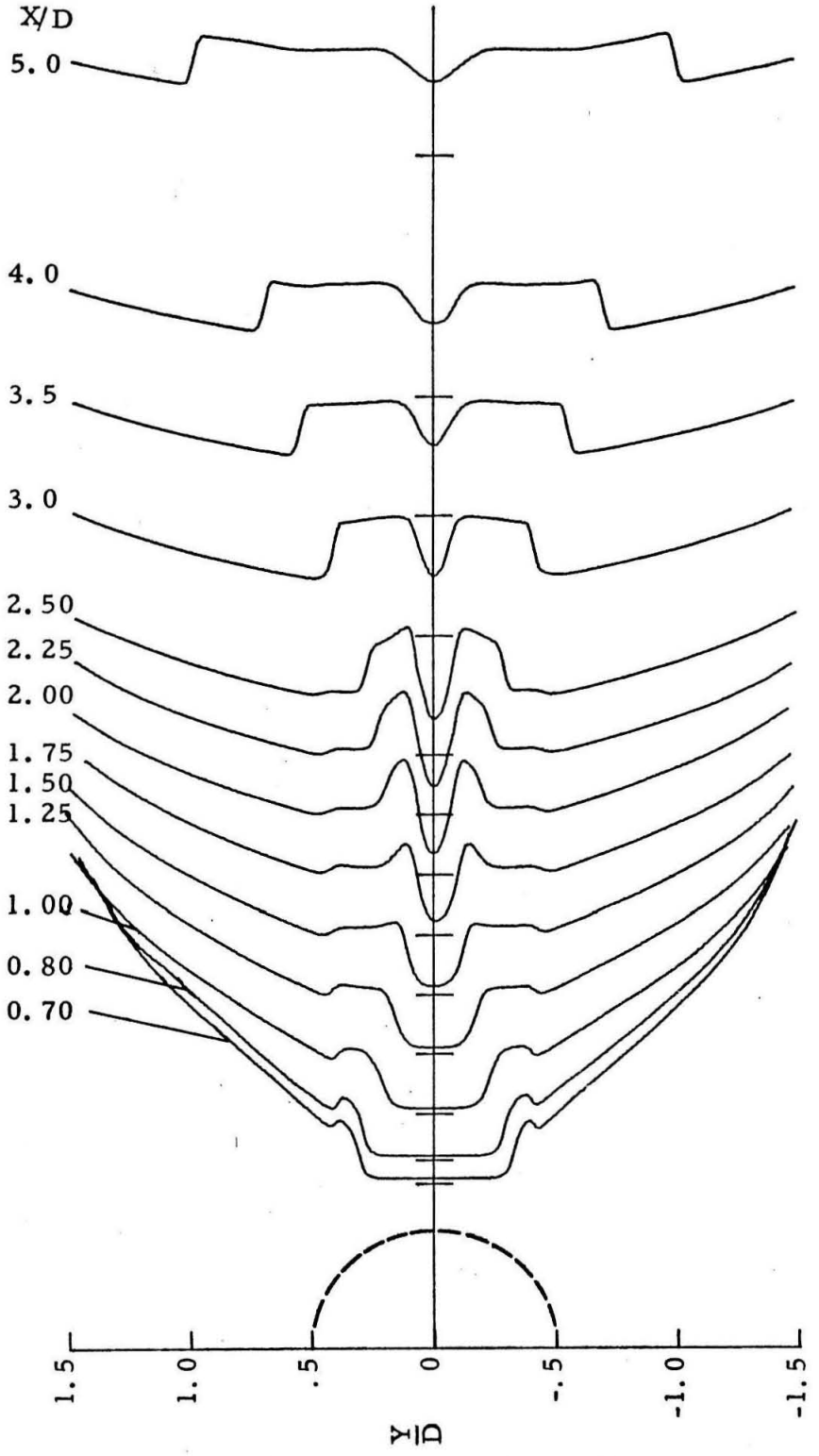

FIG.14d MEASURED PITOT PRESSURE PROFILES

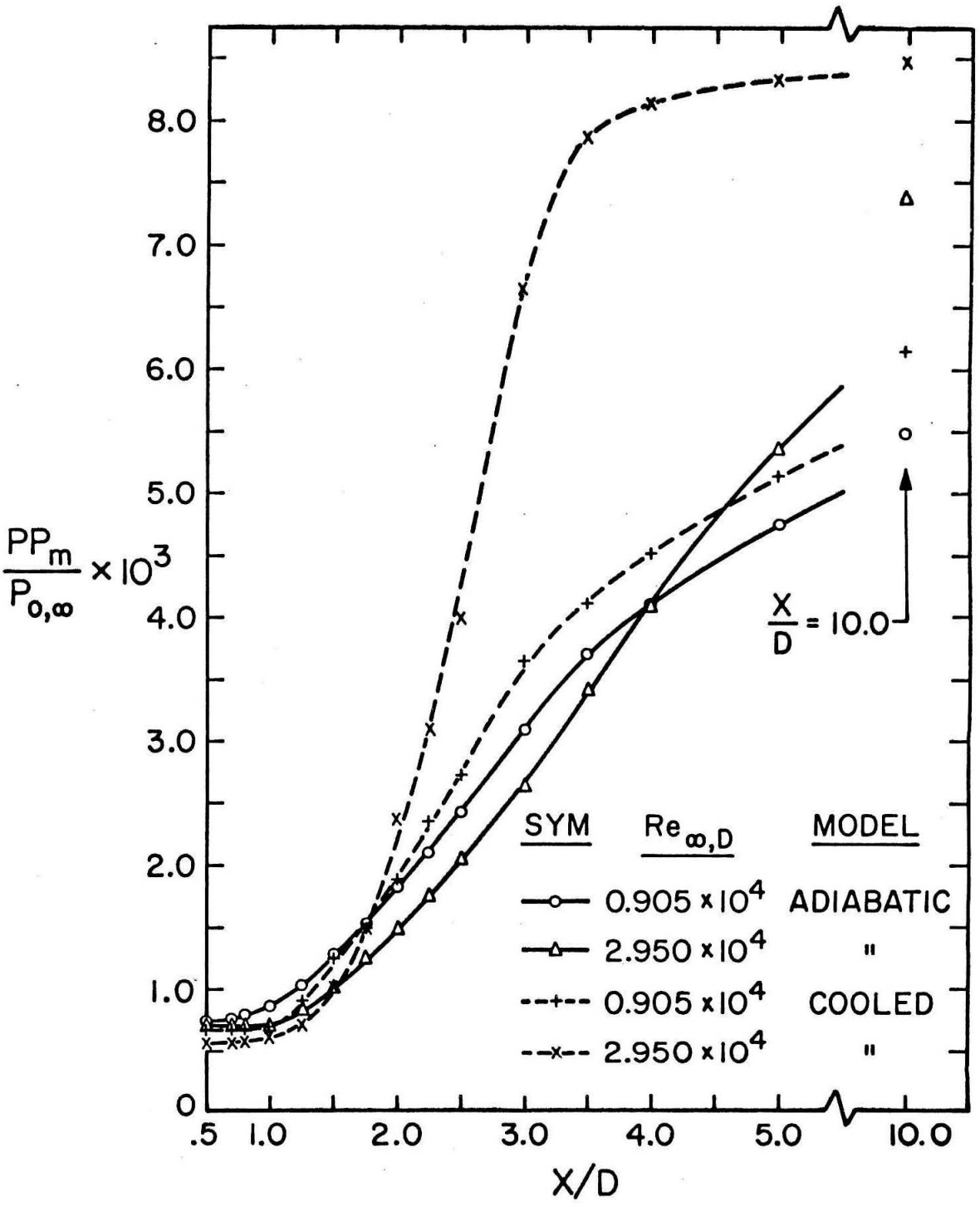

Fig. 15 MEASURED CENTERLINE PITOT PRESSURE

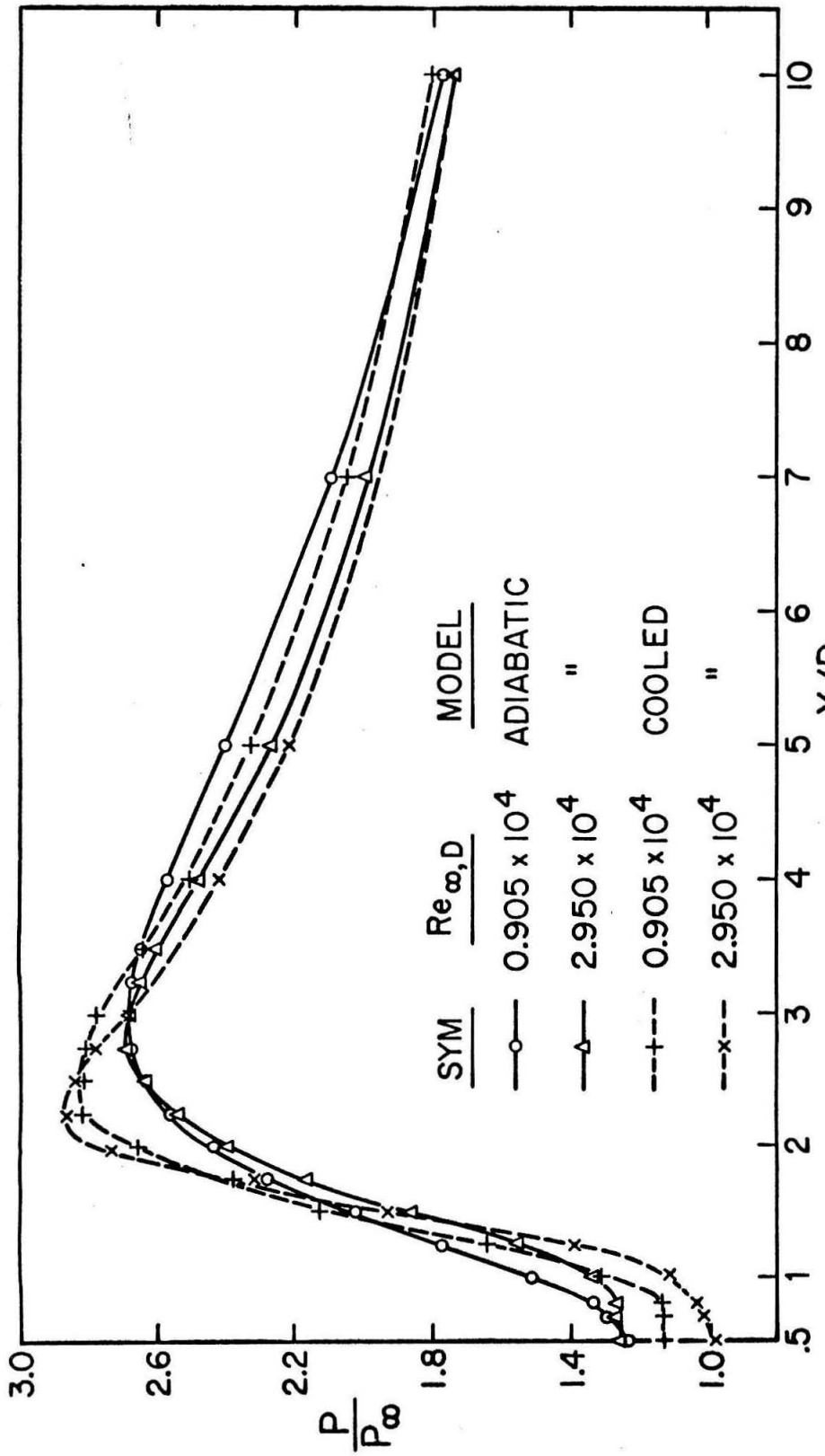

Fig. 16 CENTERLINE STATIC PRESSURE

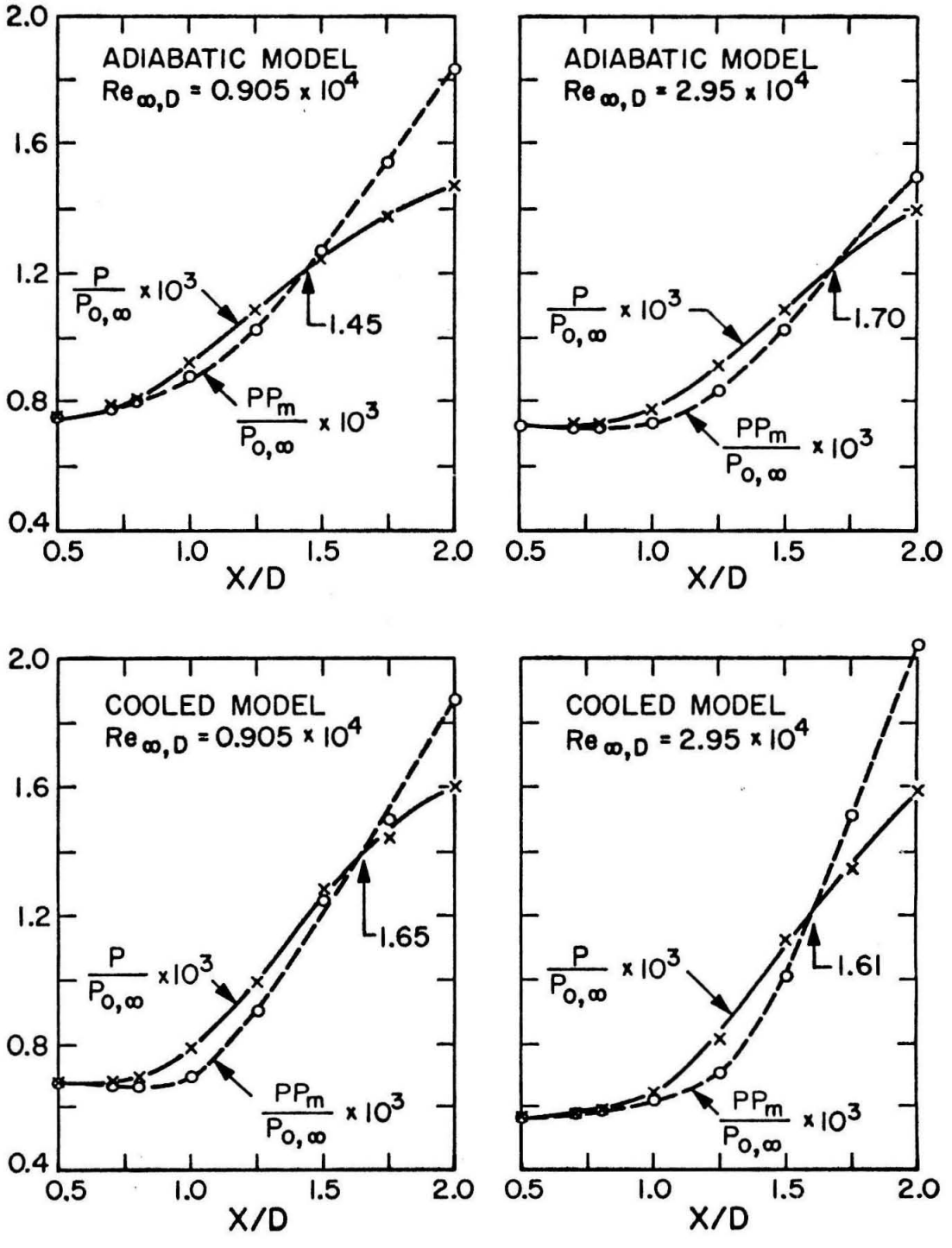

Fig. 17 LOCATION OF REAR STAGNATION POINT

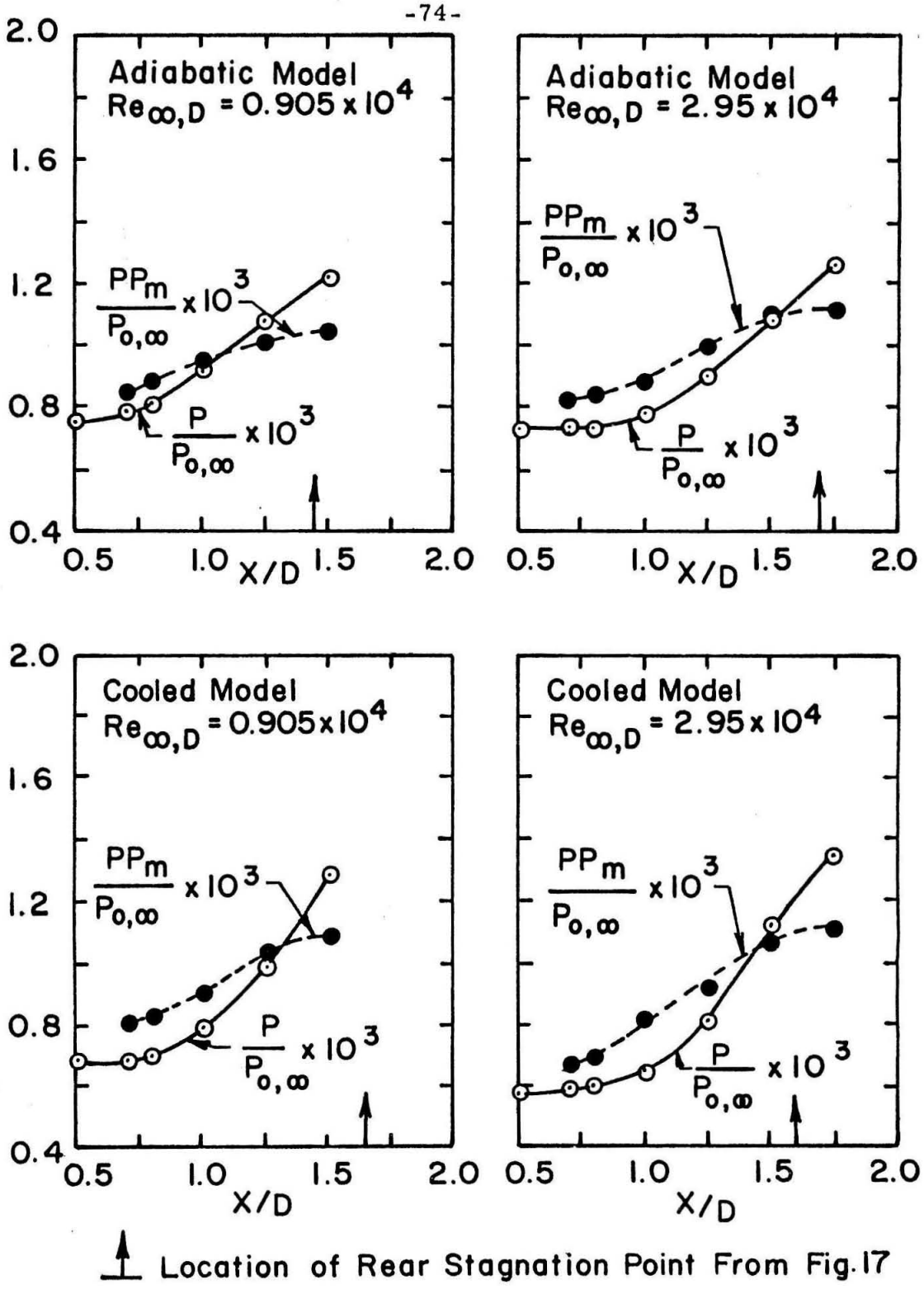

FIG. 18 MEASURED CENTERLINE PITOT PRESSURE USING LOOPED PITOT PRESSURE PROBE AND COMPARISON WITH STATIC PRESSURE

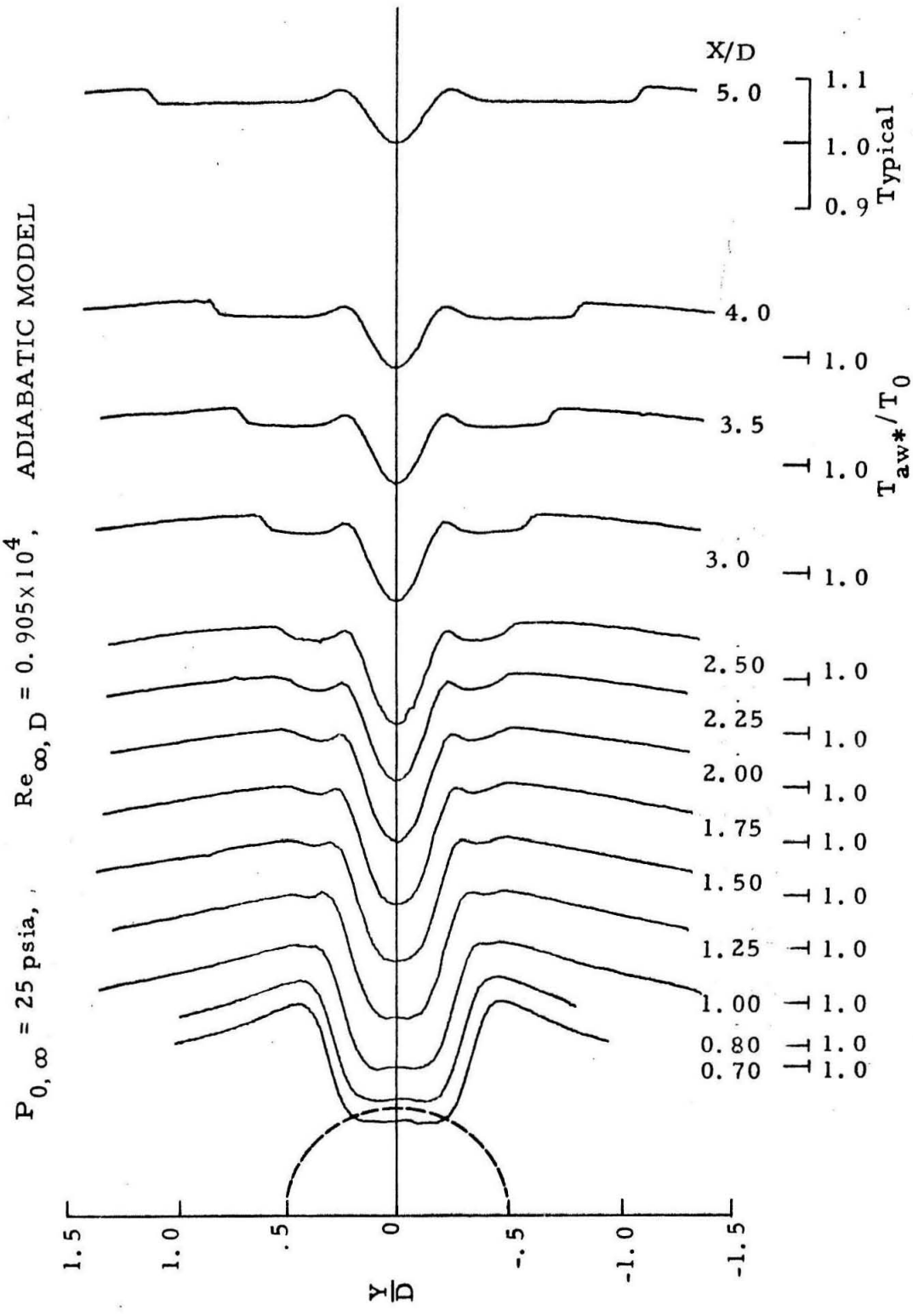

FIG. 19a INFINITE WIRE TEMPERATURE PROFILES

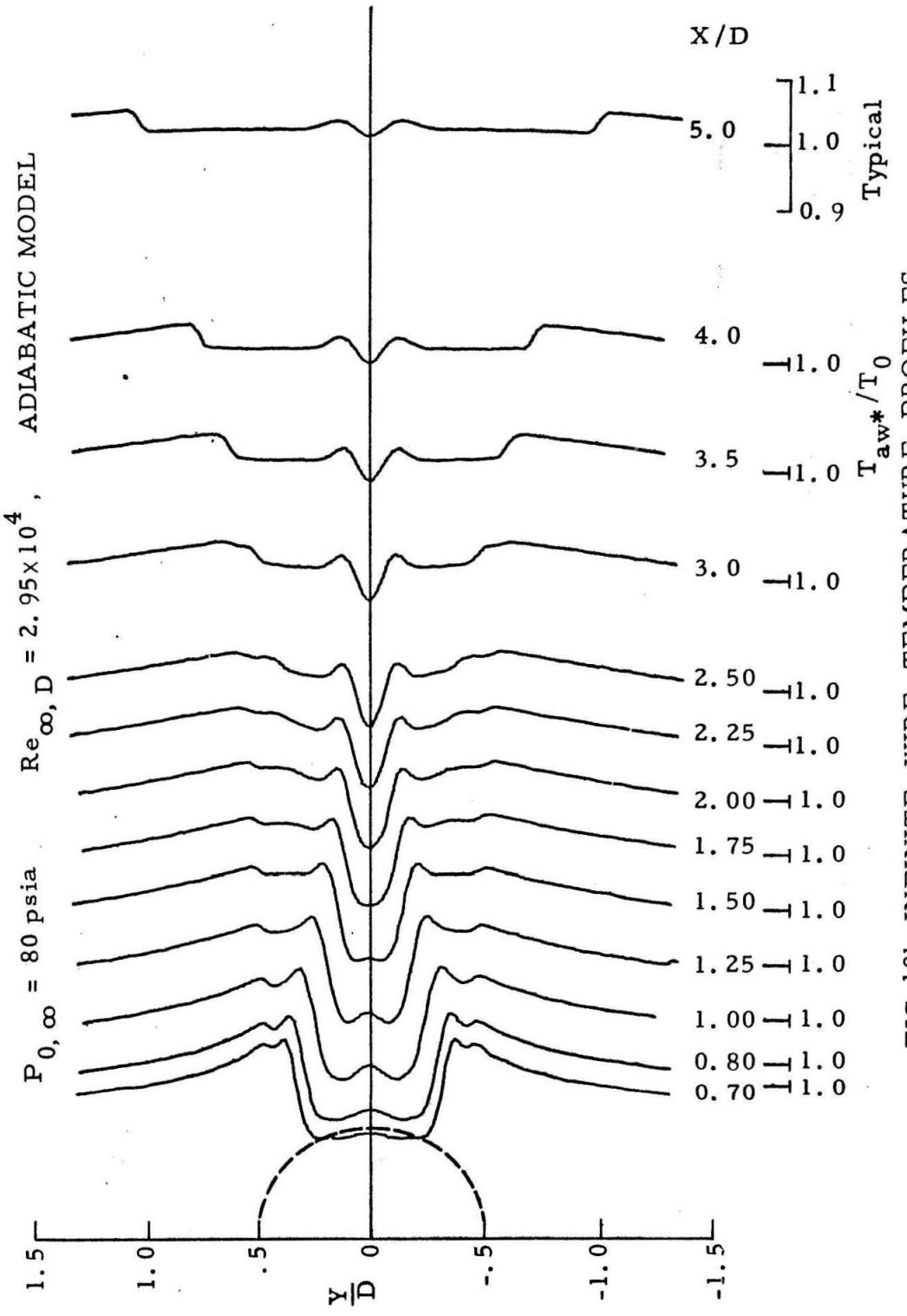

FIG. 19b INFINITE WIRE TEMPERATURE PROFILES

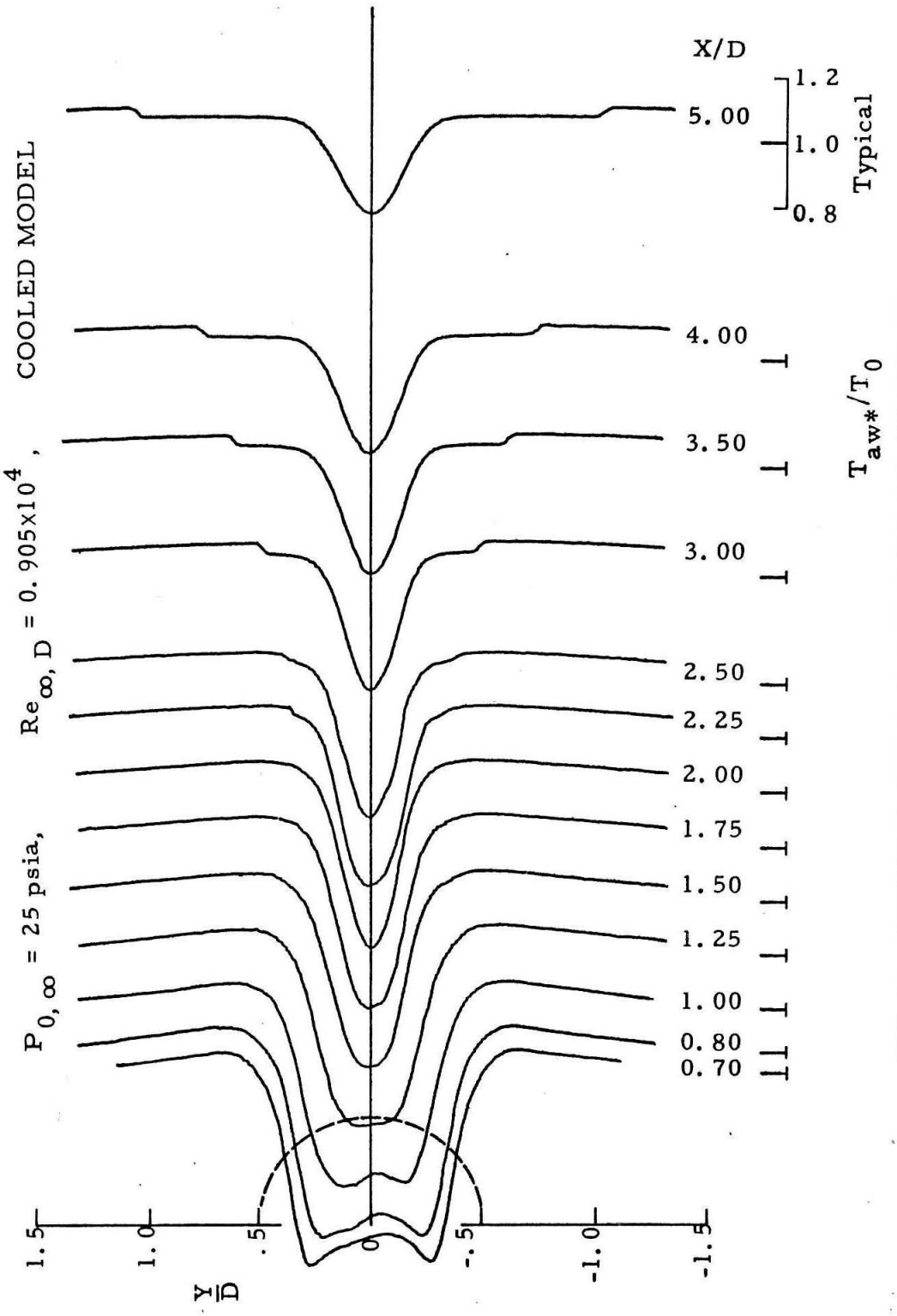

FIG. 19c INFINITE WIRE TEMPERATURE PROFILES

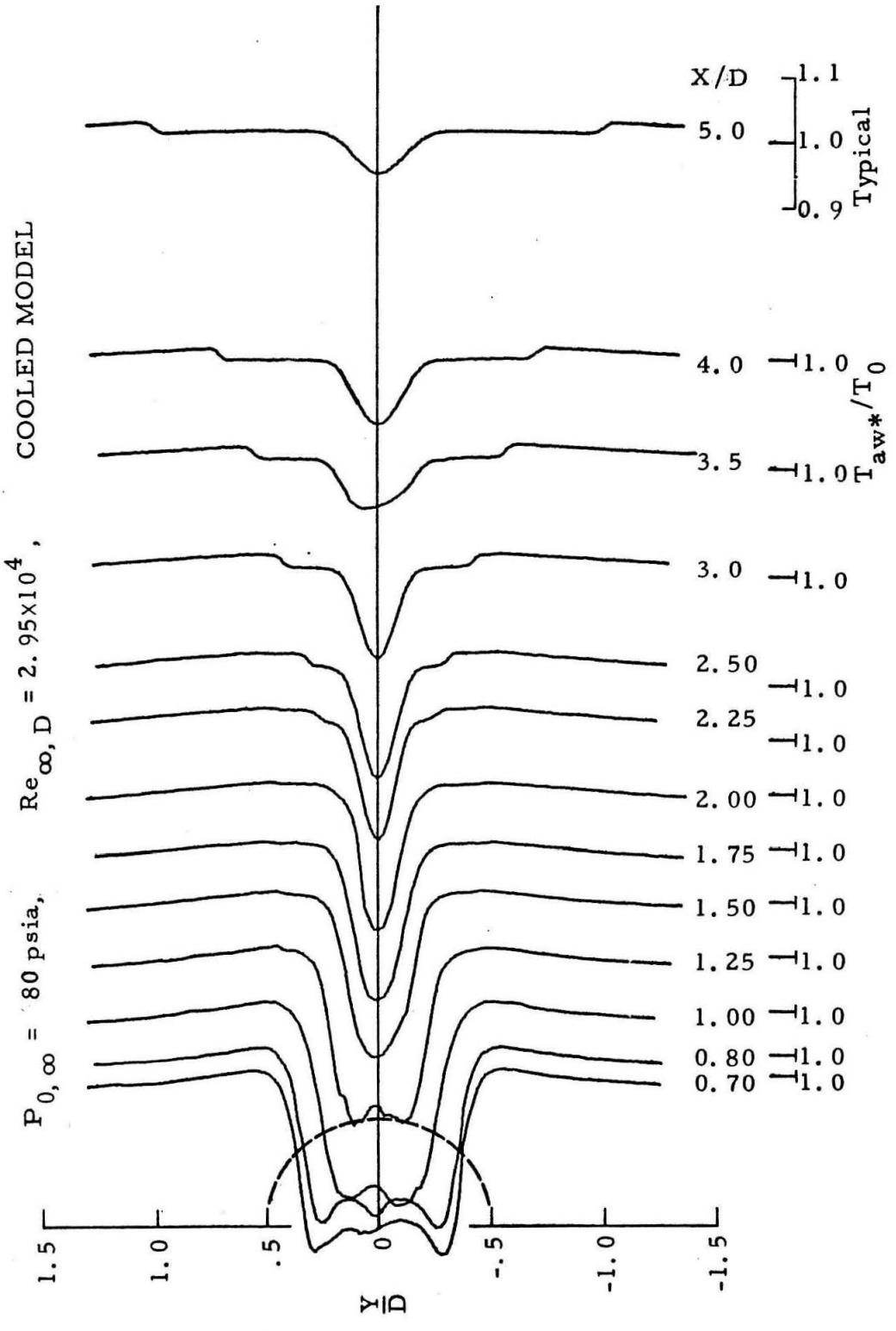

FIG. 19d INFINITE WIRE TEMPERATURE PROFILES

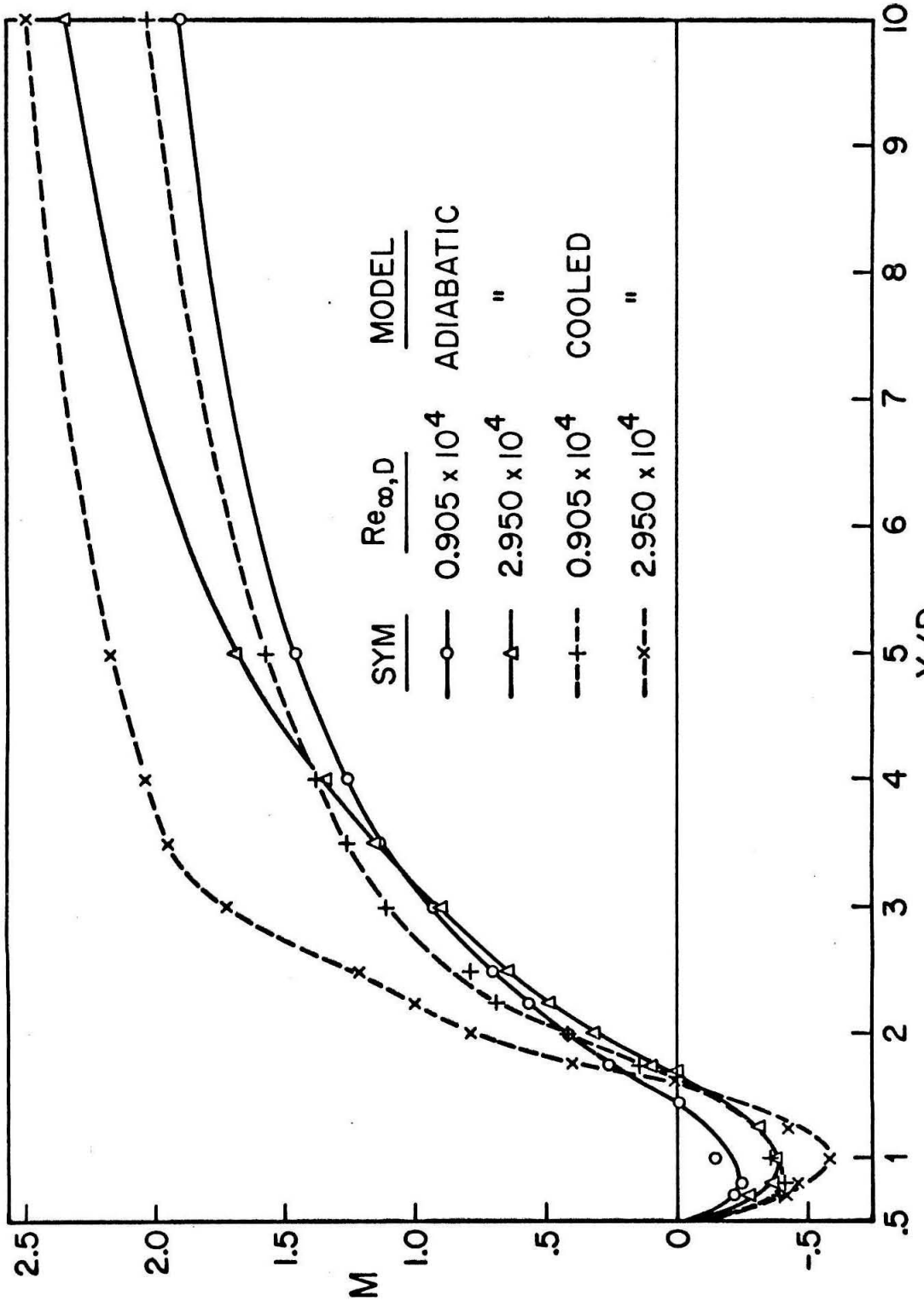

Fig. 20 CENTERLINE MACH NUMBER DISTRIBUTION

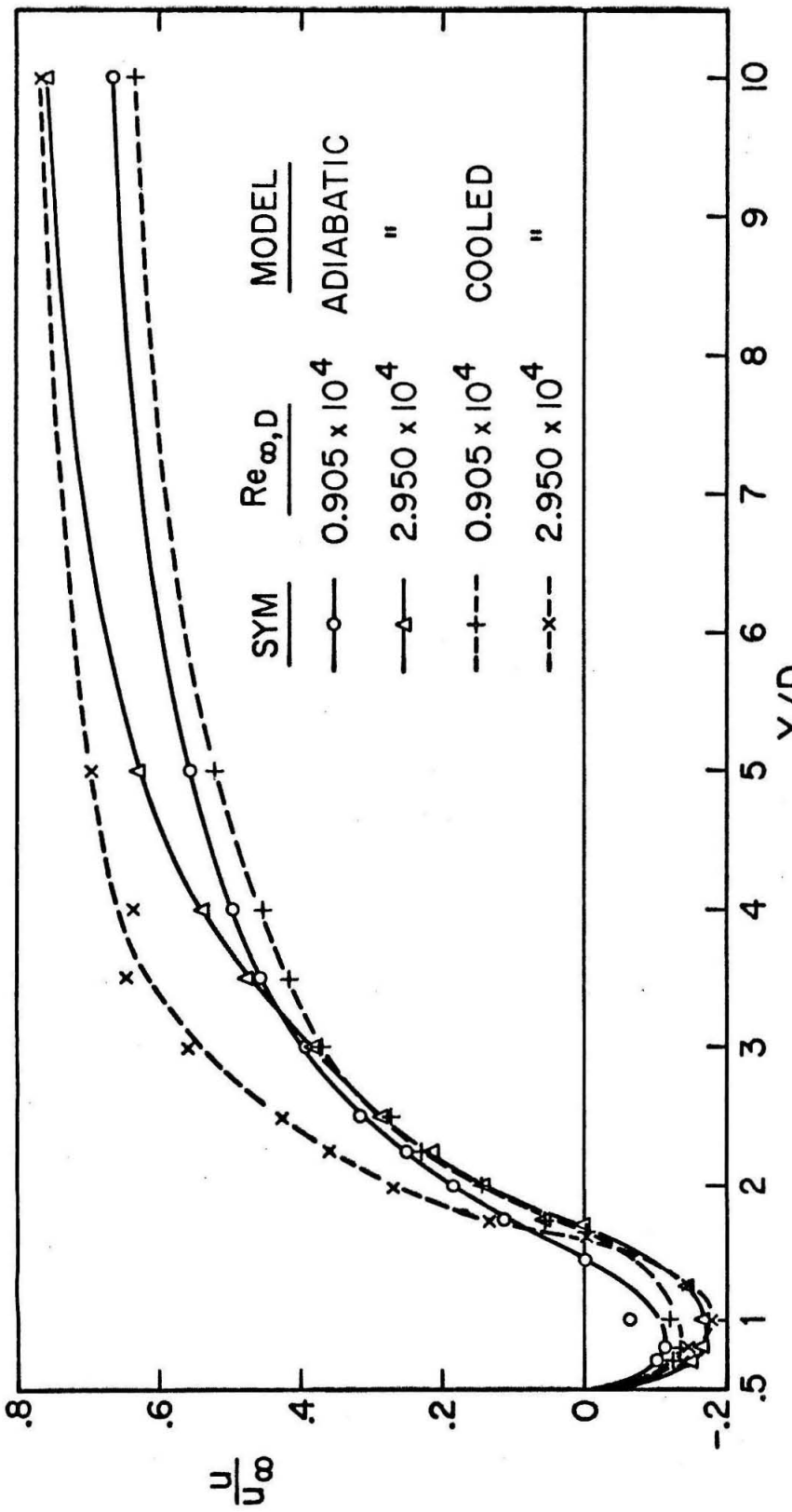

Fig. 21 CENTERLINE VELOCITY DISTRIBUTION

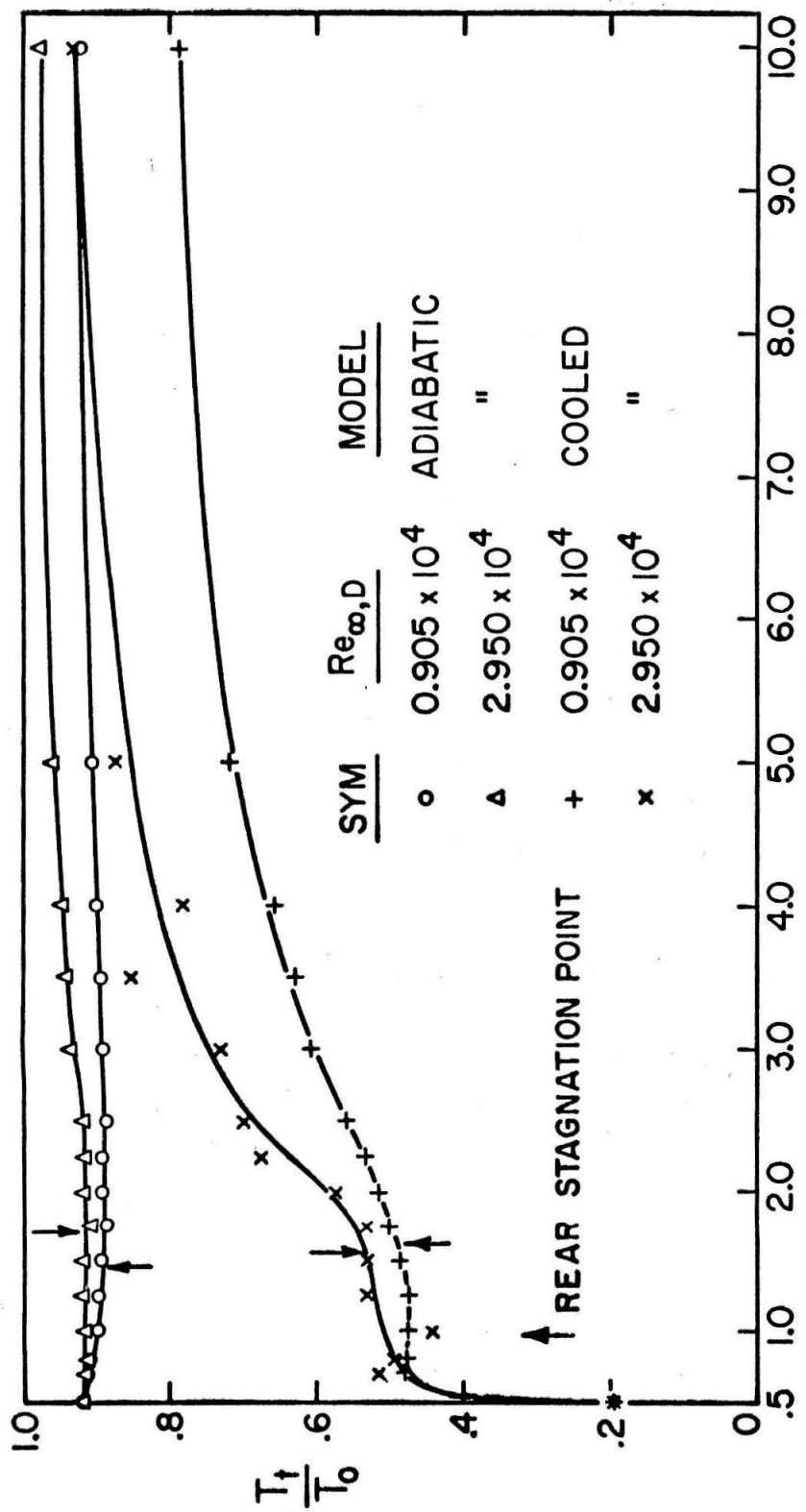

Fig. 22 CENTERLINE STAGNATION TEMPERATURE

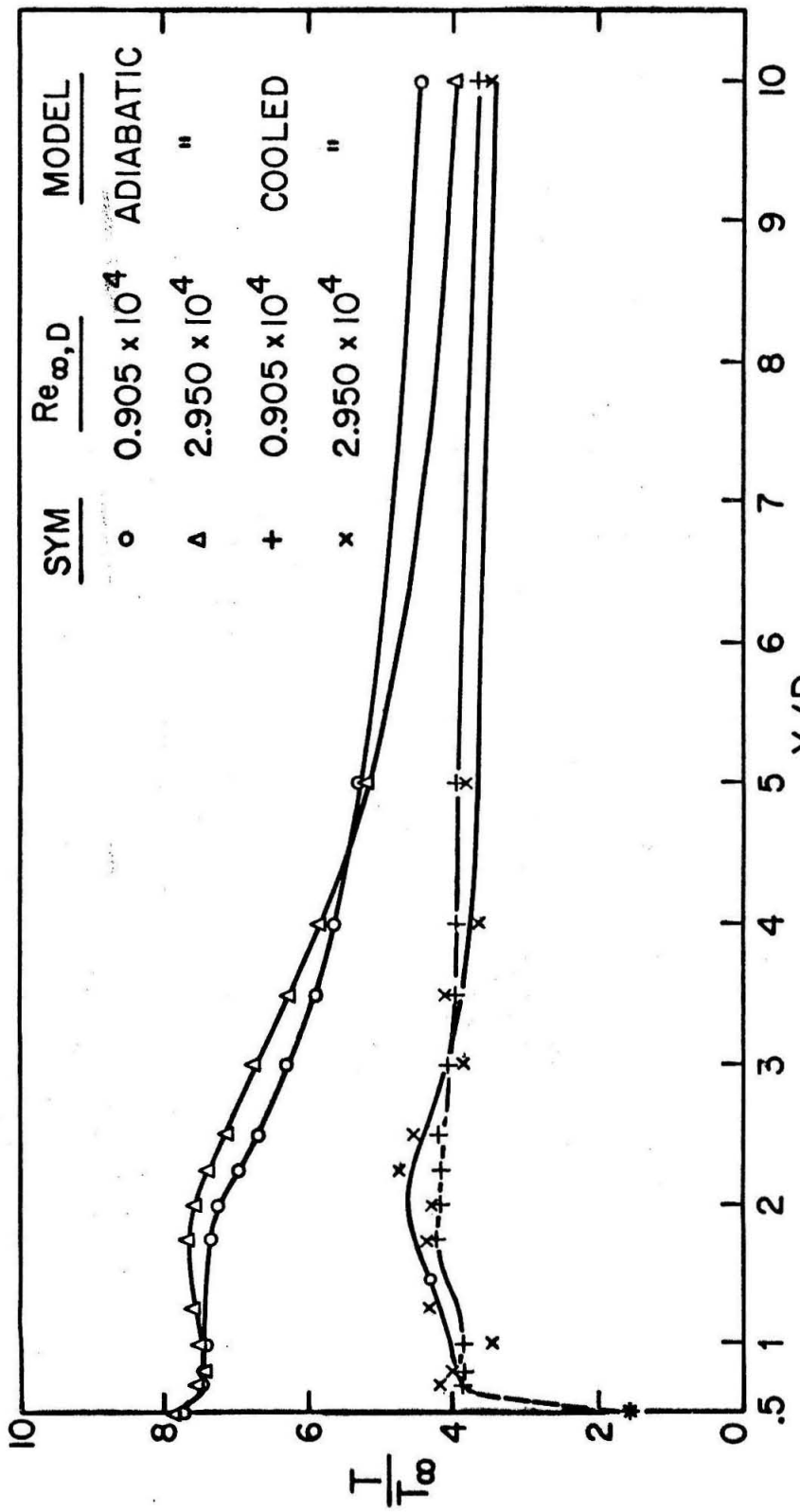

Fig. 23 CENTERLINE STATIC TEMPERATURE DISTRIBUTION

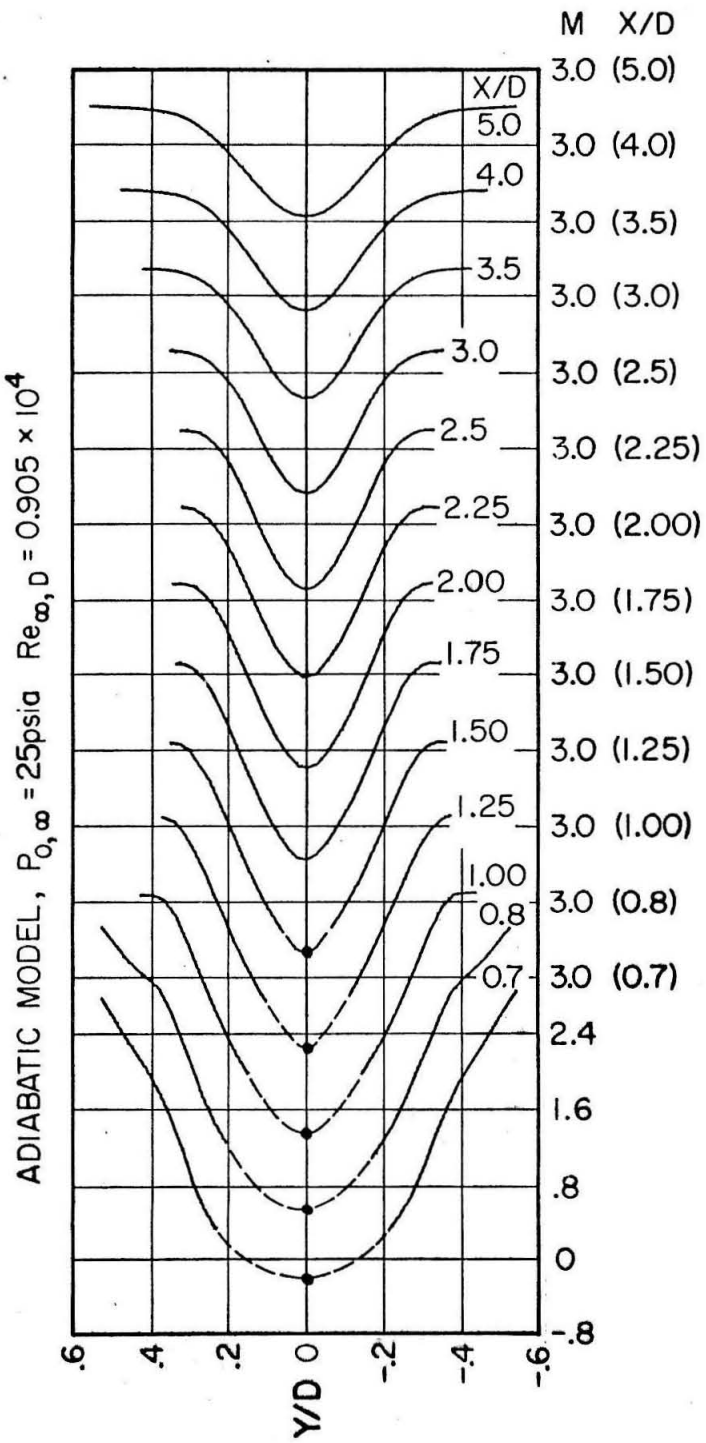

Fig. 24 a MACH NUMBER PROFILES

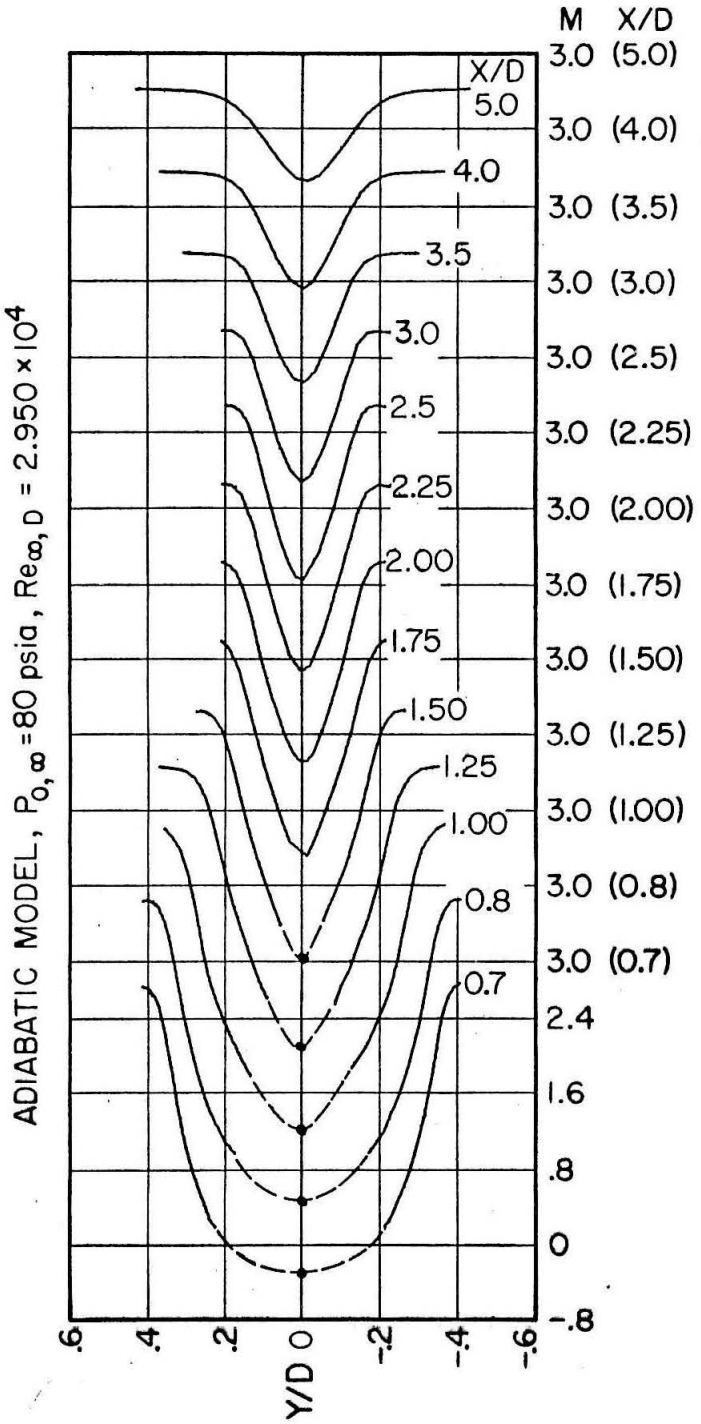

Fig. 24 b MACH NUMBER PROFILES

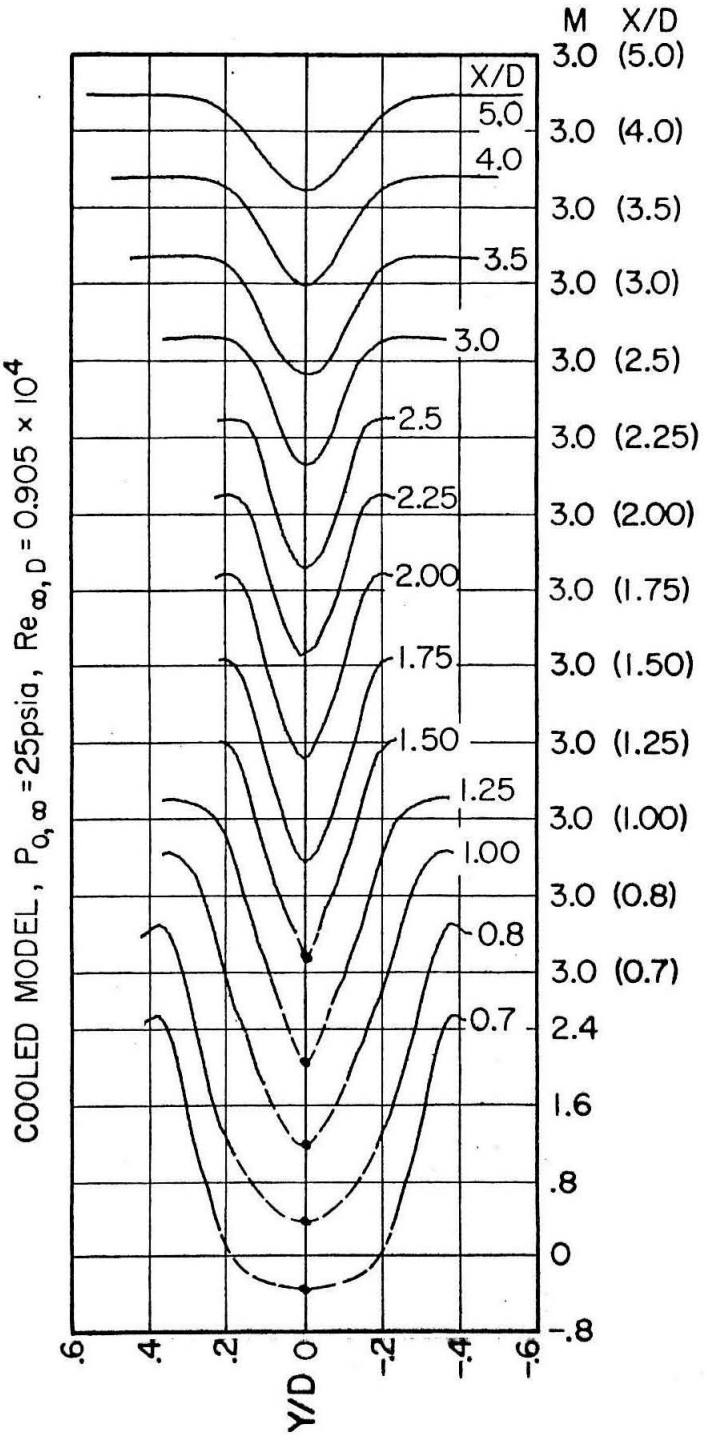

Fig. 24 c MACH NUMBER PROFILES

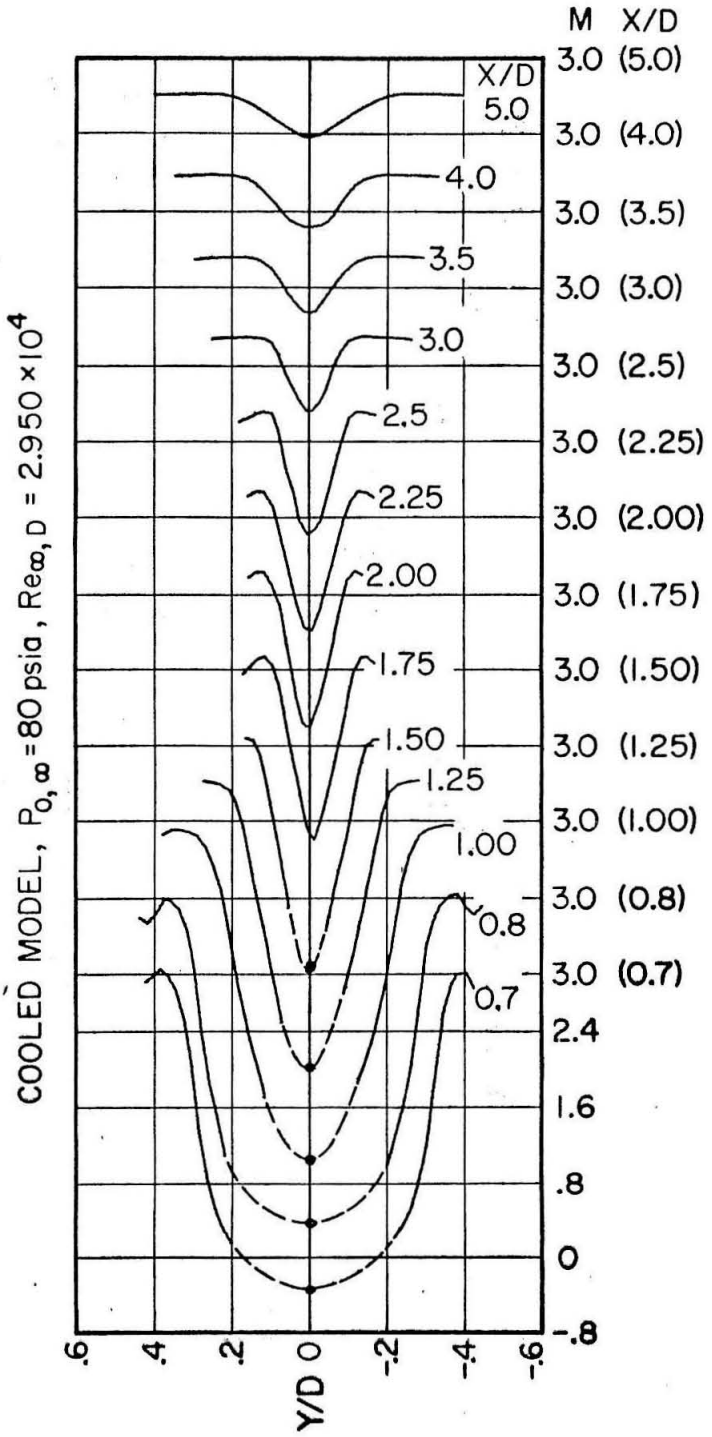

Fig. 24d MACH NUMBER PROFILES

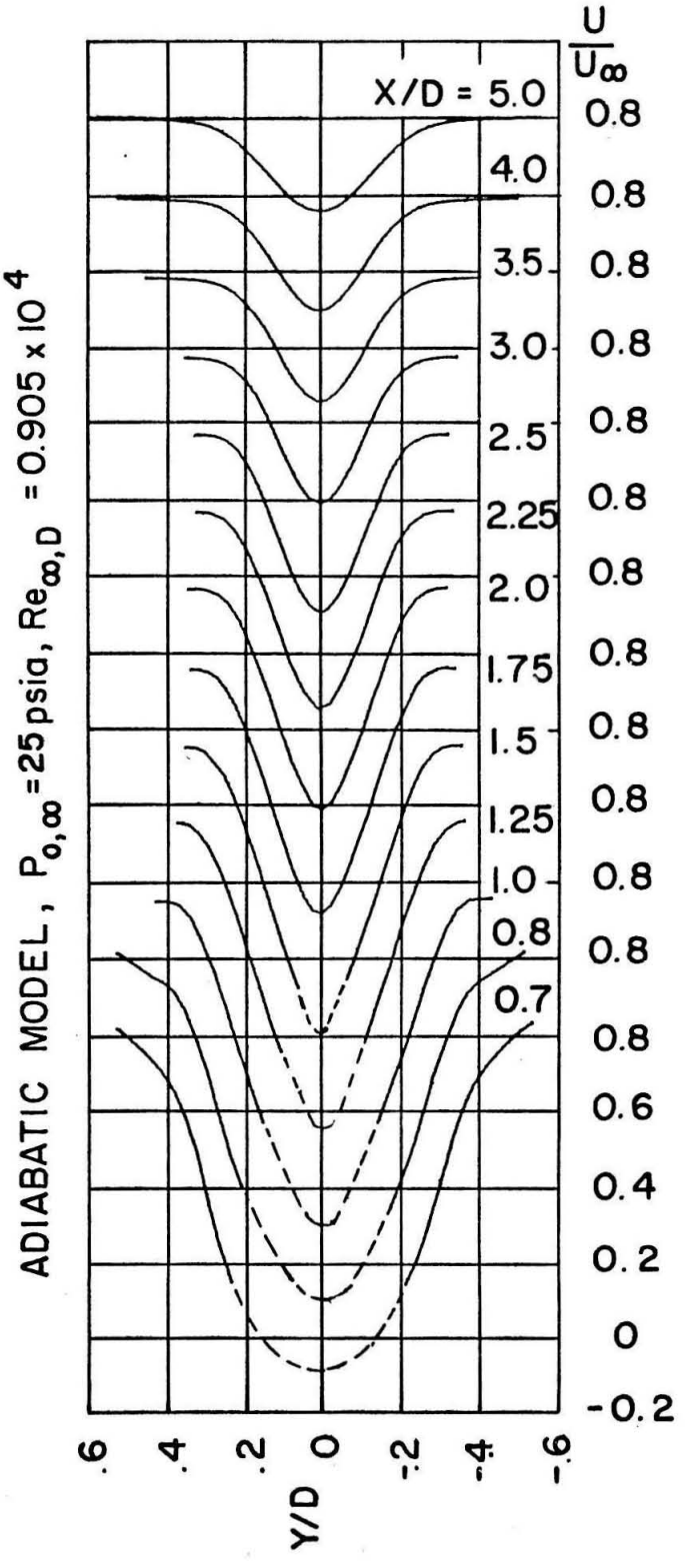

FIG.25a VELOCITY PROFILES

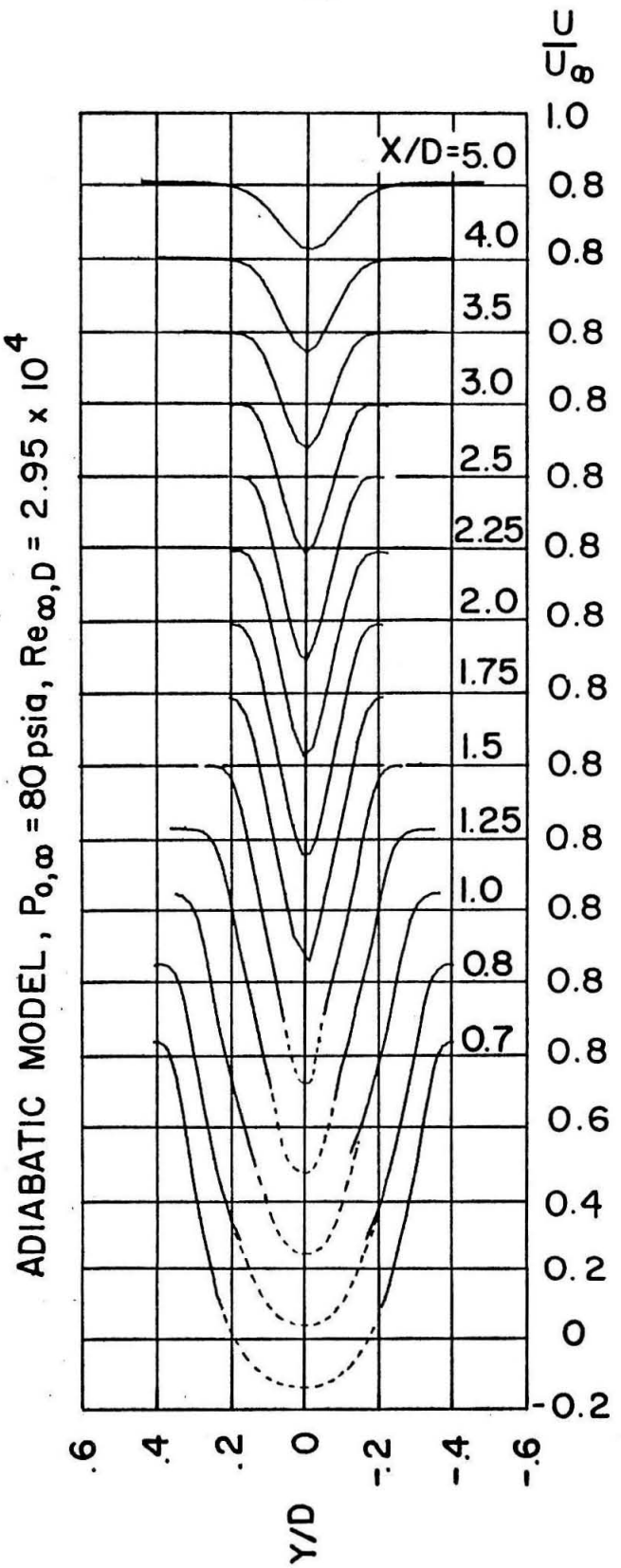

FIG.25b VELOCITY PROFILES

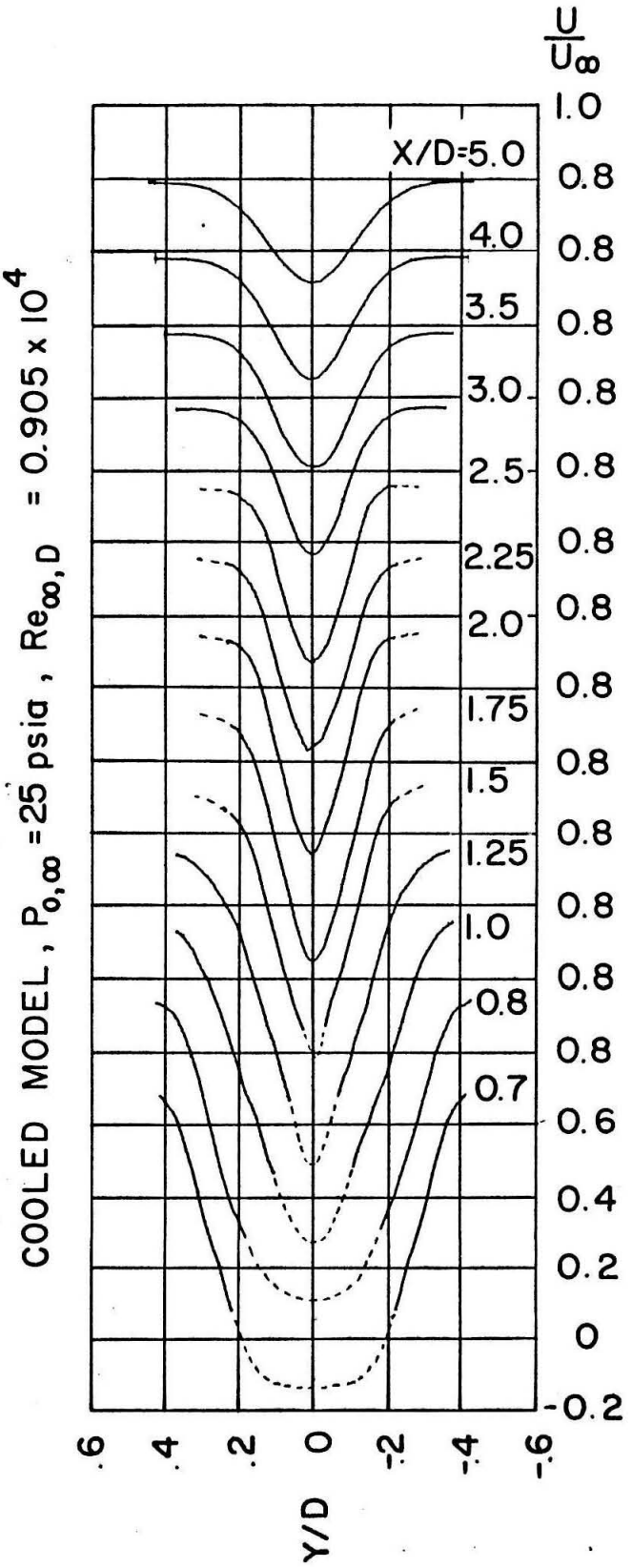

FIG.25c VELOCITY PROFILES

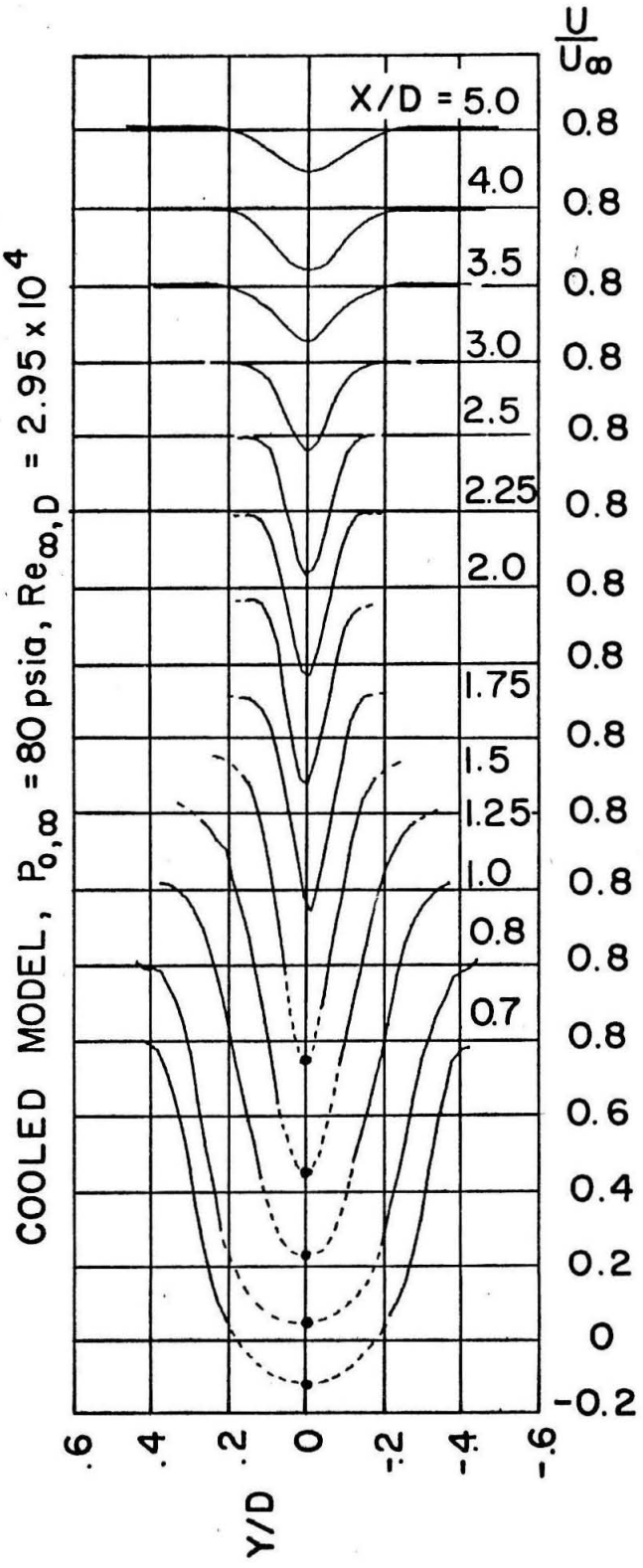

FIG.25d VELOCITY PROFILES

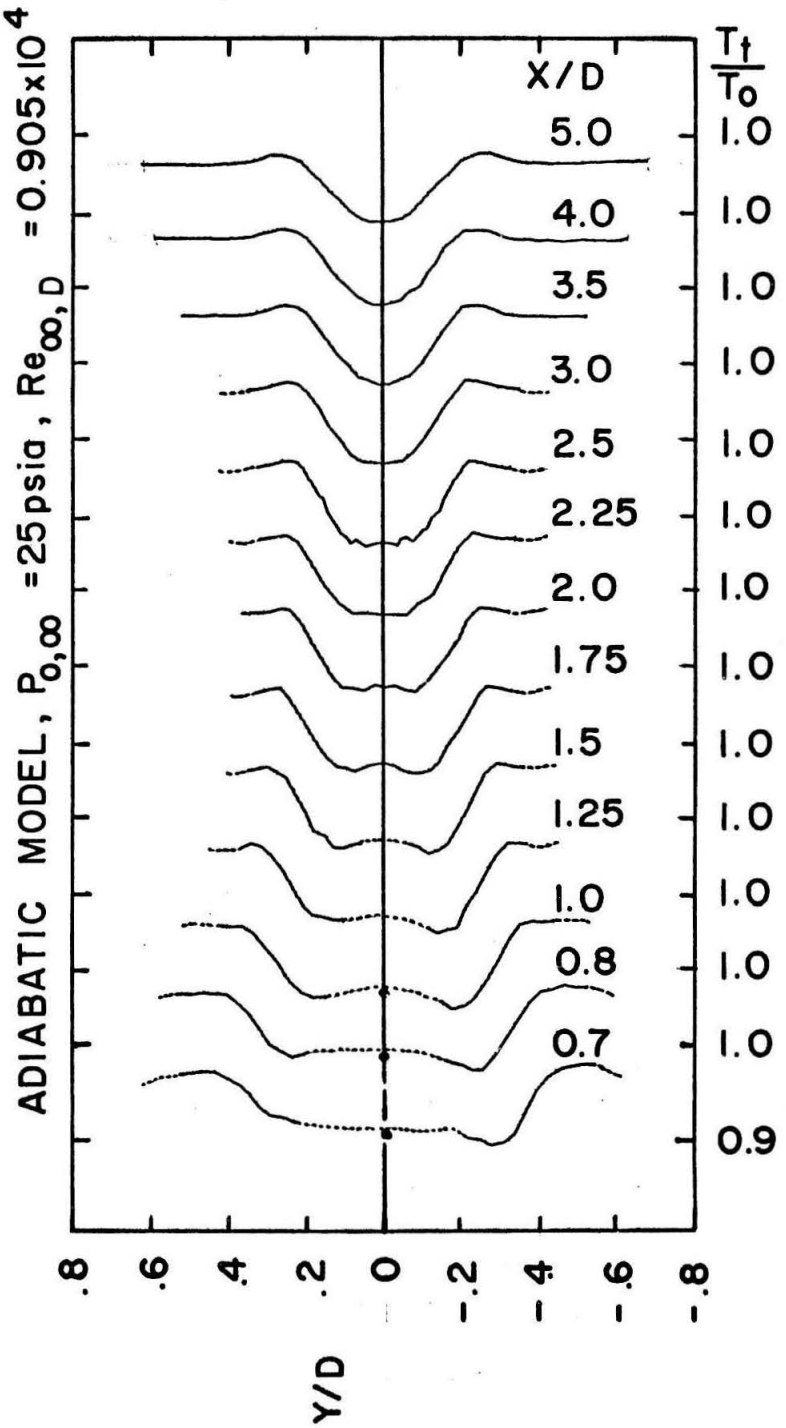

FIG.26a STAGNATION TEMPERATURE PROFILES

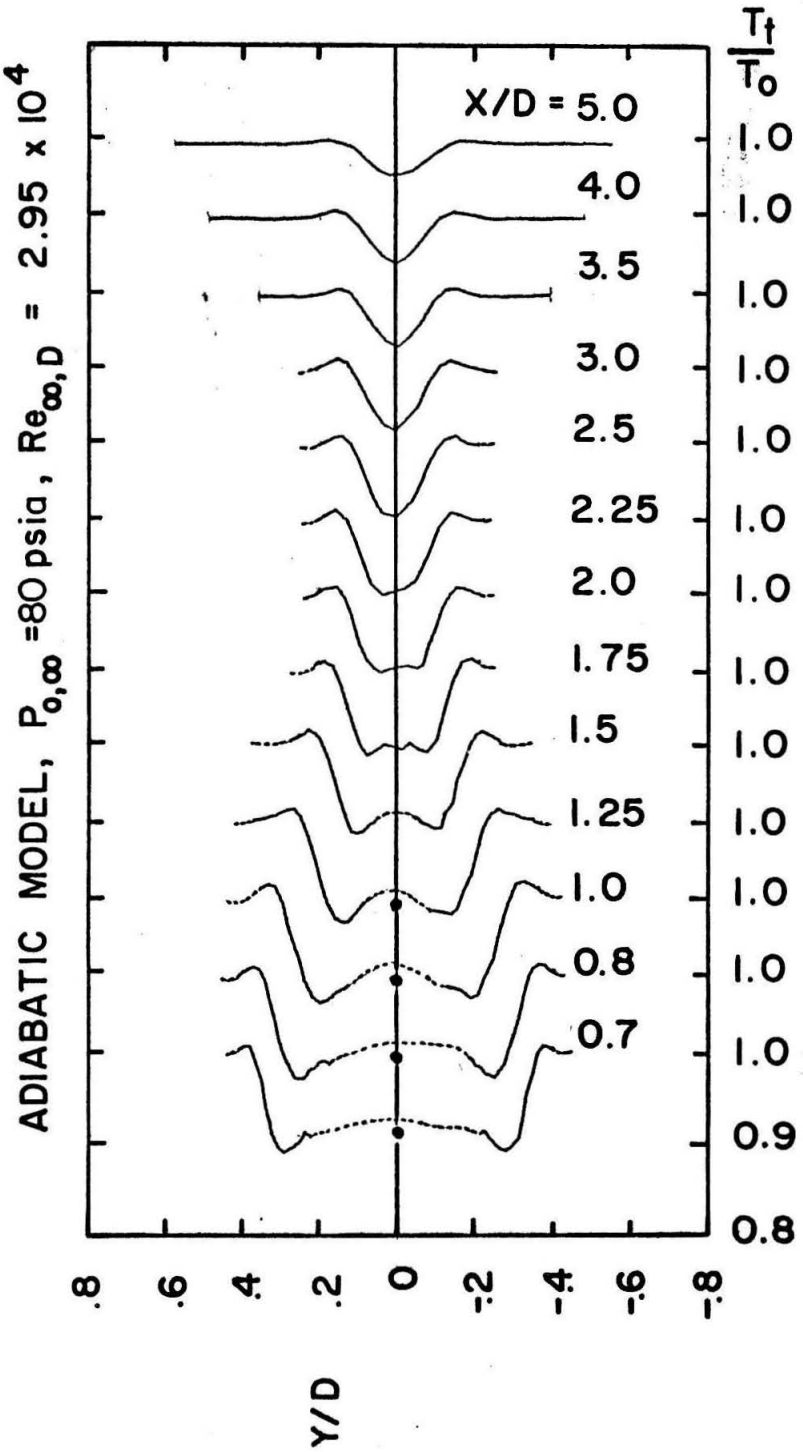

FIG.26b STAGNATION TEMPERATURE PROFILES

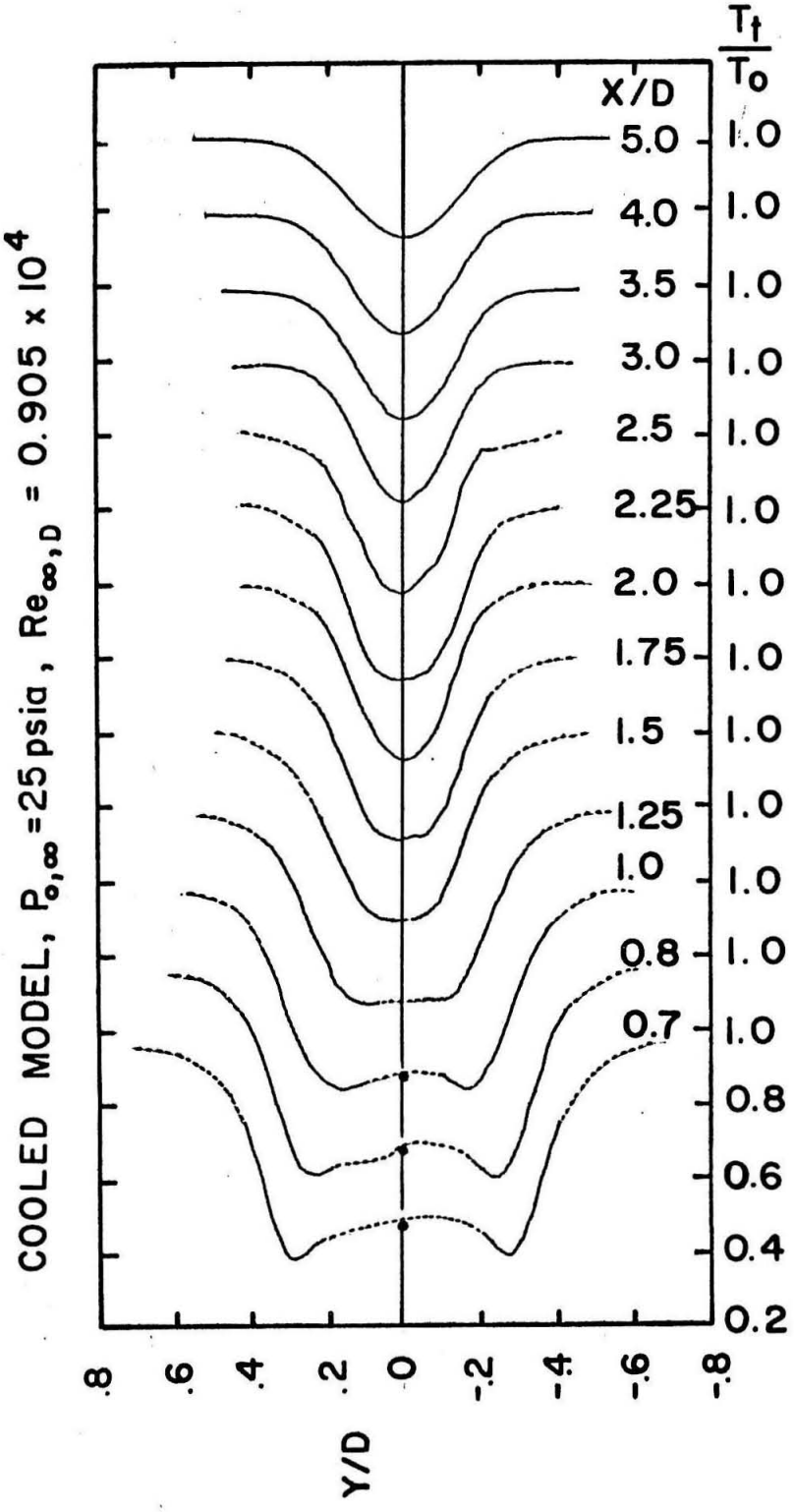

FIG.26c STAGNATION TEMPERATURE PROFILES

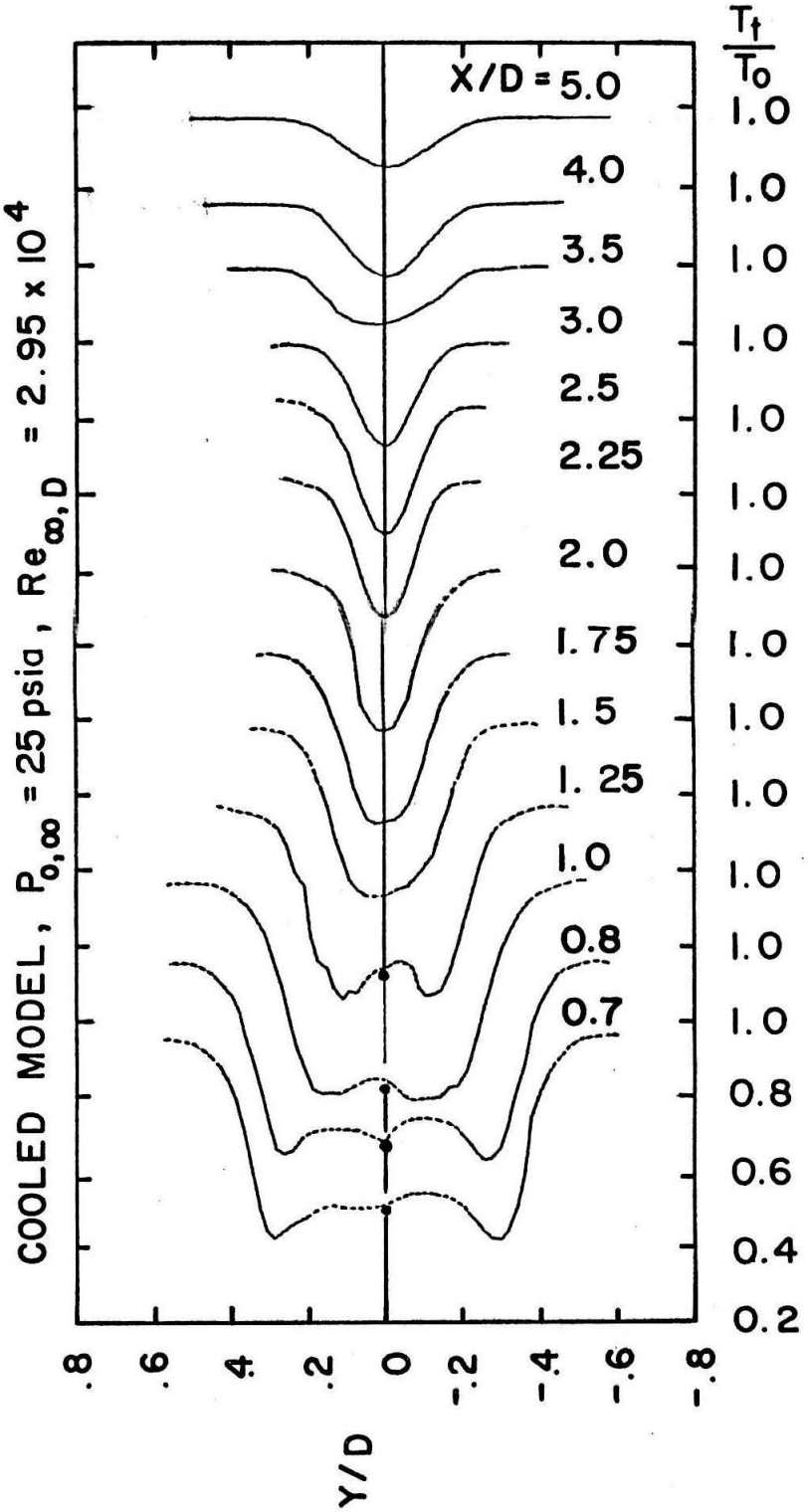

FIG.26d STAGNATION TEMPERATURE PROFILES

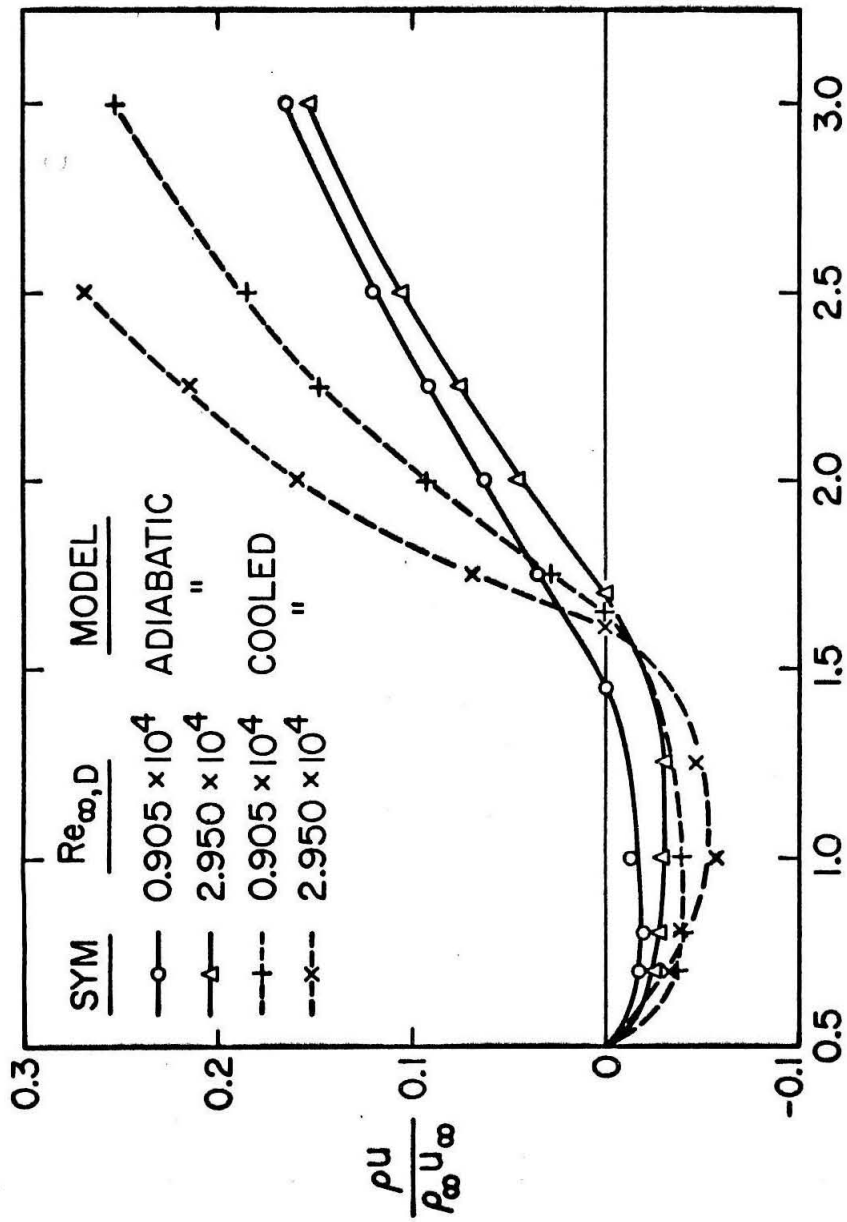

Fig. 27 CENTERLINE MASS FLOW VARIATION

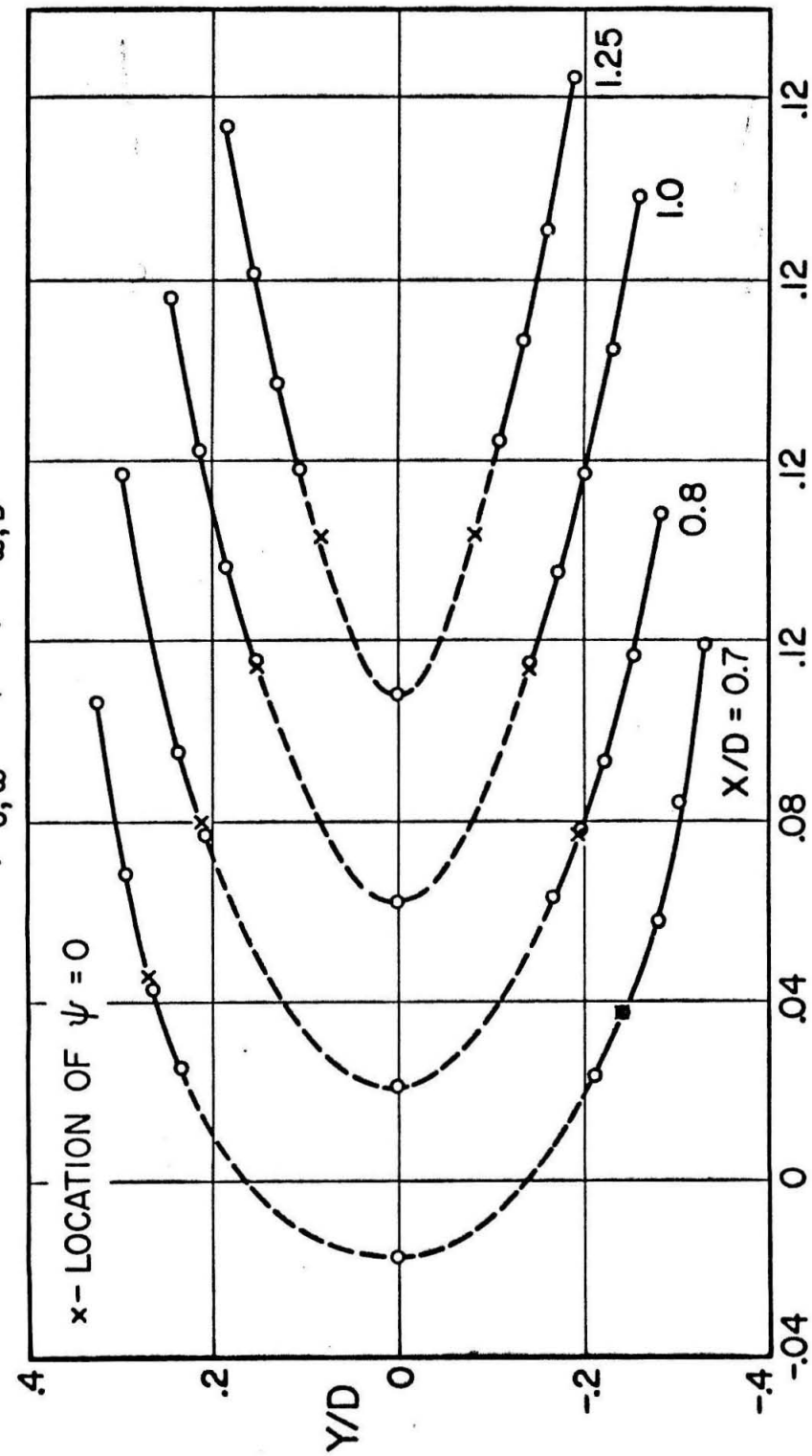

Fig.28a FAIRING OF MASS FLOW PROFILES IN REVERSE FLOW REGION

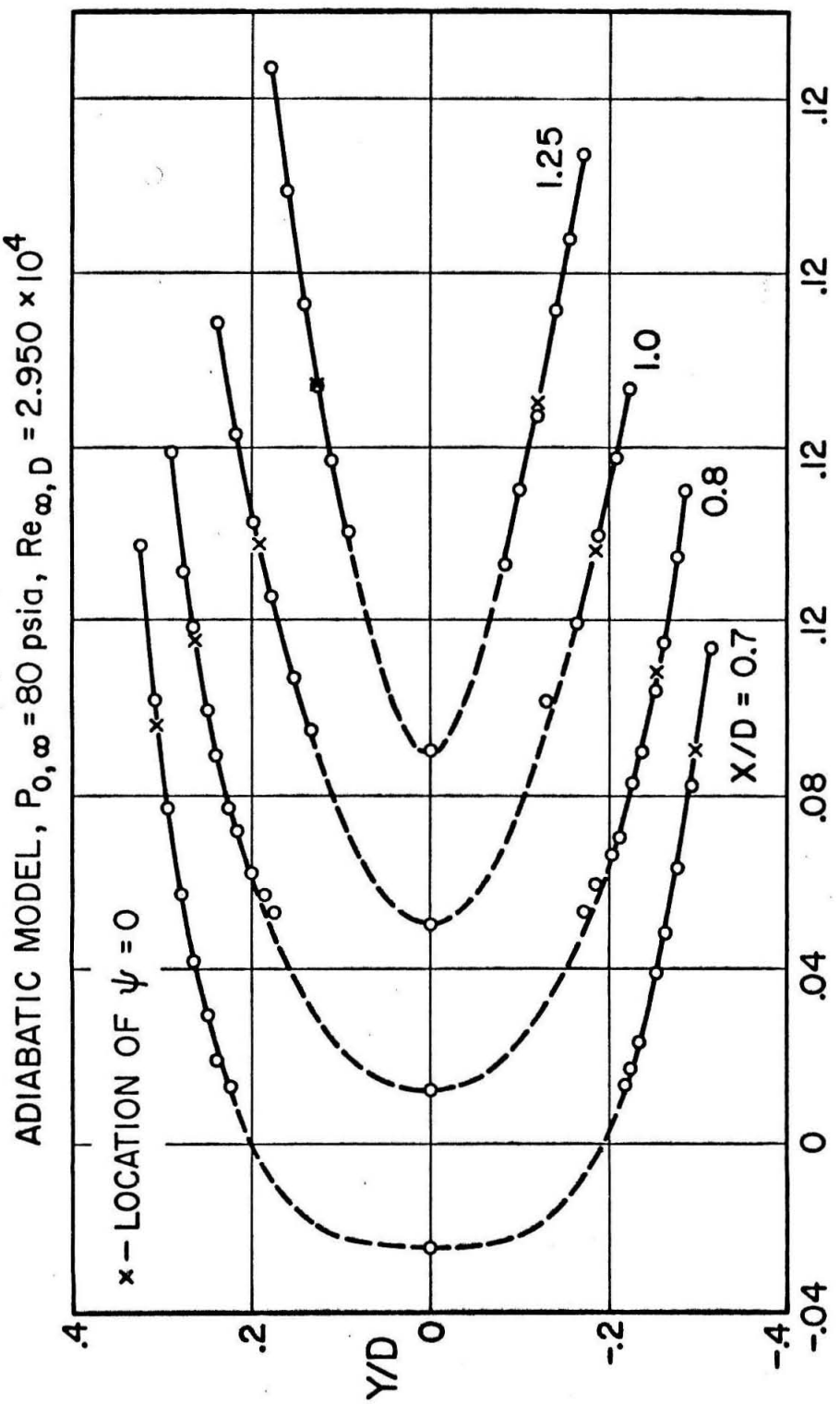

Fig. 28 b FAIRING OF MASS FLOW PROFILES IN REVERSE FLOW REGION

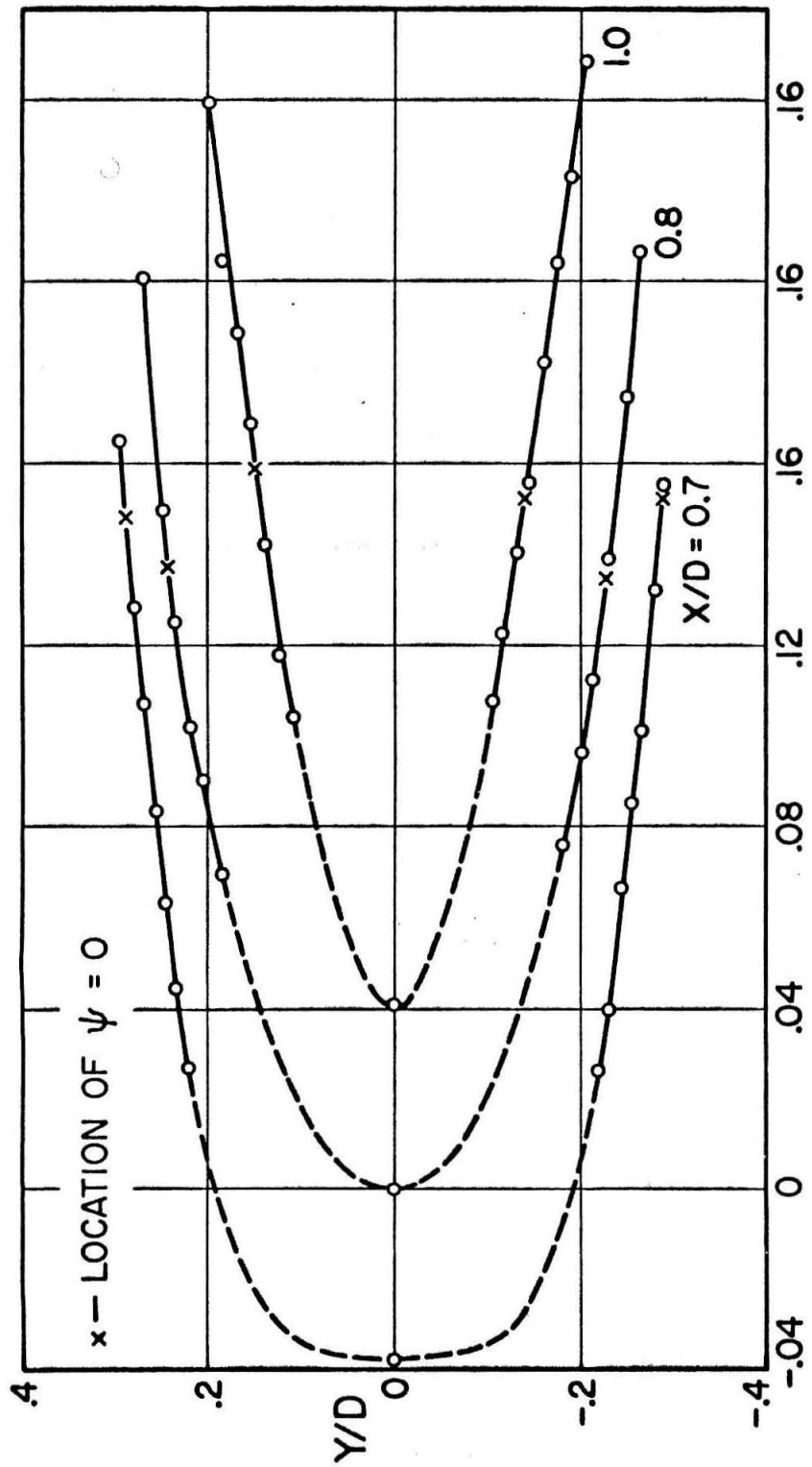

Fig. 28 c FAIRING OF MASS FLOW PROFILES IN REVERSE FLOW REGION

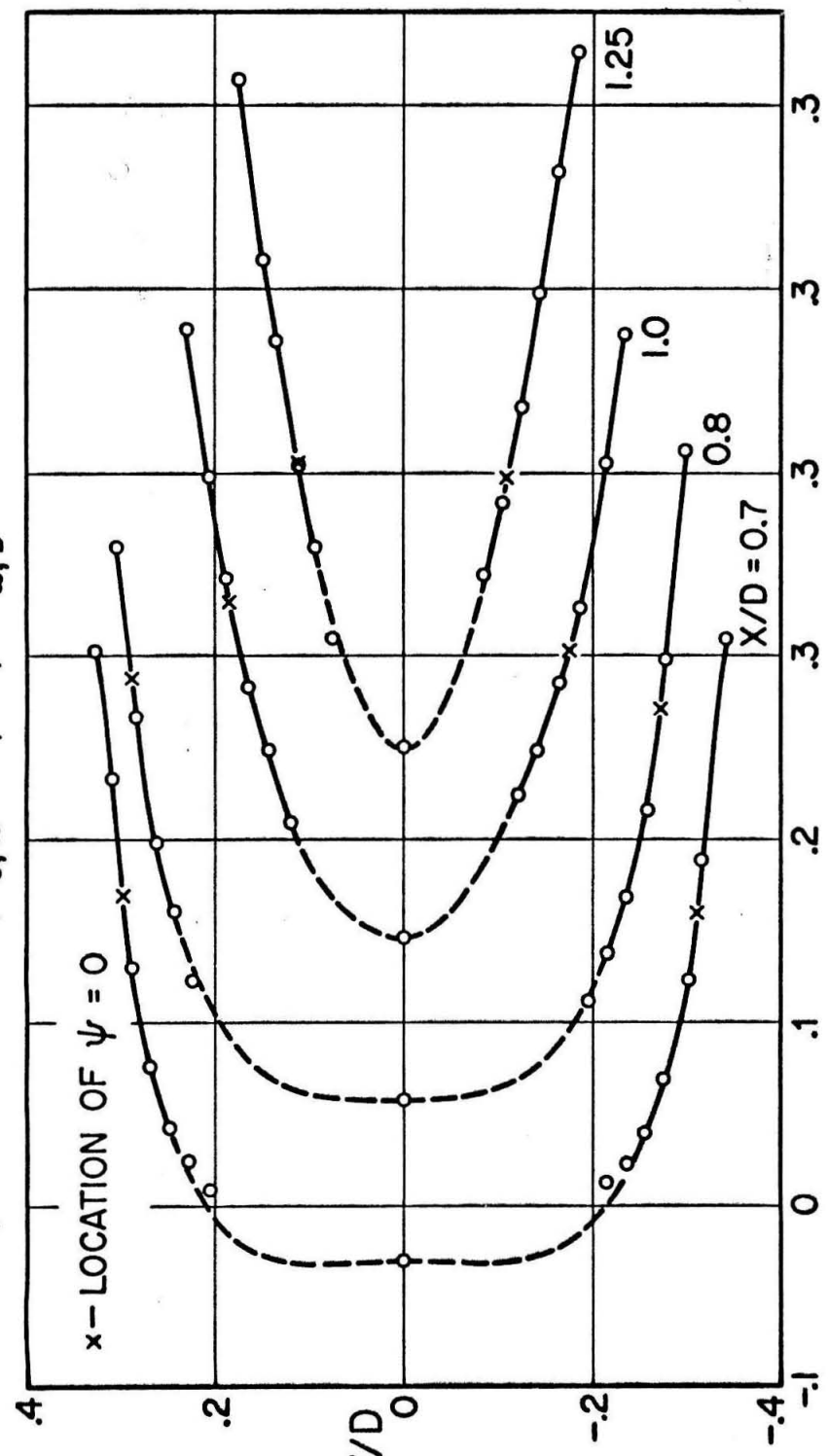

Fig. 28d FAIRING OF MASS FLOW PROFILES IN REVERSE FLOW REGION

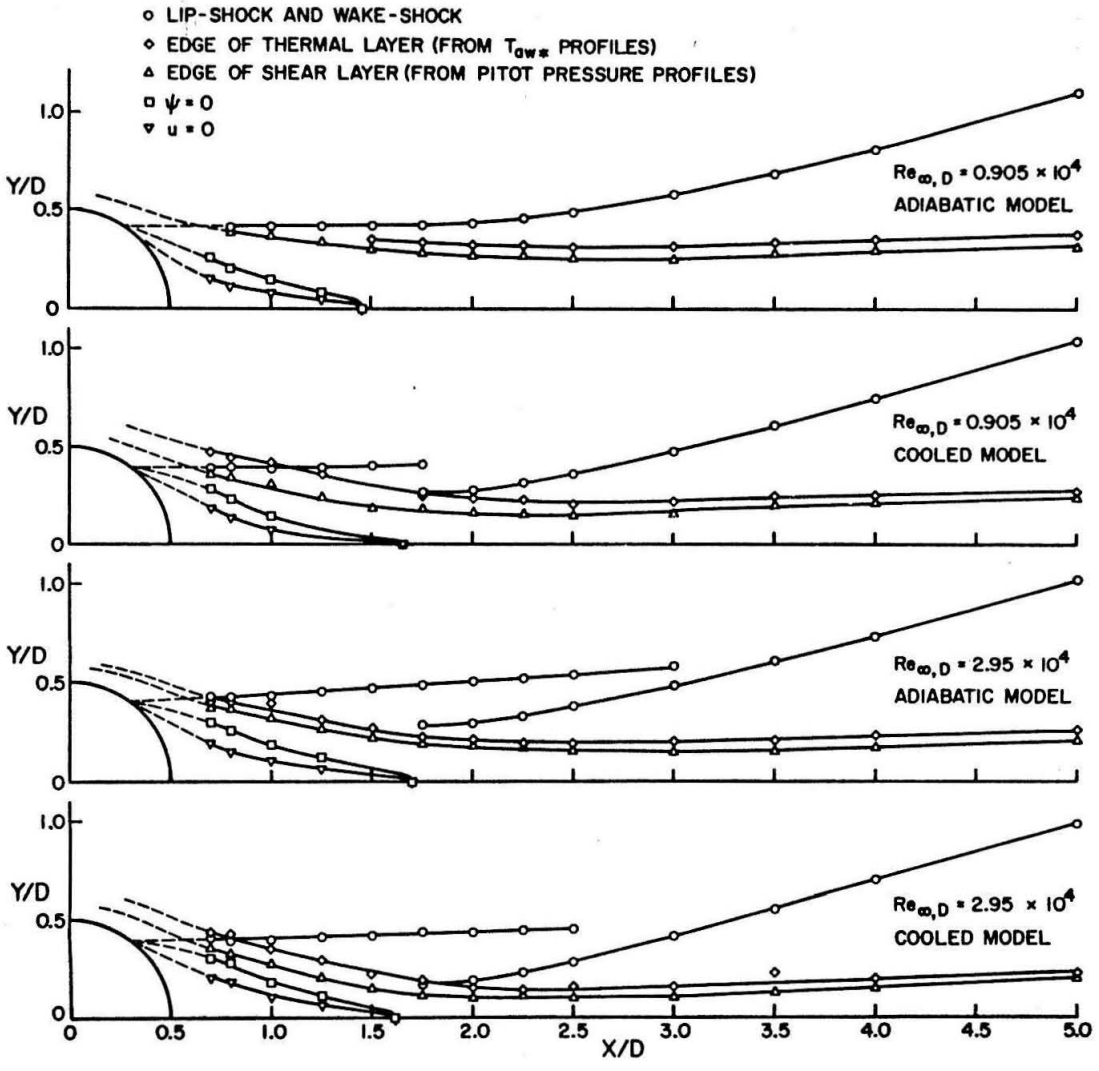

Fig. 29 NEAR-WAKE FLOW FIELD STRUCTURE

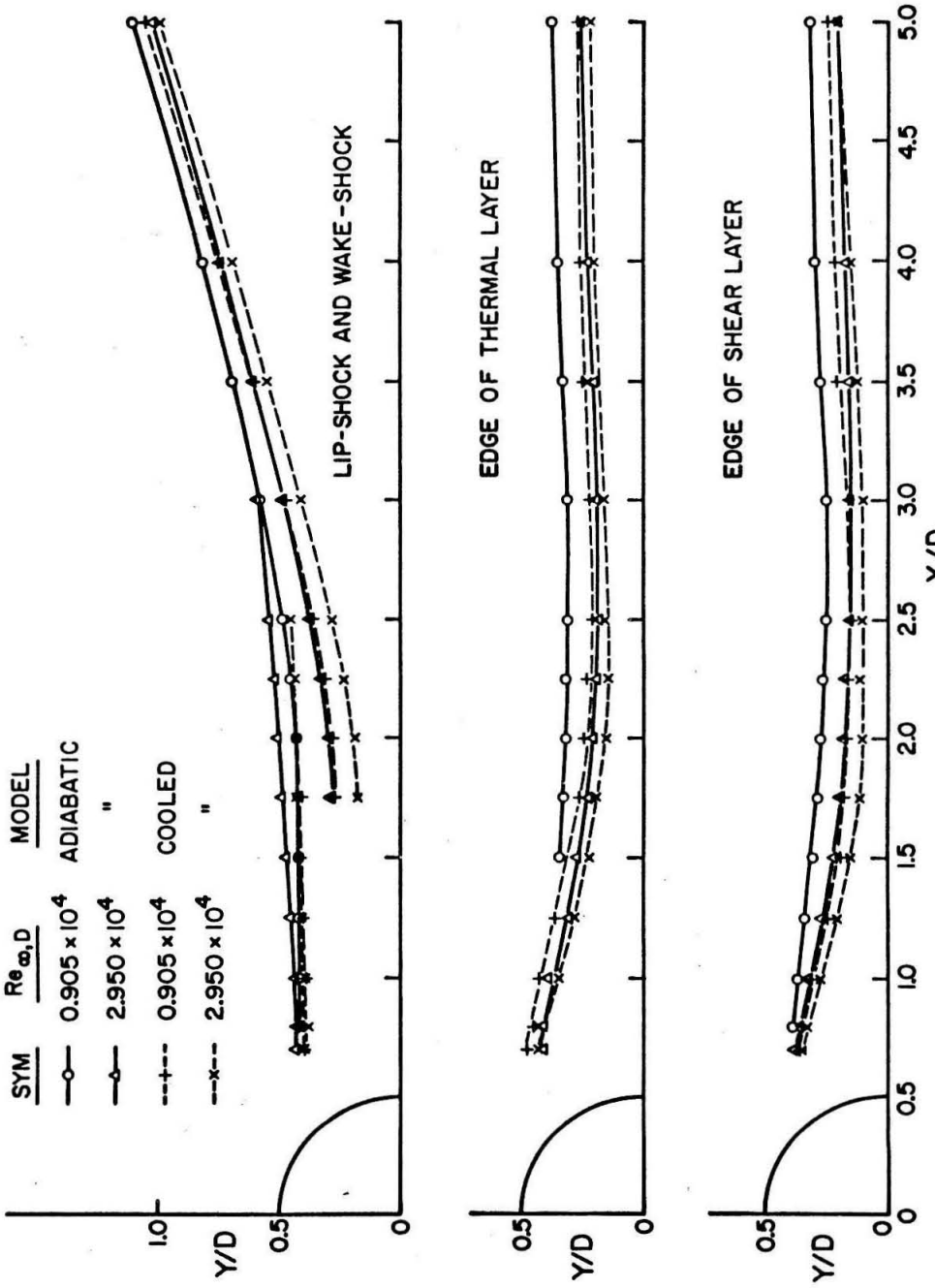

Fig. 30a EFFECT OF REYNOLDS NUMBER AND COOLING ON NEAR-WAKE

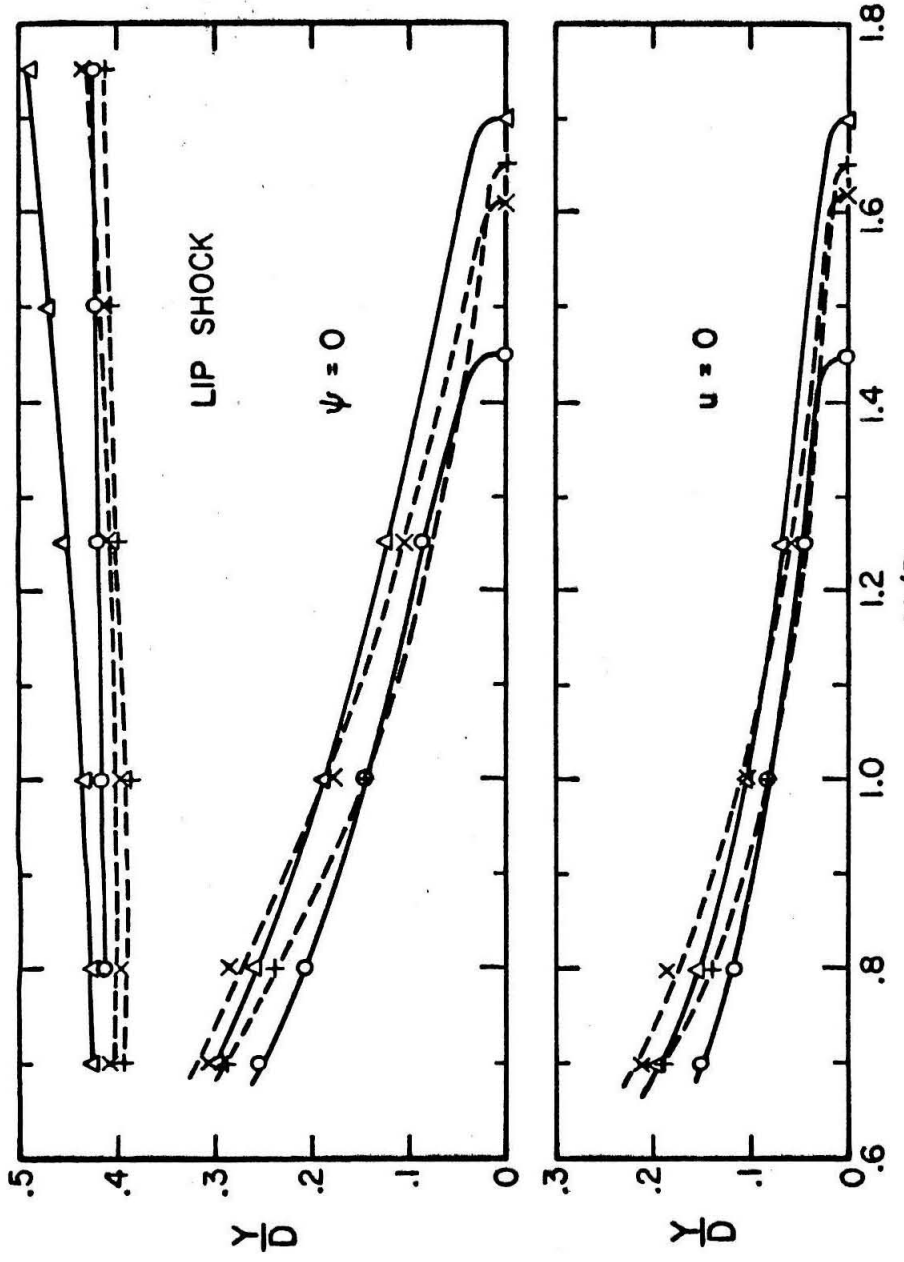

Fig.30 b EFFECT OF REYNOLDS NUMBER AND COOLING ON NEAR-WAKE

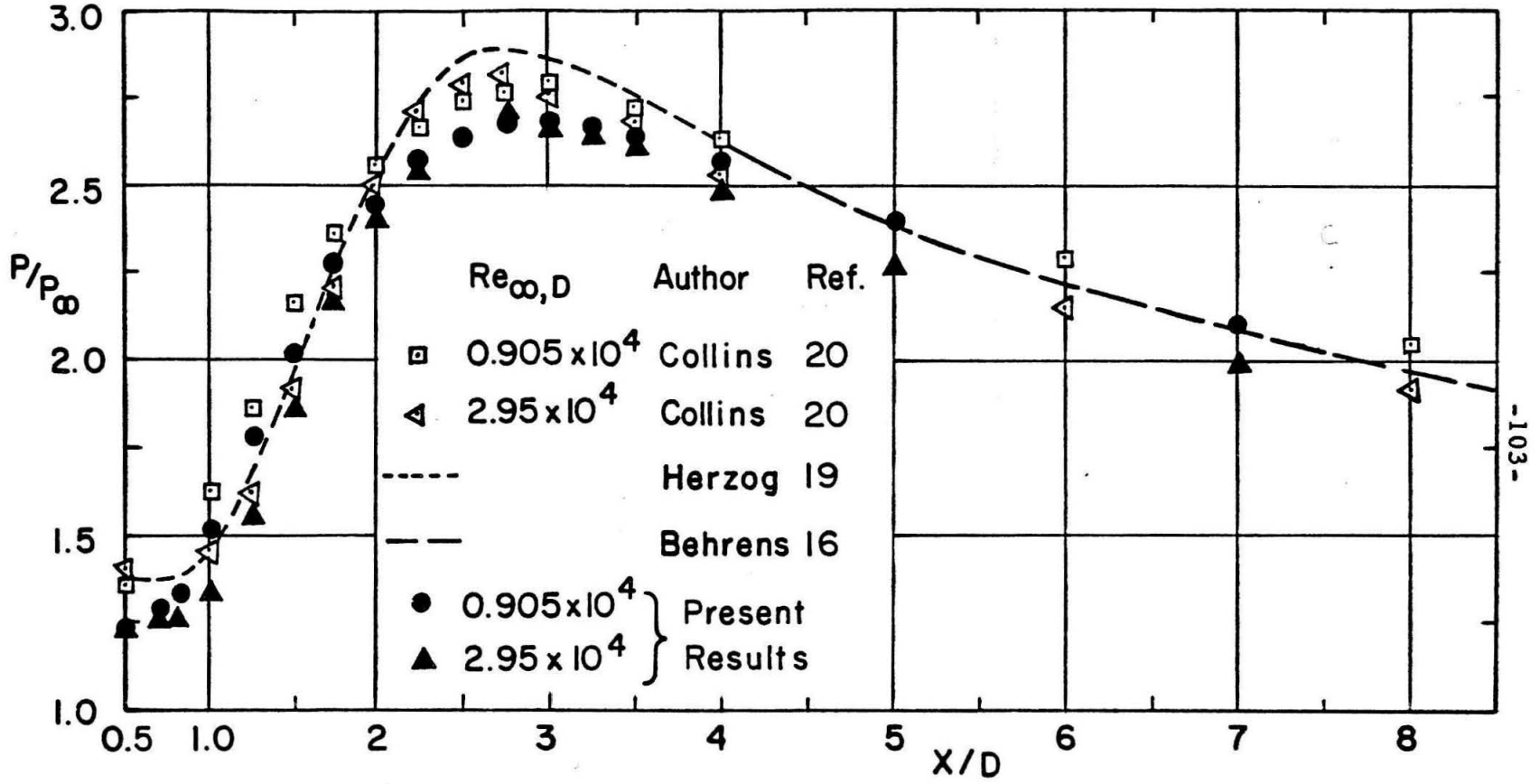

FIG. 31 COMPARISON OF CENTERLINE STATIC PRESSURE DISTRIBUTION WITH RESULTS OF OTHERS

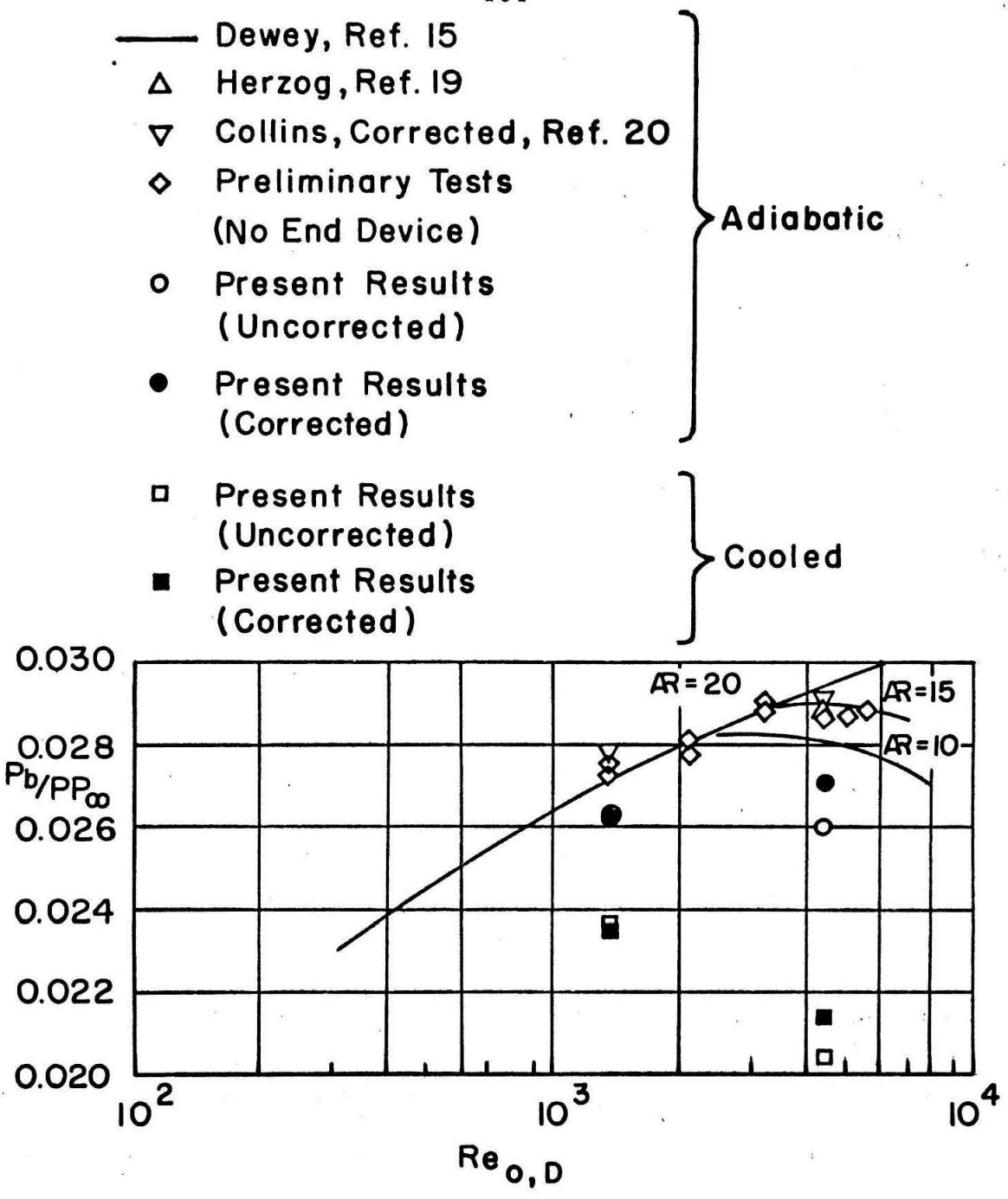

FIG. 32 BASE PRESSURE VARIATION WITH REYNOLDS NUMBER

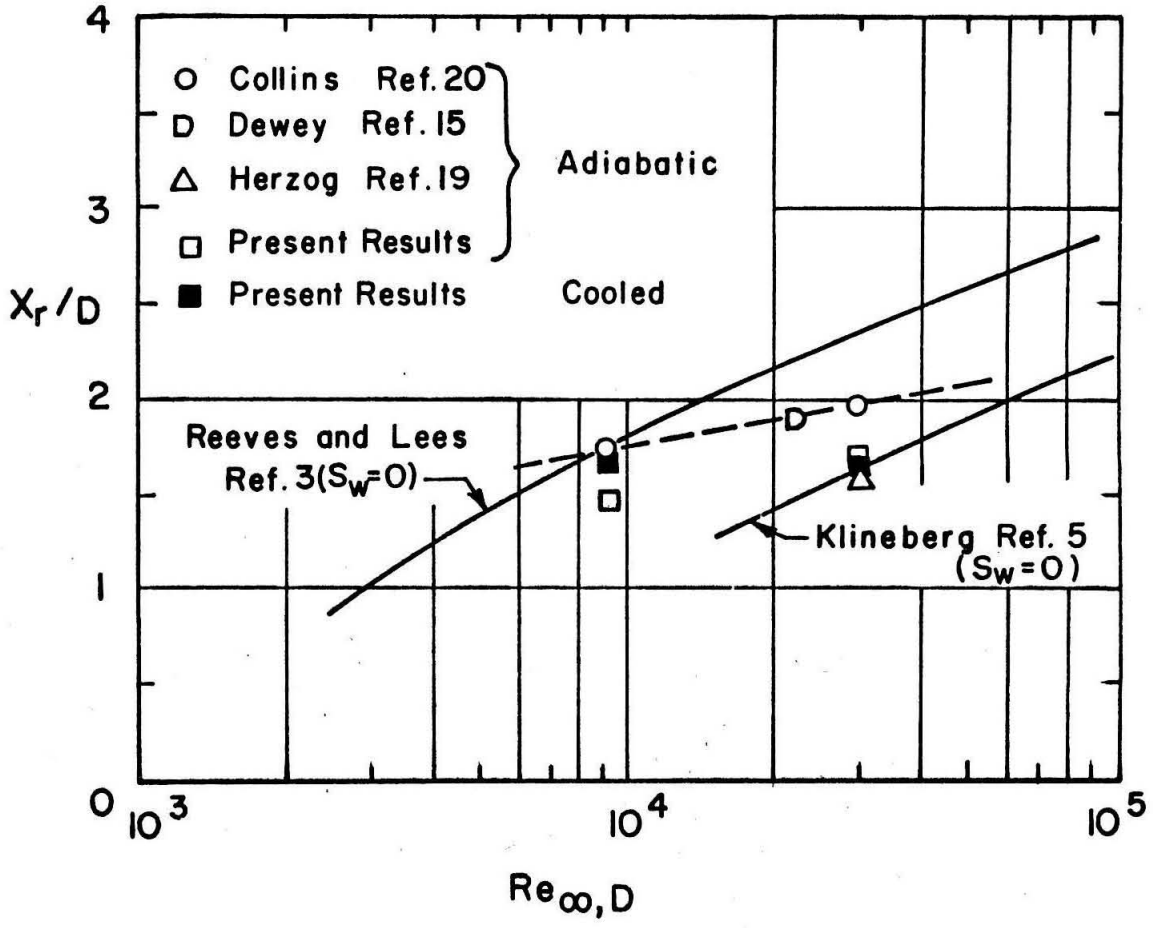

FIG.33 LOCATION OF REAR STAGNATION POINT

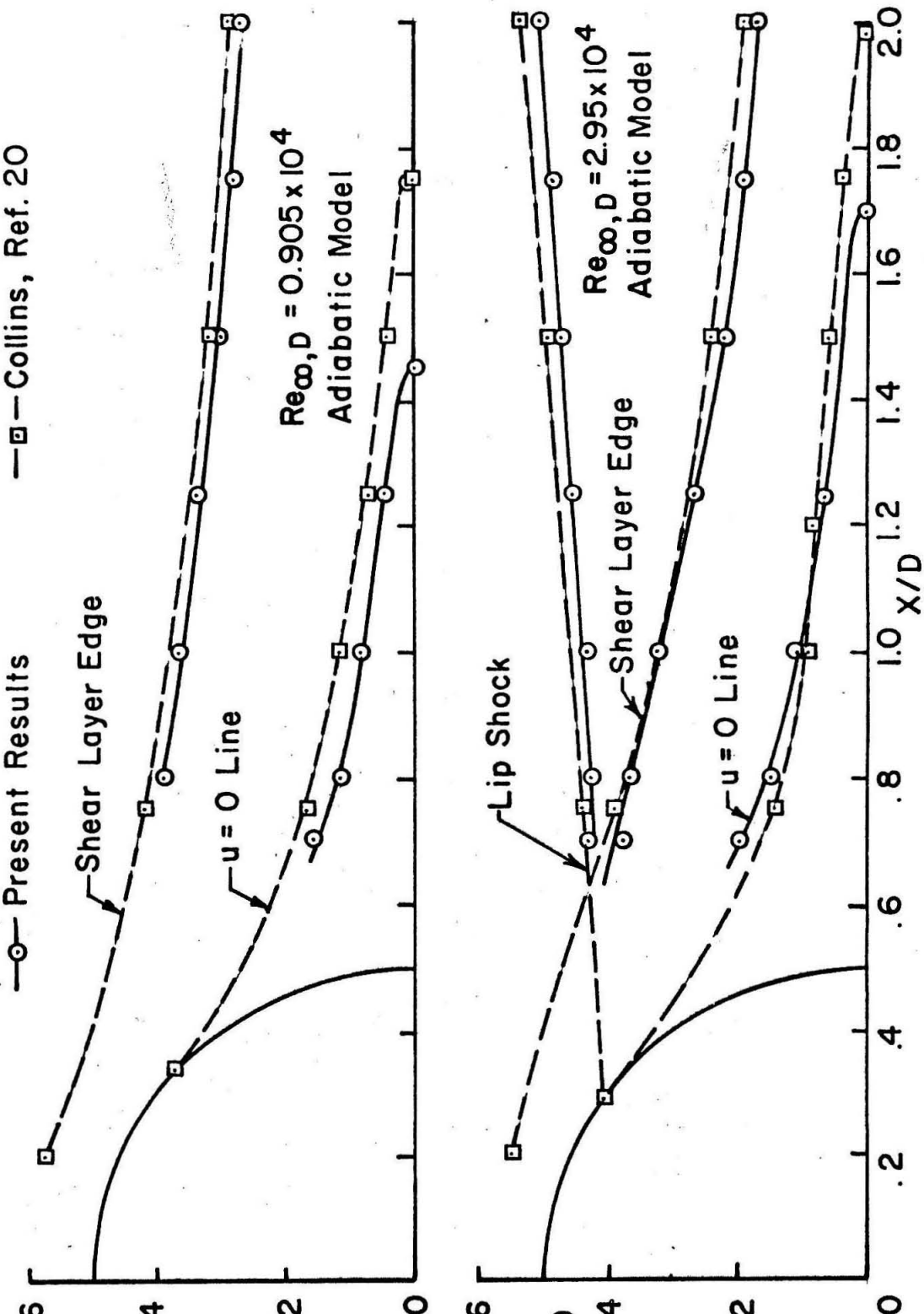

FIG. 34 NEAR-WAKE STRUCTURE-COMPARISON WITH COLLINS' RESULTS

APPENDIX A

TWO-DIMENSIONALITY OF THE FLOW

In order to obtain as good a two-dimensional flow as possible for the experiments described in the main text, preliminary tests described in this appendix were conducted. The tests were aimed primarily at minimizing the interaction and interference between the cylinder model and the side-wall boundary layer. The main criteria used in determining the two-dimensionality of the flow was the constancy of spanwise Pitot and static pressure behind the cylinder model in the symmetry plane. As pointed out by Ginoux[30] the spanwise distribution being constant does not necessarily mean that the magnitude of the quantity measured would correspond to the case of an infinite 2-dimensional flow. Therefore, in addition to obtaining as good a spanwise distribution as possible, it was indirectly confirmed, as explained later, that the values measured at the centerplane corresponded to true two-dimensional value. All these tests were conducted on an adiabatic model at a tunnel stagnation pressure of 25 psia and a stagnation temperature of 408°K at a nominal Mach number of 6.0. It is hoped that the final configuration for the end-device for obtaining two-dimensional flow arrived at by these tests would serve that purpose for the other cases in the main experiment also.

Models

The basic model as well as its adaptation to various cases is shown in Figure A1. It is a 0.2" dia. cylinder protruding into the test section. The long support prevented any significant vibration or deflection of the cylinder.

The model served as:

(a) The "basic cylinder model," when the free end butted against the opposite side wall;

(b) The "model with subsonic fences" when subsonic fences were fixed on it by means of epoxy resin;

(c) The "model with supersonic fences," when supersonic fences were fixed on it;

(d) The "model with wedge fairing of variable length," when wedge fairings were soldered onto it; and

(e) the "protruding model" as well.

For the case (d) above, the opposite port had a diamond shaped recess and thus the extent of wedge fairing protruding into the flow could be varied.

In addition to the above, the 0.2" dia. cylinder model with wedge fairings at both ends (Figure A1) used by Behrens,[16] was also used. In fact, this model was first tested before going on to case (d) and since this model showed improvement over that of the models with fences, it was decided to check on the effect of the spanwise extent of the fairing and thus led to case (d).

The subsonic fence used here had the same dimensions as that used by Collins.[20]

The dimensions of the supersonic fence were fixed by the following considerations.

i) The trailing edge of the fence should be downstream of the sonic point, which, from the results of the previous investigators, was known to be around an X/D of 3.5 from the center of the cylinder.

ii) The top and bottom edges of the fence should be beyond the separation shocks, the locations of which were obtained from Schlieren pictures taken by earlier investigators.

Side-wall Mounted Traverse Mechanism

The traverse mechanism used for making Pitot and static pressure measurements is shown in Figure A2. The vertical motion was obtained by means of a lead screw driven by a small electric motor. A 10 turn helipot potentiometer was connected to the lead screw through a worm gear. The spanwise traverse was manual and was obtained through a rack, by rotating the knob attached to the pinion. A set screw was provided to lock it in position. Backlash was prevented by hanging a weight from a thread attached to the rack and passing over a pulley and round the shaft of another potentiometer. A dial reading was provided for this spanwise traverse. The output of the potentiometer was fed into the X input of X-Y recorder and the dial reading was used to set the zero and range on the X-Y recorder.

Pitot and Static Pressure Probes

The Pitot pressure probe used in these tests is shown in Figure A-3. It had an opening of 0.006" x 0.08". The longer edges of the opening were parallel to the cylinder.

The dimensions of the static pressure probe are also shown in Figure A-3. The static holes were aligned parallel to the cylinder. The front end of the static probe was flat and sealed. When the static holes were located at an X/D of 3.0, the front end was within the re-circulating region and hence the blunt end is expected to have no appreciable effect on the static pressure measurement at X/D = 3.0.

However, in the case of the protruding cylinder model, the measurement of the static pressure had to be limited to the base region and could not be extended beyond the free end.

The Pitot and static pressure probes were simply introduced into the probe holder of the traverse and held in position by two small Allen set screws. This also permitted positioning of the probes at the desired X/D values. Leakage was prevented by two O-rings.

By using shims between the tunnel side wall and the port on which the traverse was mounted, it was possible to adjust the side wall traverse such that the probe moved parallel to the cylinder within about 0.002".

Both the Pitot and static pressures were measured by a 5 psi statham pressure transducer the output of which was recorded after suitable amplification on the X-Y recorder. The vacuum reference for the pressure transducer was maintained at less than 0.5 microns which was often checked by a McLeod gauge.

Results and Discussion

All the tests were run at a stagnation pressure of 25 psia, stagnation temperature of 408°K and nominal free stream Mach number of 6.0. The free stream Reynolds number based on the cylinder diameter of 0.2" was 0.905×10^4.

Spanwise distribution of Pitot pressure at X/D = 0.6 and X/D = 2.0, and spanwise distribution of static pressure at X/D = 3.0 for the basic cylinder model, the model with subsonic fences, the model with supersonic fences, and the model with wedge fairing at both ends (Behrens' model) are compared in Figure A-4.

The Pitot pressure distribution at X/D = 0.6 which corresponds very close to the base pressure, shows that for the basic cylinder model, the pressure increases initially as one proceeds toward the wall from the centerline and then the trend reverses and the pressure drops near the wall. The same trend is seen for the static pressure distribution at X/D = 3.0 for the basic cylinder model. The Pitot pressure distribution at X/D = 0.6 and the static pressure distribution at X/D = 3.0 for the model with subsonic fences, and the model with supersonic fences, show trends very similar to that of the basic cylinder model over the region between the fences to which the measurements had to be limited. In fact, the Pitot pressure distribution at X/D = 0.6 show greater pressure gradients for the model with fences than without it. On the other hand, it is seen that, for the model with wedge fairing at both ends, the Pitot pressure distribution at X/D = 0.6 and the static pressure distribution at X/D = 3.0 are more uniform and shows definite improvement towards two-dimensionality of the flow.

From the Pitot pressure distribution at X/D = 2.0 shown in Figure A-4, no definite conclusion as to the superiority of any configuration could be drawn. The waviness in this pressure distribution was attributed to the disturbances caused by tiny droplets of oil which formed all along the separation line on the cylinder. The difficulty of maintaining the probe in the plane of symmetry during a spanwise traverse might have also contributed to the waviness.

It may be pointed out that the pressure level in the center region is nearly the same (within experimental scatter) for all these cases

indicating that the end effects are perhaps limited to the ends only.

A sketch of the shock configurations at the root and the free end of a protruding cylinder in supersonic flow, based on the results of Sykes,[31] is shown in Figure A-5. The C_p distribution near the root, along the stagnation line, is also shown in Figure A-5. It shows very clearly the upstream interaction of the side wall boundary layer with the cylinder. Because of the λ shock formation, C_p distribution along the upstream stagnation line is quite understandable. Hence the stagnation pressure of the fluid which is going over the cylinder surface is not uniform along the span, and has a maximum somewhere between the wall and the centre. It is conjectured that most of the non-uniformity in the pressure measurements downstream of the basic cylinder model is basically caused by this non-uniformity just upstream of the model. Therefore, since the the provision of fences either subsonic or supersonic in no way influences the upstream interaction, it is understandable that they hardly improve the flow uniformity compared to the basic cylinder model. On the other hand it is felt that the wedge fairing prevents the formation of the λ shock and the associated boundary layer separation. The interaction of the oblique shock waves from the leading edge of the wedge with the bow wave of the cylinder is expected to be local, and also weaker. Hence the better performance of the wedge fairing is perhaps understandable.

Since Behrens' model did show considerable improvement in the flow, it was felt that a study to find the optimum length of the wedge projecting into the flow from the wall would be worthwhile. Hence the model with wedge fairing of variable length shown in Figure A-1 was

tested. For ease of testing, the wedge was provided on only one end and the length of the wedge projecting into the flow was varied by varying the extent to which the wedge was inserted into the recess in the port.

The pressure measurements were carried out over the half span containing the wedge since it was checked in a few cases that pressure distribution over the other half did not alter and corresponded to the case of the basic cylinder model.

Figure A-6 shows the Pitot pressure distribution at an X/D of 0.6 for various wedge projections. It is seen that up to L = 3/8" the pressure distribution almost corresponds to that of the basic cylinder model. For L = 19/32" which corresponds nearly to the case of Behrens' model (1/32" shorter), the pressure distribution has become quite uniform and beyond L = 19/32", the extent of the uniform pressure region decreases.

Figure A-7 shows the static pressure distribution at X/D = 3.0 for various wedge projection lengths. This also shows similar trend. However, the static pressure distribution does not become quite uniform for L = 19/32", though it is reasonably satisfactory. In fact, though the pressure distribution improves as L is increased further, the extent of uniform region does not. From Figure A-6 it appears that the Pitot pressure distribution at X/D = 0.6 worsens beyond L = 19/32".

Figure A-8 shows the Pitot pressure distribution for X/D = 3.0. It is seen that as L is increased beyond 19/32", the extent of the relatively uniform pressure distribution decreases. The shock from the

wedge appears first for L = $\frac{1}{2}$" indicating that the boundary layer is about 3/4". For the same reason, it is seen in Figure A-6 and A-7 that the effect of the wedge is hardly felt up to L = $\frac{1}{2}$".

On the whole it is reasonable to conclude that L = 19/32", or in other words the configuration of the Behrens' model is the optimum choice for the wedge fairing.

As pointed out at the very beginning the uniformity in the spanwise pressure distribution may not necessarily mean that the magnitude of the pressure corresponds to the true two-dimensional value. It was believed, however, that if the magnitude of the pressure in the center region was not affected when the end effects are of opposite character, then it could be assumed that the value in the center region corresponds to the two-dimensional value. With this in view some tests with the protruding cylinder model were conducted.

Figure A-9 shows the Pitot pressure distribution at X/D = 0.6 and the static pressure distribution at X/D = 3.0 for various gaps between the cylinder end and one of the walls. For G = $\frac{1}{2}$", both of these pressure distributions agree with the pressure distributions for the zero gap case (i.e. basic cylinder model) probably due to the free end being within the boundary layer of the side wall which was expected to be about 3/4" thick. For these, it is seen that the pressure increases initially as one proceeds away from the center.

For G = 1" and 1$\frac{1}{2}$", the pressure near the free end drops due to the expansion and flow around the edge (Figure A-5). The end effects in this case are obviously opposite in character to the case of G = 0. If the end effects affected the center plane pressures, then clearly at

least for G = $1\frac{1}{2}$", the pressure at the center should have been less than that for G = 0 case. In fact G = $1\frac{1}{2}$" is rather a severe case since the end is just 5 diameters away from the centerline. But it is seen from Figure A-9 that the pressure distribution in the center region and beyond is unaffected.

Hence it can be reasonably concluded that the mid-plane pressure measurements would correspond to the two-dimensional case even without any end device, but the use of wedge fairing at both ends (Behrens' model) would improve the two-dimensionality of the flow. Therefore, the configuration of the Behrens' model was used for the experiments described in the main text. It should, however, be pointed out that the two-dimensionality tests were conducted only for the adiabatic model at 10 psig stagnation pressure, whereas the near wake experiments were conducted for both adiabatic and cold models and for stagnation pressures of 10 psig and 65 psig. It is hoped that the same conclusions regarding two-dimensionality would hold good for these other cases.

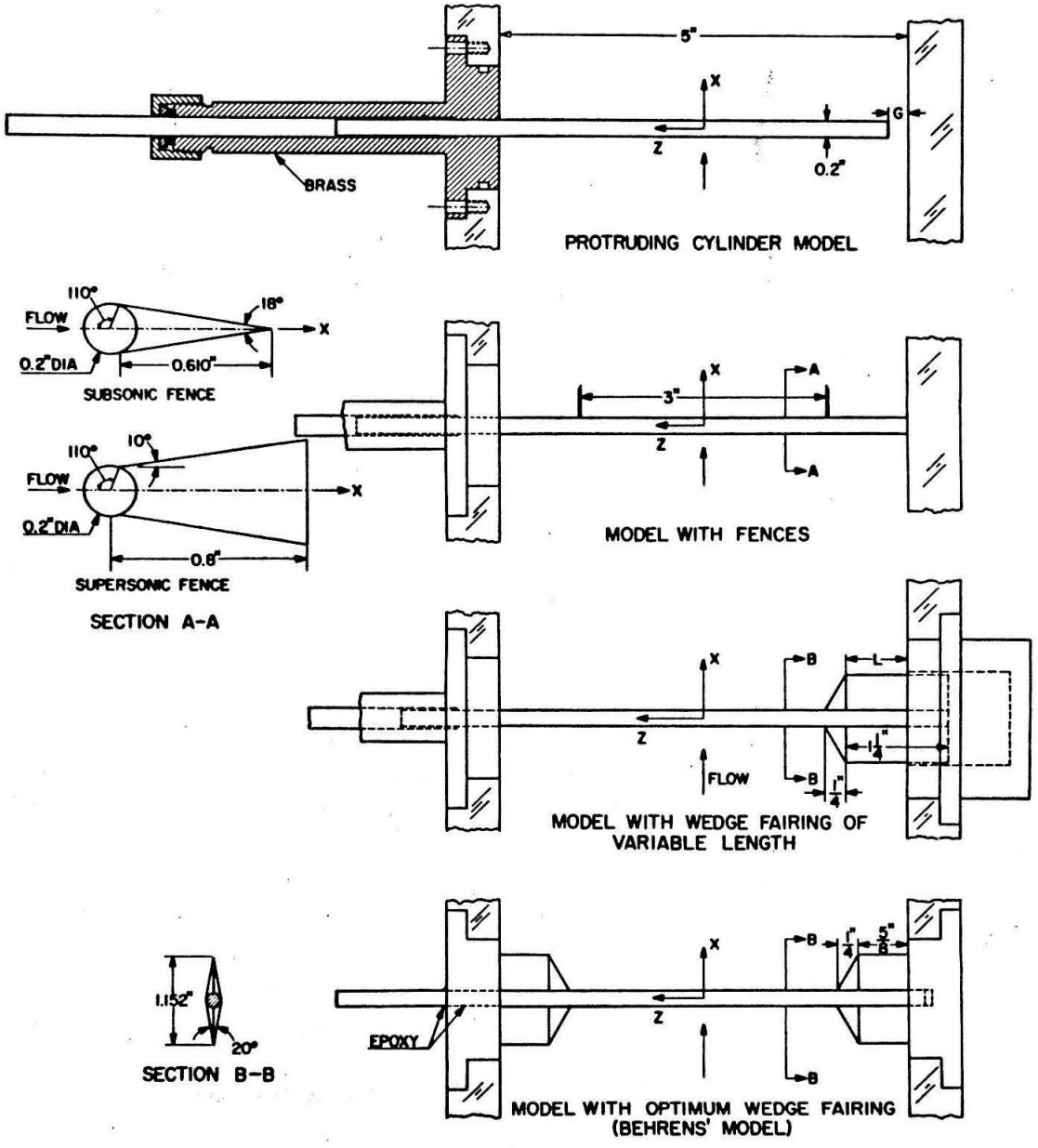

Fig. A-1 MODELS

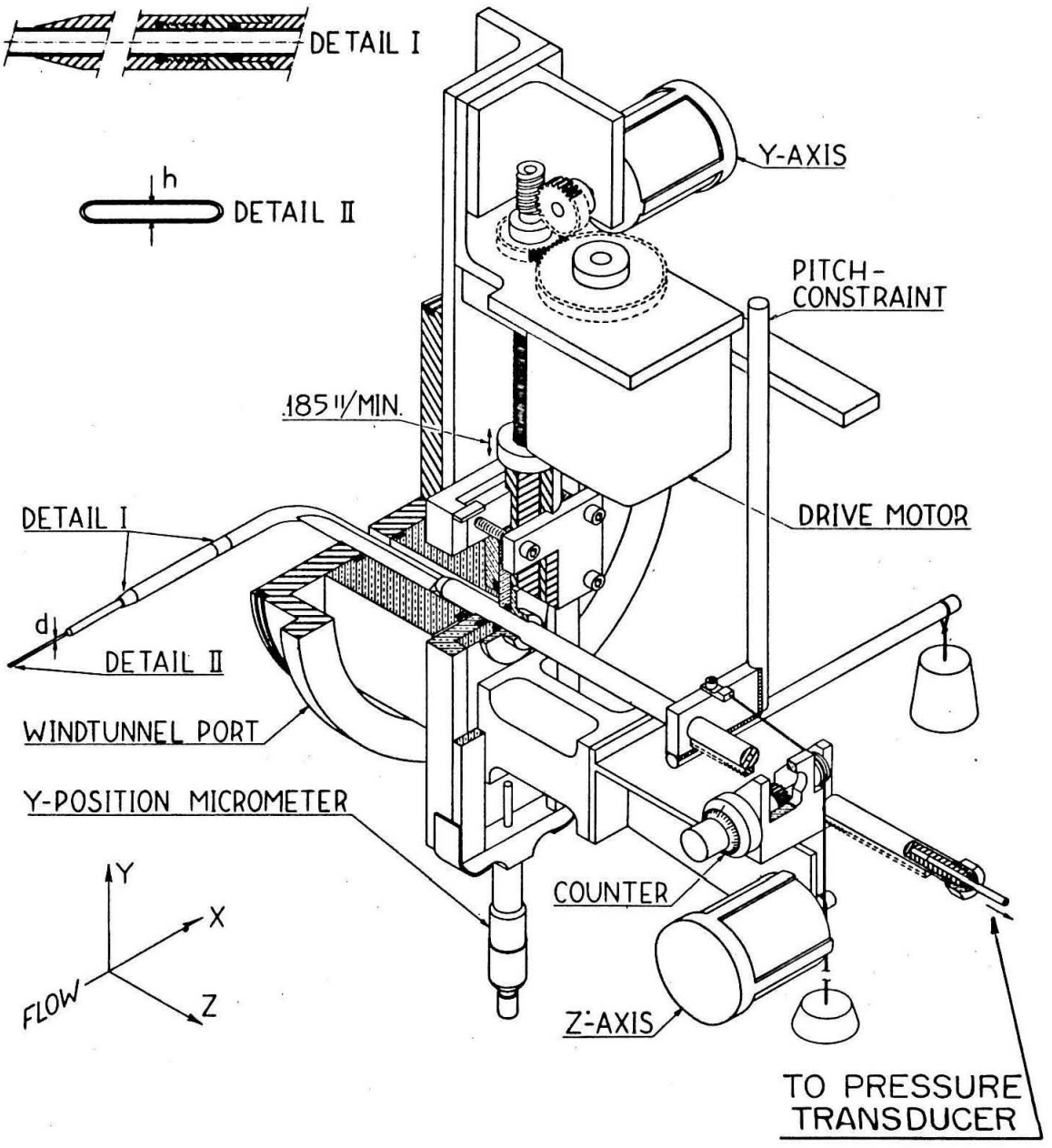

FIG.A-2 SPANWISE TRAVERSE MECHANISM

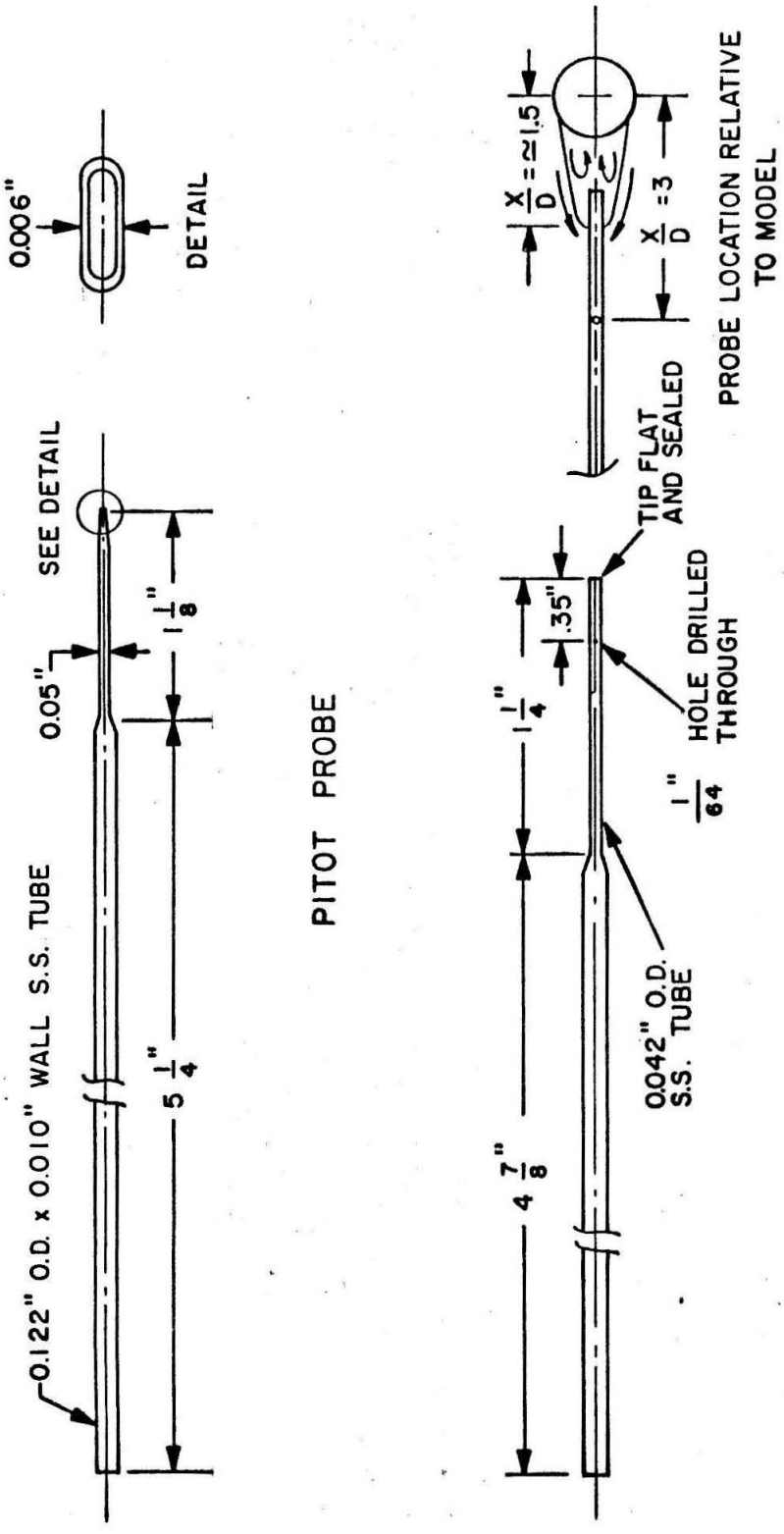

Fig. A-3 PITOT AND STATIC PRESSURE PROBES

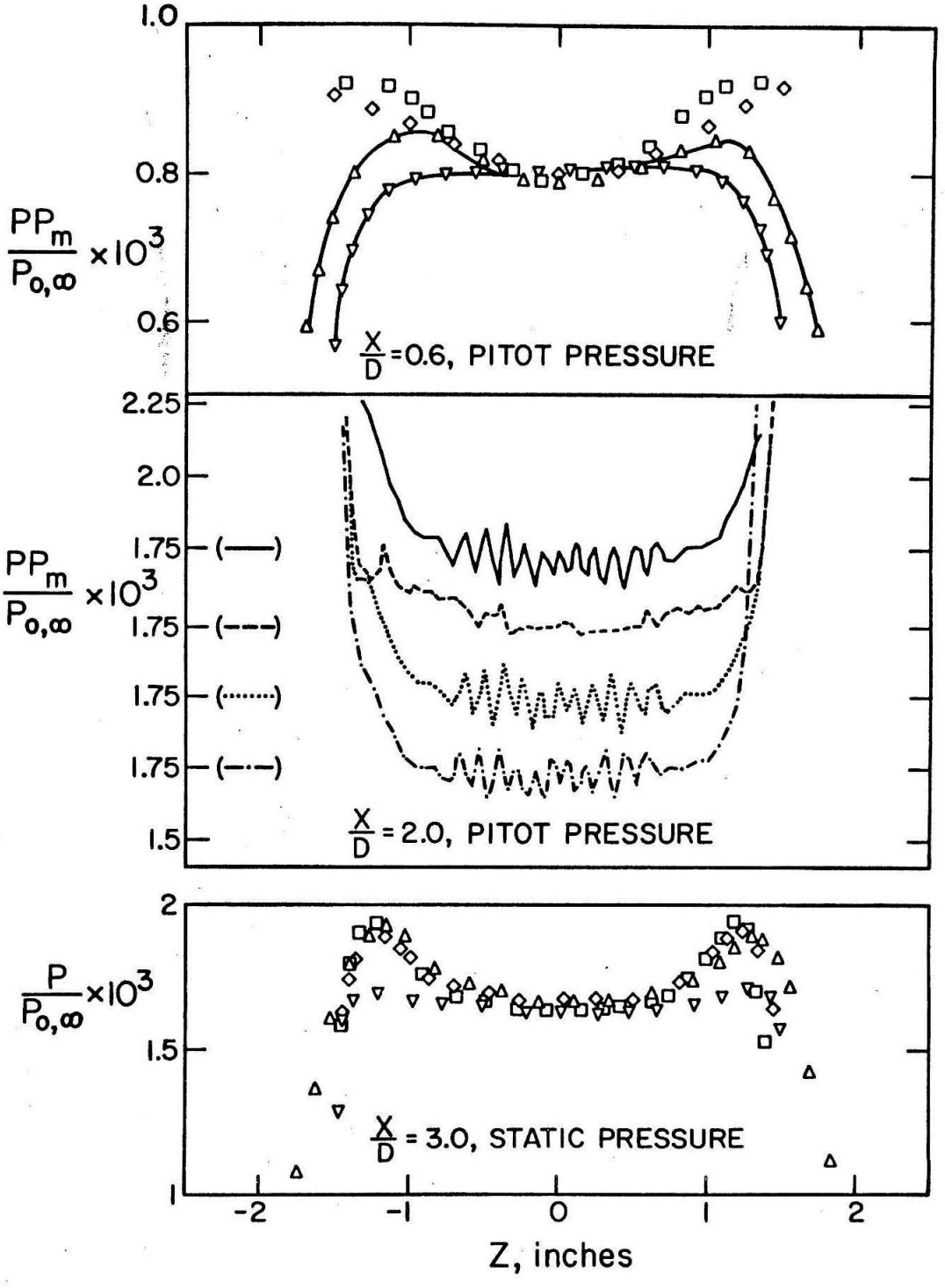

——; △ BASIC CYLINDER, ·····; ◇ CYLINDER WITH SUBSONIC FENCES

– – –; ▽ BEHRENS' MODEL, –·–·; □ CYLINDER WITH SUPERSONIC FENCES

Fig. A-4 SPANWISE PRESSURE DISTRIBUTIONS

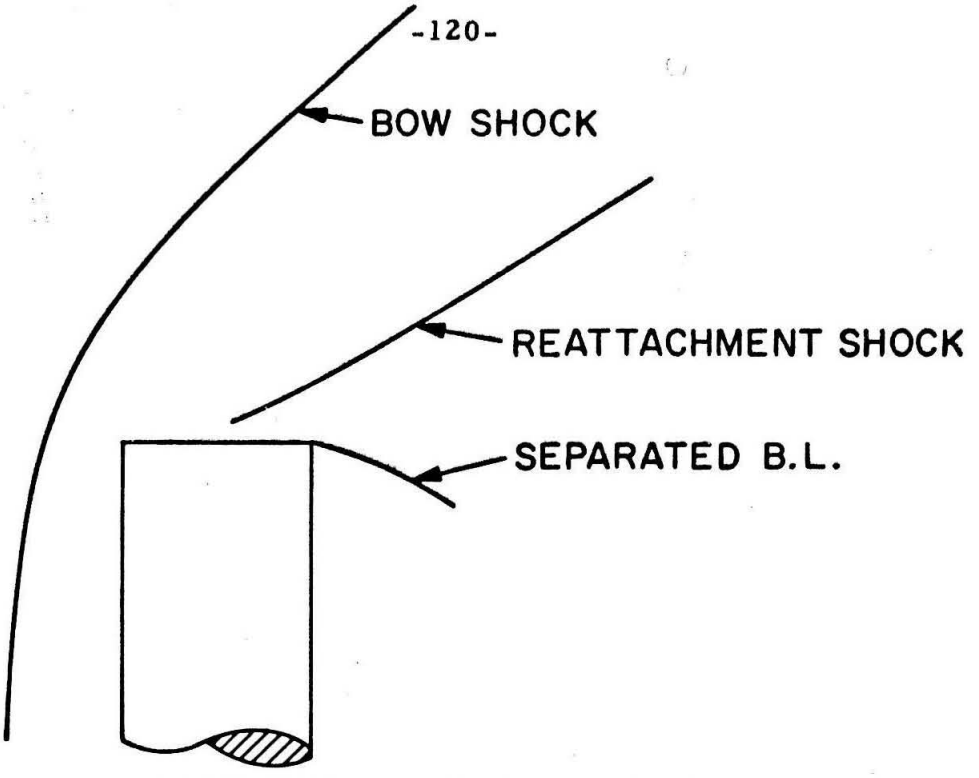

FREE-END SHOCK POSITIONS

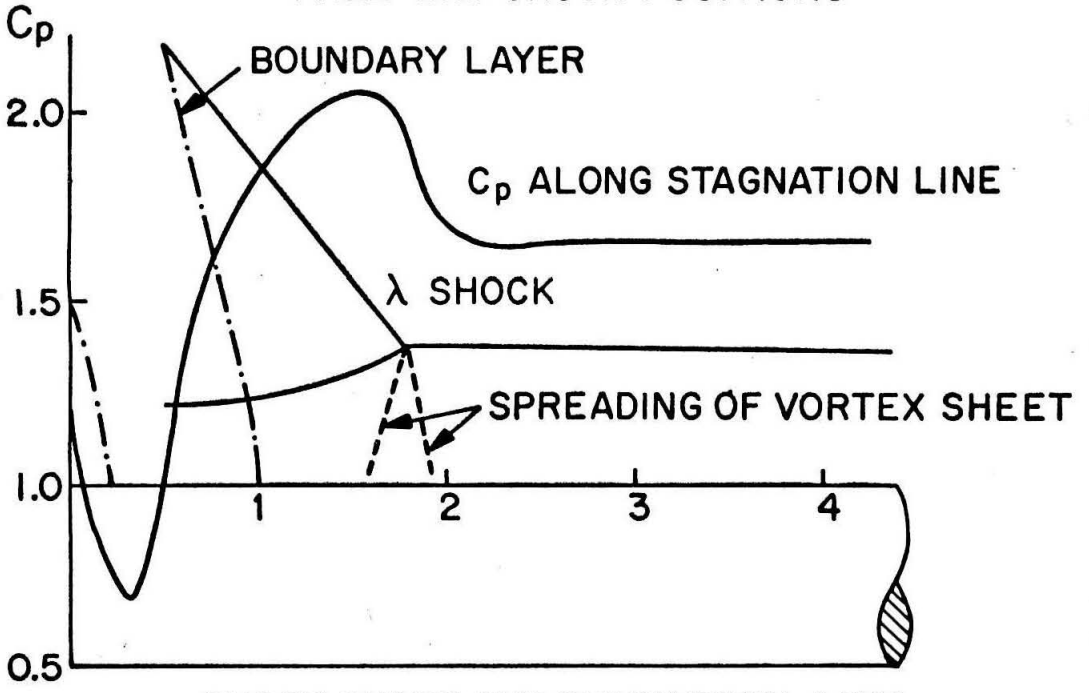

SHOCK SHAPE AND STAGNATION-LINE
PRESSURE DISTRIBUTION NEAR THE ROOT

Fig. A-5 SUPERSONIC FLOW PAST A PROTRUDING CYLINDER

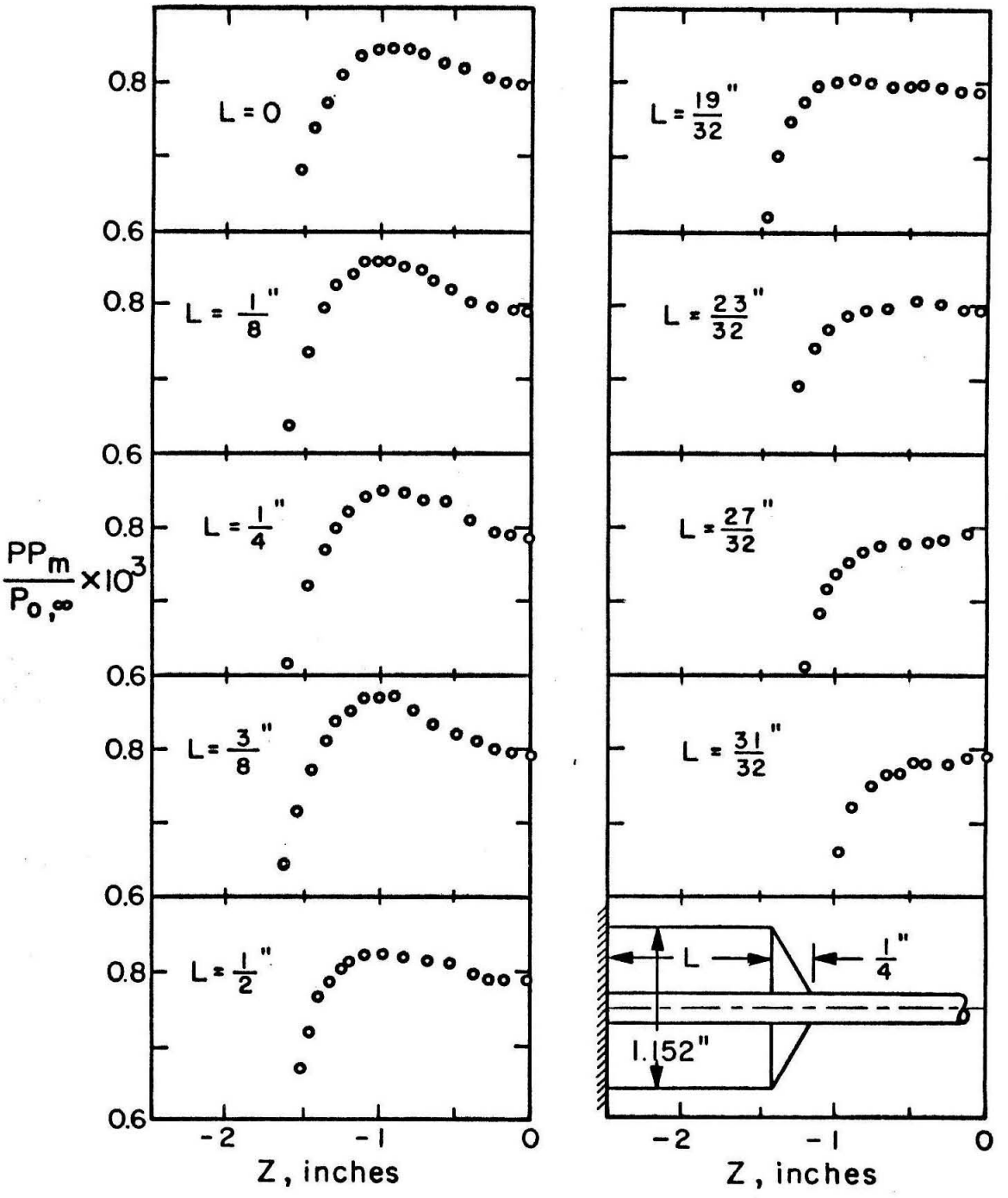

Fig. A-6 PITOT PRESSURE DISTRIBUTION FOR THE MODEL WITH WEDGE OF VARIABLE LENGTH AT X/D = 0.6

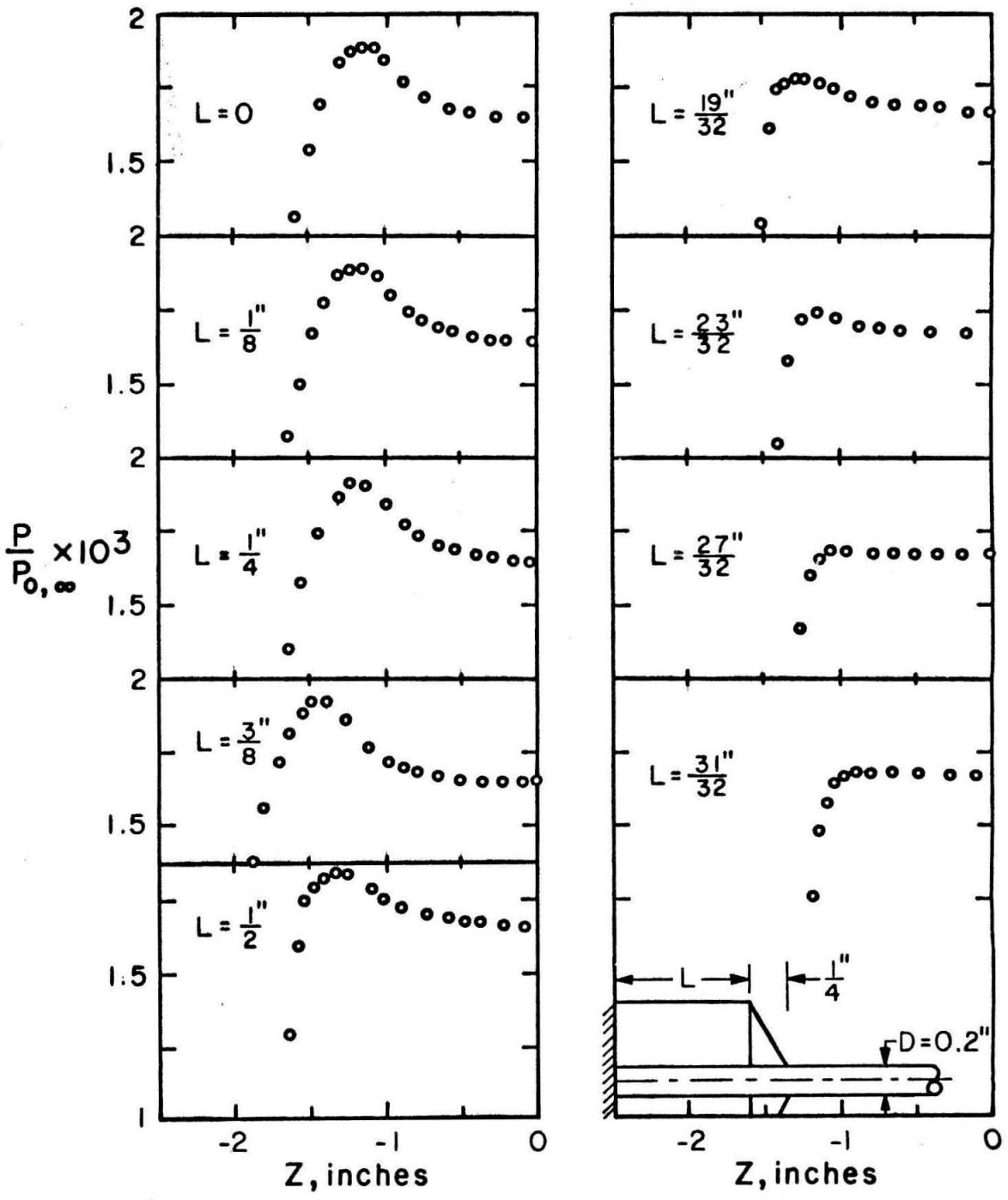

Fig. A-7 STATIC PRESSURE DISTRIBUTION FOR THE MODEL WITH WEDGE OF VARIABLE LENGTH AT X/D = 3.0

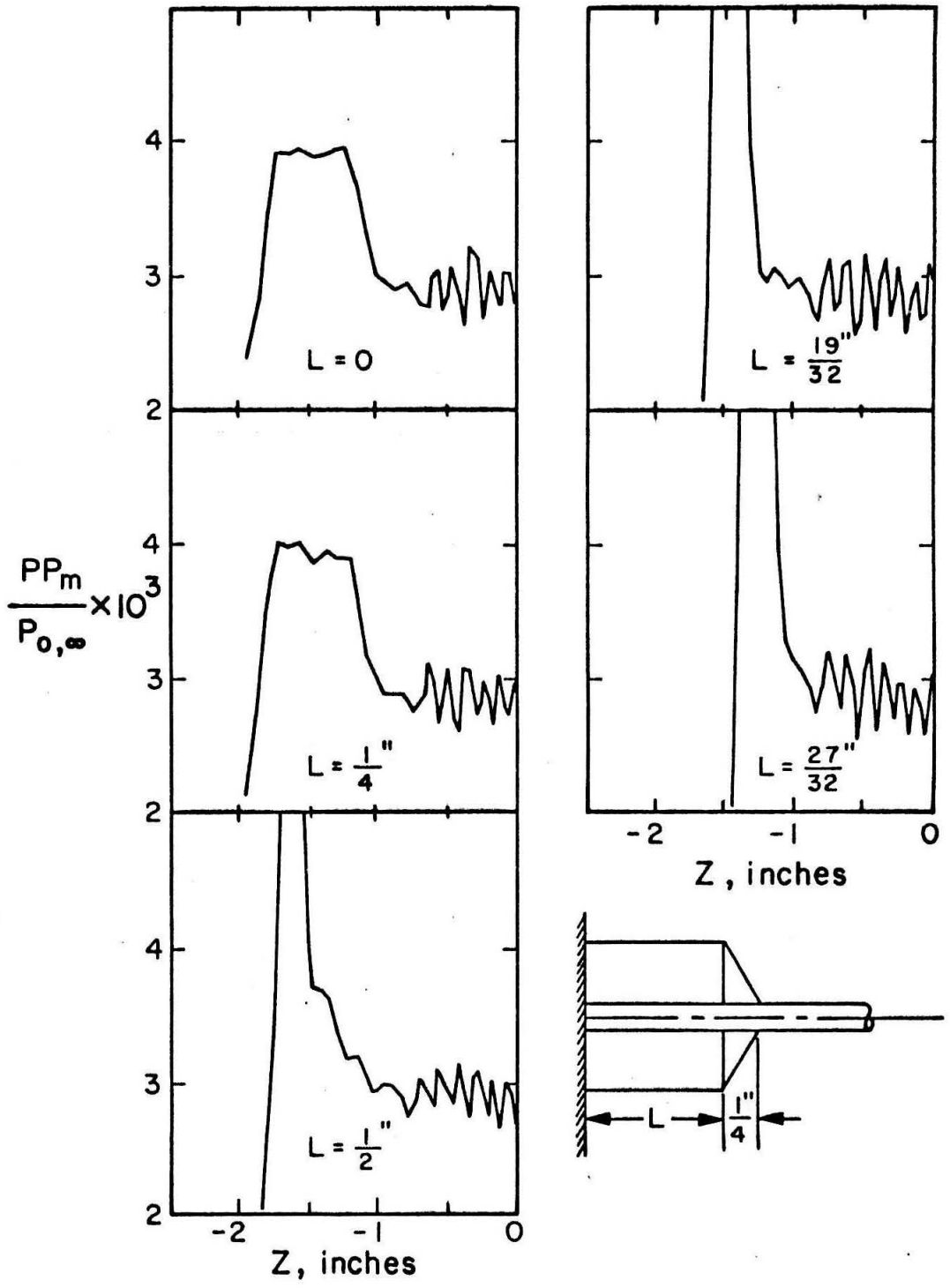

Fig. A-8 PITOT PRESSURE DISTRIBUTION FOR THE MODEL WITH WEDGE OF VARIABLE LENGTH AT X/D = 3.0

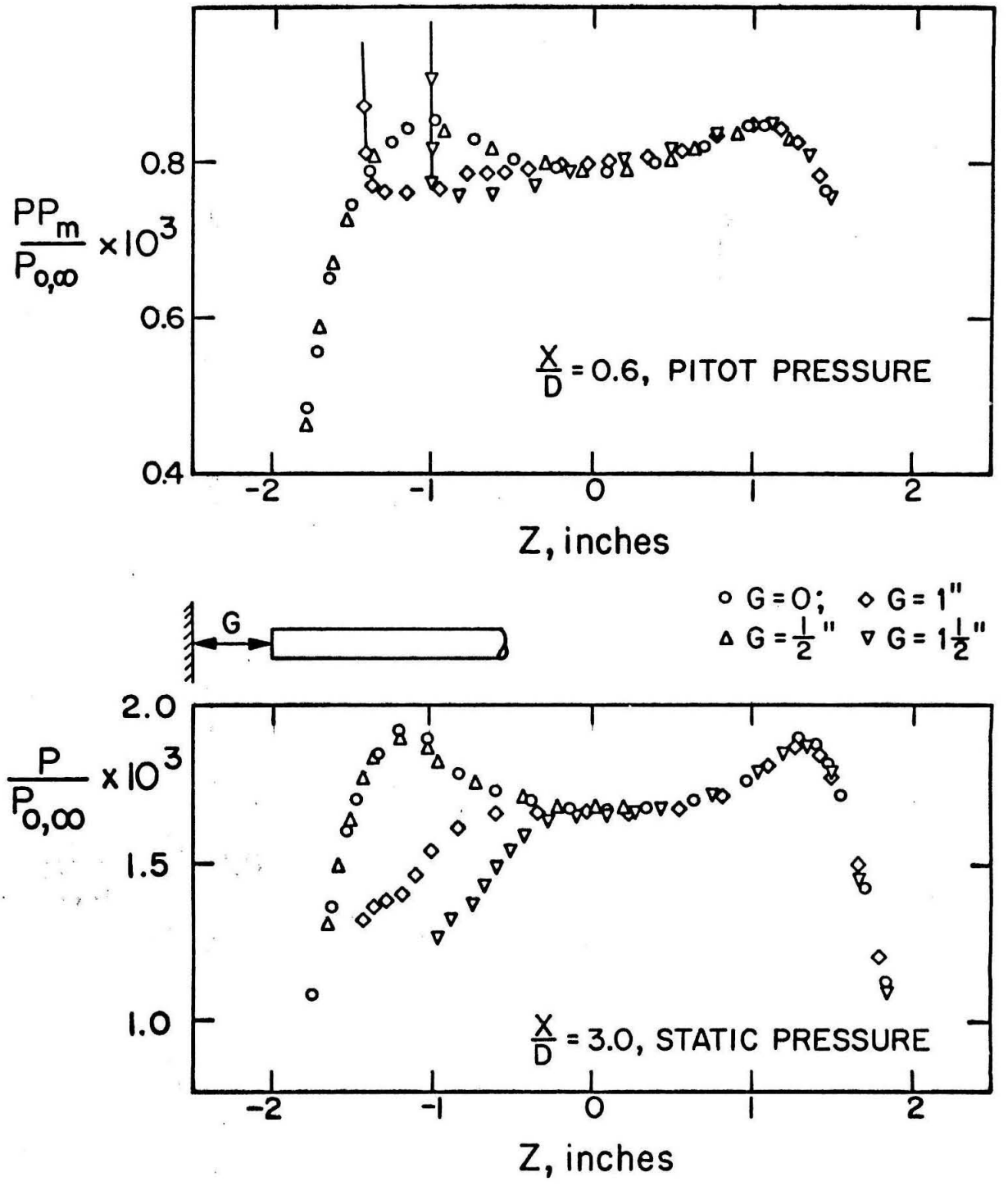

Fig.A-9 PRESSURE DISTRIBUTIONS FOR THE PROTRUDING CYLINDER MODEL

APPENDIX B

VISCOUS CORRECTIONS TO MEASURED PITOT PRESSURE

Brief Review

The ideal Pitot pressure (PP_i) is given by

$$PP_i = P + \tfrac{1}{2}\rho u^2 \quad \text{for incompressible flow}$$

$$\frac{PP_i}{P} = \left(1 + \frac{\gamma-1}{2} M^2\right)^{\frac{\gamma}{\gamma-1}} \quad \text{for } M < 1$$

and

$$\frac{PP_i}{P} = \left(\frac{\gamma+1}{2} M^2\right)^{\frac{\gamma}{\gamma-1}} \Big/ \left(\frac{2\gamma}{\gamma+1} M^2 - \frac{\gamma-1}{\gamma+1}\right)^{\frac{1}{(\gamma-1)}} \quad \text{for } M > 1$$

The last expression is from the Rankine-Hugoniot relations for normal shocks. When the local Reynolds number based on the Pilot probe is small, the measured pressure will differ from this ideal pressure because of viscous effects. The correction to the measured Pitot pressure to obtain the ideal pressure has been the subject of study by many workers. Among them the recent publication by Schaaf[27] is a review and gives many references to the related work. The results of Sherman[24] and Potter et. al.[25] provide considerable experimental data to evaluate the viscous corrections to the measured Pitot pressure.

Figure B-1 shows the experimental results of Sherman[24] for the Pitot pressure correction, for M = 0.1 to 0.7. Results for both open-ended and source shaped tubes are given in this figure. It can be noticed that the corrections for the source shaped probe is more than that of the open end tube. The results of the source shaped probe agree quite well with the theoretical and experimental results of Homann[23] for spherical-headed probes in oil (M = 0).

Figure B-2 shows the correction factors for the supersonic case taken from results of Potter and Bailey[25] and Sherman[24] (Figure I-2 in reference (25)). It is seen that there is no variation in the correction factor with Mach number for the range of 1.8 to 5.8 covered by these data.

The theoretical and experimental results of Homann,[23] for incompressible flow, agree with each other reasonably well. Though no theory has been worked out for the compressible subsonic case, the reason for the increase in the measured stagnation pressure as compared with the ideal one is essentially the same as for the incompressible case, namely the viscous ramming effect as the Reynolds number reduces.

For the supersonic case the experimental data (Figure B-2) indicate that as the Reynolds number is decreased, there is apparently first a decrease in the measured Pitot pressure below that of PP_i, followed by a reversal and an abrupt increase as the Reynolds number is further decreased.

Probstein and Kemp[32] have analyzed the viscous and incipient merged layers of the shock on the basis of Navier-Stokes and shock wave conservation equations simplified according to strong shock and constant density shock layer assumptions. Their solutions for an adiabatic probe and $\gamma = 11/9$ did not exhibit a minimum for PP_m/PP_i for intermediate values of $Re_{2r}(\rho_2/\rho_1)^{\frac{1}{2}}$ as shown in Figure B-2. However, such a minimum was obtained for very cooled probes.

The theory of Levinsky and Yoshihara[33] used the Navier-Stokes equations and integrated the viscous, compressible flow equations

between the body and infinity along the stagnation streamline with the shock included. They found that PP_m/PP_I was relatively unaffected by cooling and it predicted $PP_m/PP_I < 1$ in the viscous layer regime. The results of this theory agree closely with the experimental results for $Re_{2r}(\rho_2/\rho_1)^{\frac{1}{2}}$ greater than 200 (Figure 11 and Figure 15 of Reference (25)). However, a reversal in the behavior and a rapid increase in $PP_m/PP_I > 1$ as shown in Fig. B-2 is not predicted by this theory.

Sedov et al[26] found theoretical expressions for PP_m/PP_i for supersonic flow taking PP_m to be the stagnation pressure behind a curved shock, calculated on the basis of conservation equations across the shock along the stagnation line taking into account the viscous and heat flow terms downstream of the shock, but assuming that the variation of viscous terms and of heat flow was small. The expressions for PP_m/PP_i for both 2-dimensional and 3-dimensional flows were obtained in terms of Re_{2R} and $\lambda_1 = u_1/a^*$ where Re_{2R} is the Reynolds number based on the conditions downstream of the shock and the radius of curvature of the shock. The results indicate that PP_m/PP_i decreases below 1.0 as Re_{2R} is reduced. However, in order to compare this theory with the experimental results, Re_{2R} had to be related to Re_{2r}.

From NACA technical report R-1 by Van Dyke and Gorden,[34] we find that R/r for a sphere, for $\gamma = 1.6$, is about 1.47. Using this value we found $(PP_m - PP_i)/PP_i$ as predicted by this theory of Sedov[26] was about twice as much as that given by the experiments in the range where the results of Levinsky and Yoshihara[33] agreed closely with the experimental results. This quantitative disagreement may probably

be due to the thin shock assumption made in reference (26) being not valid even in this flow regime.

A second order asymptotic analysis of the curved shock structure expanded in terms of the small parameter $1/Re_{2R}$ in a manner very similar to that done by Bush[35] was carried out. However, the final results for PP_m/PP_i did not show any dip as Reynolds number was decreased. PP_m/PP_i was always greater than 1.0 and increased as the Reynolds number decreased, a behavior similar to that obtained by Probstein and Kemp.[32]

Thus, one finds that there is no suitable theory to date to predict the viscous effects on impact probes for the supersonic flow. Therefore analytical expressions, giving the corrections to measured Pitot pressure, agreeing reasonably with the experimental data for both subsonic and supersonic flows and as well having a smooth transition from one to the other had to be obtained, more or less, on an emperical basis.

Emperical Formulation

(a) Subsonic flow:

Analytical expressions were fitted to experimental results of Sherman,[24] Figure B-1, for both open ended tube and source shaped probes. They are,

$$\frac{PP_m - PP_i}{\frac{1}{2}\rho u^2} = \frac{6.82}{Re_d} - 0.1136 \quad \text{for open ended tubes}$$

and

$$\frac{PP_m - PP_i}{\frac{1}{2}\rho u^2} = \frac{15.6}{3.0 + Re_d} - 0.02Re_d \quad \text{for source shaped probes.}$$

It can be shown from an analysis similar to that done by Homann[23] that, for incompressible flow, the correction for a two-dimensional probe is half that of an axisymmetric probe. It was assumed that this holds good in compressible subsonic flow also. The standard probe used in these experiments was of the open tube type and was 0.008" by 0.051" outside dimensions (an aspect ratio of approximately 6). Hence it was considered more appropriate to consider this probe as two-dimensional and take half the corrections of the axisymmetric probe. Hence

$$\frac{PP_m - PP_i}{\frac{1}{2}\rho u^2} = \frac{3.41}{Re_H} - 0.0568 \qquad \text{for the standard probe,}$$

where Re_H is based on H, the outside thickness of the probe.

The probe used for reverse flow measurements, shown in Fig. 5 has pressure orifices on the surface of a 0.022" tube. Therefore, the corresponding axisymmetric probe would be a spherical headed probe. Since the results of Sherman[24] for source shaped probes in air agreed with the incompressible flow results of Homann[23] for spherical-headed probes in oil, it was considered reasonable to take the corrections for this reverse flow-probe to be half that of the corrections for the source-shaped probe given by Sherman.[24] Hence

$$\frac{PP_m - PP_i}{\frac{1}{2}\rho u^2} = \frac{7.8}{3.0 + Re_d} - 0.001\, Re_d$$

was taken as the correction formula for this special probe used in reverse flow regions where flow was always subsonic.

Due to lack of any experimental data for Mach number 0.7 to 1.0, it was assumed that the above relations hold even up to M = 1.0.

(b) Supersonic flow

The corrections to the measured Pitot pressure for supersonic flow was considered to be made up of two parts, the one associated with the viscous subsonic flow after the shock and ahead of the Pitot probe and the other associated with the curved shock. It was further assumed that the first part was given by the expressions given earlier for subsonic flow if the quantities are based on conditions behind the shock. That is

$$\frac{PP_m - PP_i}{\frac{1}{2}\rho_2 u_2^2} = \frac{6.82}{Re_{2d}} - 0.1136$$

for axi-symmetric open-ended probes, or

$$\frac{PP_m - PP_I}{\frac{1}{2}\rho_2 u_2^2} = \frac{3.41}{Re_{2H}} - 0.0568$$

for two-dimensional open-ended probes.

The correction associated with the curved shock was obtained by taking the difference between the overall correction given by the experimental results of Potter and Bailey[25] (Figure B-2) minus the corrections given by the above expressions due to the viscous subsonic part. Note that the experimental data for the supersonic case are given in terms of PP_m/PP_i versus $Re_{2r}(\rho_2/\rho_1)^{\frac{1}{2}}$ and that the effect of Mach number in M = 1.7 to 6.0 range on the correction, if any, is completely submerged in the experimental scatter. Therefore in order to subtract the "Subsonic part" of the correction, it has to be expressed in terms of PP_m/PP_i, $Re_{2r}(\rho_2/\rho_1)^{\frac{1}{2}}$ and Mach number.

i.e. $$\left(\frac{PP_m}{PP_i} - 1\right)_{sub.} = \frac{\frac{1}{2}\rho_2 u_2^2}{PP_i}\left[\frac{3.41}{Re_{2r}(\rho_2/\rho_1)^{\frac{1}{2}}} \cdot \left(\frac{\rho_2}{\rho_1}\right) - 0.1136\right]$$

where $\frac{1}{2}\frac{\rho_2 u_2^2}{PP_i}$ and $\frac{\rho_2}{\rho_1}$ are just functions of Mach number.

After obtaining the values of the correction associated with shock emperically, an analytical expression was found which agrees reasonably with these values as functions of Mach number and $Re_{2d}\left(\frac{\rho_2}{\rho_1}\right)^{\frac{1}{2}}$, keeping in mind that the "shock corrections" should be zero at M = 1.0 and that the overall corrections should vary little with Mach number beyond M = 1.7. The expression obtained for this "shock correction" was

$$\left(\frac{PP_m}{PP_i} - 1\right)_{shock} = -\left\{\frac{F}{80 + 0.536\,F^{2.1336}}\right\}$$

where $F = Re_{2r}\left(\frac{\rho_2}{\rho_1}\right)^{\frac{1}{2}}\frac{M^2}{M^2-1}$

The overall correction in supersonic flow is then given by

$$\left(\frac{PP_m}{PP_I} - 1\right)_{total} = \left(\frac{PP_m}{PP_I} - 1\right)_{sub} + \left(\frac{PP_m}{PP_I} - 1\right)_{shock}.$$

The overall correction as given by the above expression is also shown in Figure (B-2). It is seen that the agreement is reasonably good.

It should be pointed out that the above formulation is purely emperical and was undertaken in order to incorporate the viscous correction into the iteration scheme in the mean flow data reduction program and the separation of the overall correction into "subsonic correction" and "shock correction" is really not meaningful in the merged layer regime.

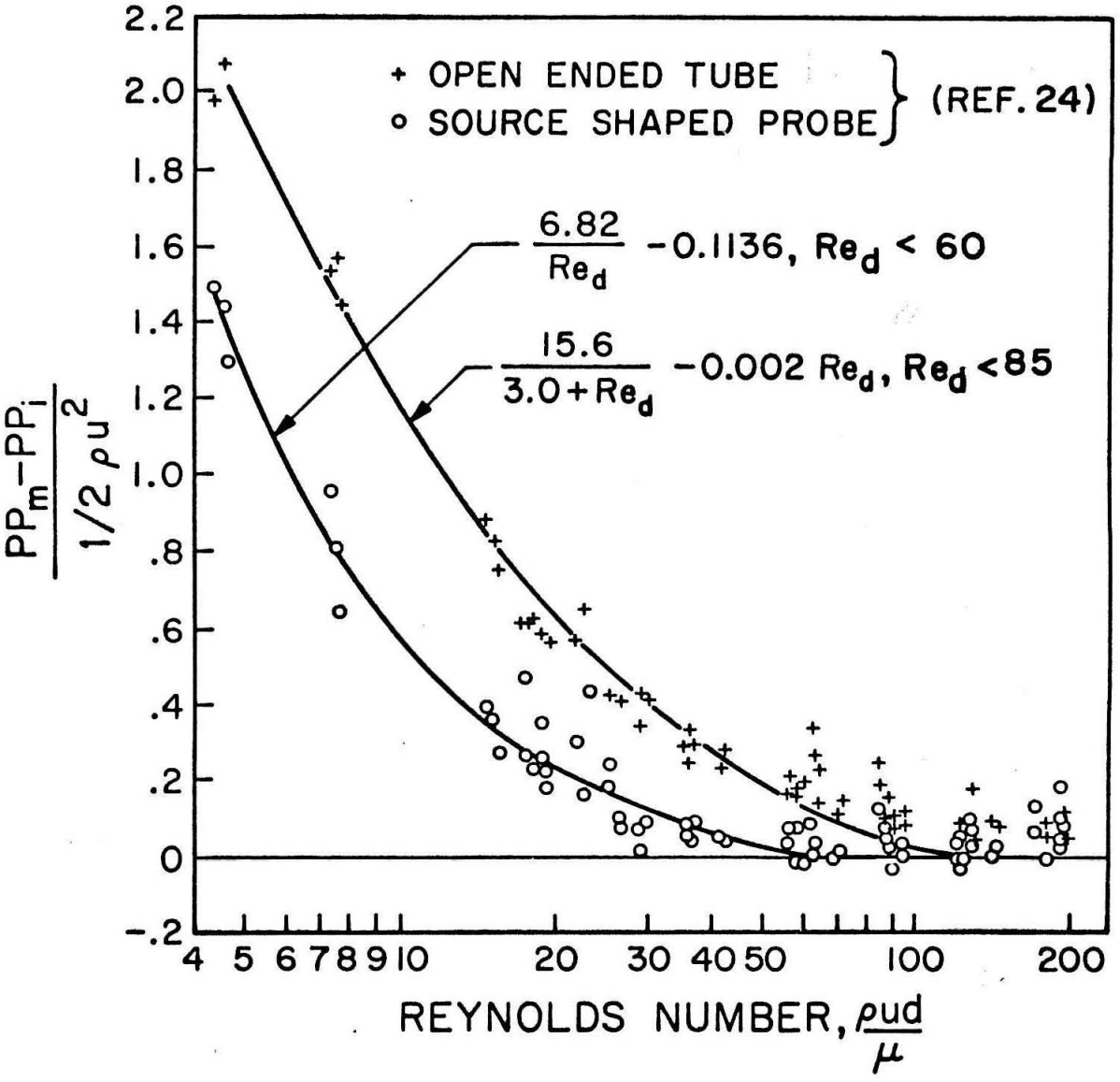

Fig.B-1 VISCOUS CORRECTION TO MEASURED PITOT PRESSURE ($0.1 < M < 0.67$)

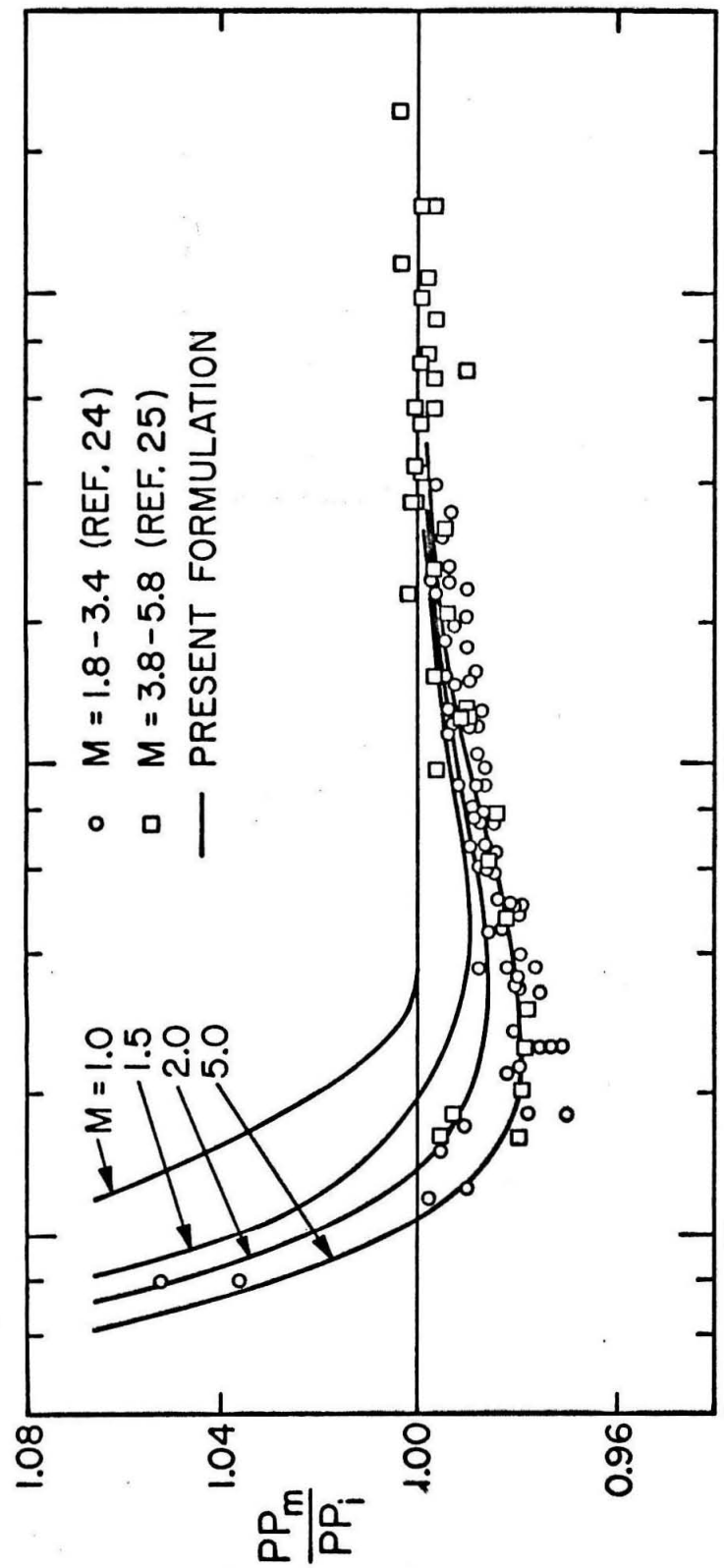

Fig.B-2 VISCOUS CORRECTION TO MEASURED PITOT PRESSURE IN SUPERSONIC FLOW

REFERENCES

1. Crocco, L. and Lees, L.: "A Mixing Theory for the Interaction Between Dissipative Flows and Nearly Isentropic Streams," J. Aero. Sci., 19:10, 649-676 (1952).

2. Chapman, D. R., Kuehn, D. M. and Larson, H. K.: "Investigation of Separated Flows in Supersonic and Subsonic Streams with Emphasis on the Effect of Transition," NACA Report 1356 (1958).

3. Reeves, B. L. and Lees, L.: "Theory of Laminar Near Wake of Blunt Bodies in Hypersonic Flow," AIAA Journal, 3:11, 2061 (Nov. 1965).

4. Grange, J. M., Klineberg, J. M. and Lees, L.: "Laminar Boundary Layer Separation and Near-Wake Flow for a Smooth Blunt Body at Supersonic and Hypersonic Speeds," AIAA Journal, 5:6, 1089 (June 1967).

5. Klineberg, J. M.: "Theory of Laminar Viscous-Inviscid Interactions in Supersonic Flow," Ph.D. Thesis, California Institute of Technology, Pasadena, Calif. (1968).

6. Chapman, D. R.: "A Theoretical Analysis of Heat Transfer in Regions of Separated Flow," NACA TN 3792 (Oct. 1956).

7. Baum, E., King, H. H. and Denison, M. R.: "Recent Studies of the Laminar Base-Flow Region," AIAA Journal, 2:9, 1527 (Sept. 1964).

8. Feldman, S.: "Trails of Axi-Symmetric Hypersonic Blunt Bodies Flying Through the Atmosphere," Avco-Everett, Research Report 82 (Dec. 1959); Also J. Aero. Sci., 28, 433-448 (1961).

References (Cont.)

9. Lykoudis, P. S.: "Theory of Ionized Trails for Bodies at Hypersonic Speeds," Rand RM-2682-1-PR (May 1961, revised Oct. 1961).

10. Lees, L. and Hromas, L.: "Turbulent Diffusion in the Wake of a Blunt-Nosed Body at Hypersonic Speeds," J. Aero. Sci., 29, 976-993 (1962).

11. Kubota, T.: "Laminar Wake with Streamwise Pressure Gradient II," GALCIT Internal Memorandum No. 9 (April 1962).

12. Gold, H.: "Laminar Wake with Arbitrary Initial Profiles," AIAA Journal, 2:5, 948-949 (1964).

13. Lees, L. and Gold. H.: "Stability of Laminar Boundary Layers and Wakes at Hypersonic Speeds. Part I. Stability of Laminar Wakes," Fundamental Phenomena in Hypersonic Flow, ed. by J. Gordon Hall, Cornell Univ. Press, 310-343 (1966).

14. McCarthy, J. F., Jr.: "Hypersonic Wakes," GALCIT Hypersonic Research Project, Memorandum No. 67 (July 1962).

15. Dewey, C. F., Jr.: "Near Wake of a Blunt Body at Hypersonic Speeds," AIAA Journal, 3:6, 1001-1010 (1965);
Also "Measurements in Highly Dissipative Regions of Hypersonic Flows. Part II. The Near Wake of a Blunt Body at Hypersonic Speeds," Ph.D. Thesis, California Institute of Technology, Pasadena, Calif. (1963).

16. Behrens, W.: "Flow Field and Stability of the Far Wake Behind Cylinders at Hypersonic Speeds," Ph. D. Thesis, Calif. Inst. of Technology, Pasadena, Calif. (1966);
Also "The Far Wake Behind Cylinders at Hypersonic Speeds. Part I. Flowfield," AIAA Journal, 5:12, 2135 (Dec. 1967).

17. Mohlenhoff, W.: "Experimental Study of Helium Diffusion in the Wake of a Circular Cylinder at M = 5.8," GALCIT Hypersonic Research Project, Memorandum No. 54 (May 1960).

18. Kingsland, L., Jr.: "Experimental Study of Helium and Argon Diffusion in the Wake of a Circular Cylinder at M = 5.8," GALCIT Hypersonic Research Project, Memorandum No. 60 (June 1961).

19. Herzog, R. R.: "Nitrogen Injection Into the Base Region of a Hypersonic Body," GALCIT Hypersonic Research Project, Memorandum No. 71 (August 1964).

20. Collins, D. J.: "The Near Wake of a Two-Dimensional Hypersonic Blunt Body with Mass Addition," Ph. D. Thesis, Calif. Inst. of Technology, Pasadena, Calif. (1969).

21. Batt, R. G.: "Experimental Investigation of Wakes Behind Two-Dimensional Slender Bodies at M = 6," Ph. D. Thesis, Calif. Inst. of Technology, Pasadena, Calif. (1967).

22. Baloga, P. E. and Nagamatsu, H. T.: "Instrumentation of the GALCIT Hypersonic Wind Tunnels," GALCIT Hypersonic Research Project, Memorandum No. 29 (July 1955).

23. Homann, F.: "Der Einfluss grosser Zihigkeit bei der Stromung un den Zylinder und un die Kugel," ZAMM, 16 (1936).

24. Sherman, F. S.: "New Experiments on Impact-Pressure Interpretation in Supersonic and Subsonic Rarefied Air Streams," NACA TN 2995 (Sept. 1963).

25. Potter, J. L. and Bailey, A. B.: "Pressures in the Stagnation Regions in the Viscous-Layer to Merged-Layer Regimes of Rarefied Flow," Arnold Engineering Development Center, AEDC-TDR-63-168 (Sept. 1963).

26. Sedov, L. I., Michailova, M. P. and Chernyi, G. G.: "On the Influence of Viscosity and Heat Conduction on the Gas Flow Behind a Strong Shock Wave," translated from Vestnik Mosovskovo Universiteta, No. 3, 1953 by Ronald F. Probstein, WADC TN 59-349 (Oct. 1959).

27. Schaaf, S. A.: "The Pitot Probe in Low Density Flows," AGARD Report 525 (January 1966).

28. Zakkay, V. and Cresci, R. J.: "An Experimental Investigation of the Near Wake of a Slender Cone at M_∞ = 8 and 12," AIAA Journal, 4:1, 41 (Jan. 1966).

29. Muntz, E. P. and Softley, E. J.: "Study of Laminar Near Wakes," AIAA Journal, 4:6, 961 (June 1966).

30. Ginoux, J. J.: "On the Existence of Cross Flows in Separated Supersonic Streams," T. E. C. A. Tn 6, Rhode-Saint-Genese Belgium (1962).

31. Sykes, D. M.: "The Supersonic and Low Speed Flows Past Circular Cylinders of Finite Length Supported at One End," J. Fluid Mech., 12, pt. 3, 367 (1962).

32. Probstein, R. F. and Kemp, N. H.: "Viscous Aerodynamic Characteristics in Hypersonic Rarefied Gas Flow," J. Aero. Sci., 27:3 (March 1960).

33. Levinsky, E. S. and Yoshihara, H.: "Rarefied Hypersonic Flow Over a Sphere," Hypersonic Flow Research, ed. by F. R. Riddell, Academic Press (1962).

34. Van Dyke, M. D. and Gordon, H. S.: "Supersonic Flow Past a Family of Blunt Bodies," NASA Technical Report R-1 (1959).

35. Bush, W. B.: "On the Viscous Hypersonic Blunt Body Problem," J. Fluid Mech., 20, pt. 3 (1964).